SLAC–PUB–10811
October 2004

Testing Quantum Chromodynamics with Antiprotons *

Stanley J. Brodsky
Stanford Linear Accelerator Center
Stanford University, Stanford, California 94309
E-mail: sjbth@slac.stanford.edu

Presented at the
International School of Physics "Enrico Fermi"
Course CLVIII – "Hadron Physics"
Varenna, Italy
June 22–July 2, 2004

*Work supported by the Department of Energy under contract number DE–AC02–76SF00515.

Abstract

The antiproton storage ring HESR to be constructed at GSI will open up a new range of perturbative and nonperturbative tests of QCD in exclusive and inclusive reactions. I discuss 21 tests of QCD using antiproton beams which can illuminate novel features of QCD. The proposed experiments include the formation of exotic hadrons, measurements of timelike generalized parton distributions, the production of charm at threshold, transversity measurements in Drell-Yan reactions, and searches for single-spin asymmetries. The interactions of antiprotons in nuclear targets will allow tests of exotic nuclear phenomena such as color transparency, hidden color, reduced nuclear amplitudes, and the non-universality of nuclear antishadowing. The central tool used in these lectures are light-front Fock state wavefunctions which encode the bound-state properties of hadrons in terms of their quark and gluon degrees of freedom at the amplitude level. The freedom to choose the light-like quantization four-vector provides an explicitly covariant formulation of light-front quantization and can be used to determine the analytic structure of light-front wave functions. QCD becomes scale free and conformally symmetric in the analytic limit of zero quark mass and zero β function. This "conformal correspondence principle" determines the form of the expansion polynomials for distribution amplitudes and the behavior of non-perturbative wavefunctions which control hard exclusive processes at leading twist. The conformal template also can be used to derive commensurate scale relations which connect observables in QCD without scale or scheme ambiguity. The AdS/CFT correspondence of large N_C supergravity theory in higher-dimensional anti-de Sitter space with supersymmetric QCD in 4-dimensional space-time has important implications for hadron phenomenology in the conformal limit, including the nonperturbative derivation of counting rules for exclusive processes and the behavior of structure functions at large x_{bj}. String/gauge duality also predicts the QCD power-law fall-off of light-front Fock-state hadronic wavefunctions with arbitrary orbital angular momentum at high momentum transfer. I also review recent work which shows that the diffractive component of deep inelastic scattering, single spin asymmetries, as well as nuclear shadowing and antishadowing, cannot be computed from the LFWFs of hadrons in isolation.

1 Introduction

Quantum Chromodynamics is a remarkable theory. Not only does it provide a consistent description of the strong and nuclear interactions in terms of quark and gluon degrees of freedom at short distances, but its non-Abelian Yang Mills gauge theory structure also provides the foundation for the electroweak interactions and the eventual unification of the electrodynamic, weak, and hadronic forces at very short distances. The theory has extraordinary properties, such as color confinement [1], asymptotic freedom [2, 3], a complex vacuum structure, and predicts an array of new forms of hadronic matter such as gluonium and hybrid states [4]. The phase structure of QCD [5] implies the formation of a quark-gluon plasma in high energy heavy ion collisions [6] as well insight into the evolution of the early universe [7].

The asymptotic freedom property of QCD explains why the strong interactions become weak at short distances, thus allowing hard processes to be interpreted directly in terms of the perturbative interactions of quark and gluon quanta. This in turn leads to factorization theorems [8, 9] for both inclusive and exclusive processes [10] which separate the hard scattering subprocesses which control the reaction from the nonperturbative physics of the interacting hadrons.

More recently, a remarkable duality has been established between supergravity string theory in 10 dimensions and conformal supersymmetric extensions of QCD [11, 12, 13, 14]. The AdS/CFT correspondence is now leading to a new understanding of QCD at strong coupling and the implications of its nearly-conformal structure.

The Lagrangian density of QCD [15] has a deceptively simple form:

$$\mathcal{L} = \overline{\psi}(i\gamma_\mu D^\mu - m)\psi - \frac{1}{4}G^2_{\mu\nu} \tag{1}$$

where the covariant derivative is $iD_\mu = i\partial_\mu - gA_\mu$ and where the gluon field strength is $G_{\mu\nu} = \frac{i}{g}[D_\mu, D_\nu]$. The structure of the QCD Lagrangian is dictated by two principles: (i) local $SU(N_C)$ color gauge invariance – the theory is invariant when a quark field is rotated in color space and transformed in phase by an arbitrary unitary matrix $\psi(x) \to U(x)\psi(x)$ locally at any point x^μ in space and time; and (ii) renormalizability, which requires the appearance of dimension four interactions. In principle, the only parameters of QCD are the quark masses and the QCD coupling determined from a single observable at a single scale.

Solving QCD is extremely challenging because of the non-Abelian three-point and four-point gluonic couplings contained in its Lagrangian. Exact solutions are known for $QCD(1+1)$ at $N_C \to \infty$ by 't Hooft [16]. The one-space one-time theory can be solved numerically to any precision at finite N_C for any coupling strength and number of quark flavors using discretized light-cone quantization (DLCQ) [17, 18, 19, 20]. One can use DLCQ to calculate the entire spectrum of virtually any 1+1 theory, its discrete bound states as well as the scattering continuum. The main emphasis of the DLCQ method applied to QCD is the determination of the wavefunctions of the hadrons from first principles.

Currently the most important computational tool for making predictions in strong-coupling QCD(3+1) is lattice gauge theory [21] which has made enormous progress in recent years particularly in computing mass spectra and decay constants. Lattice gauge theory can only provide limited dynamical information because of the difficulty of continuing predictions from Euclidean to Minkowski space. At present, results are limited to large quark and pion masses such that the ρ meson is stable [22]. The DLCQ solutions for 1+1 quantum field theories could provide a powerful test of lattice methods.

Other important nonperturbative QCD methods are Dyson-Schwinger techniques [23] and the transverse lattice [24] which combines DLCQ methods for the one space and one time theory with lattice methods in transverse space. The Dyson-Schwinger methods account well for running quark mass effects, and in principle can give important hadronic wavefunction information. The transverse lattice method has recently provided the first computation of the generalized parton distributions of the pion [24].

Light Front Wavefunctions [20]: The concept of a wave function of a hadron as a composite of relativistic quarks and gluons is naturally formulated in terms of the light-front Fock expansion at fixed light-front time [25], $\tau = x \cdot \omega$. The four-vector ω, with $\omega^2 = 0$, determines the orientation of the light-front plane; the freedom to choose ω provides an explicitly covariant formulation of light-front quantization [26]. The light-front wave functions (LFWFs) $\psi_n(x_i, k_{\perp_i}, \lambda_i)$, with $x_i = \frac{k_i \cdot \omega}{P \cdot \omega}$, $\sum_{i=1}^n x_i = 1$, $\sum_{i=1}^n k_{\perp_i} = 0_\perp$, are the coefficient functions for n partons in the Fock expansion, providing a general frame-independent representation of the hadron state. The λ_i are the eigenvalues of the spin projections S^z in the $\hat{z}$ direction. Angular momentum conservation for each Fock state implies

$$J^z = \sum_i^n S_i^z + \sum_i^{n-1} L_i^z \tag{2}$$

where L_z is one of the $n-1$ relative orbital angular momentum. Relativity and quantum theory require that the number of Fock states cannot be bounded. However, the probability of massive Fock states with invariant mass $\mathcal{M}$ falls-off at least as fast as $1/\mathcal{M}^2$.

The LFWFs are boost invariant; i.e., independent of Lorentz frame. In principle, they are solutions of the LF Heisenberg equation where H_{LF} is computed from the theory quantized at fixed τ. As I will review in these lectures, given the LFWFs, one can calculate a myriad of dynamical processes. The LFWFs of hadrons are thus centerposts of the theory [27].

The Light-Front Fock state expansion provides a number of new perspectives for QCD:

Intrinsic Glue and Sea: Even though QCD was motivated by the successes of the parton model, QCD predicts many new features which go well beyond a three-quark bound state description of the proton. Since the number of Fock components cannot be limited in relativity and quantum mechanics, the nonperturbative wavefunction of

a proton contains gluons and sea quarks, including heavy quarks, at any resolution scale. Thus there is no scale Q_0 in deep inelastic lepton-proton scattering where the proton can be approximated by its valence quarks. The sea-quark distributions $Q(x)$ and $\overline{Q}(x)$ are not equal [28].

Initial and Final-State Interactions: Although it has been more than 35 years since the discovery of Bjorken scaling [29] in electroproduction [30], there are still many issues in deep-inelastic lepton scattering and Drell-Yan reactions which are only now being understood from a fundamental basis in QCD. In contrast to the parton model, final-state interactions in deep inelastic scattering and initial state interactions in hard inclusive reactions cannot be neglected – leading to $T-$odd single spin asymmetries [31, 32, 33] and diffractive contributions [34, 35]. This in turn implies that the structure functions measured in deep inelastic scattering are not probability distributions computed from the square of the LFWFs computed in isolation [34].

Novel Nuclear Phenomena: In the case of nuclei, QCD predicts that nuclear wavefunctions contain "hidden color" [36] components: color configurations not dual to the usual nucleonic degrees of freedom. For example, the scaling of the deuteron's reduced form factor suggests that the probability of six-quark Fock states with a color configuration orthogonal to that of the proton and neutron is of order of 15%. I will also discuss in these lectures other surprising features of QCD which contrast with standard nuclear physics descriptions, such as "color transparency" [37], the physical origin of antishadowing [38] and its nonuniversal character [39]. As I will discuss, the antishadowing of nuclear structure functions is quark-flavor specific; this implies that part of the anomalous NuTeV [40] result for $\sin^2\theta_W$ could be due to the non-universality of nuclear antishadowing for charged and neutral currents.

I will also several topics in which the underlying conformal symmetry of QCD plays a crucial role:

AdS/CFT Correspondence and QCD: The AdS/CFT correspondence [11, 12, 13, 14] between superstring theory in 10 dimensions and supersymmetric Yang Mills theory in 3+1 dimensions can provide important information on QCD phenomena without reliance on perturbation theory. As I will discuss in these lectures, one can use this connection to establish the form of QCD wavefunctions at large transverse momentum $k_\perp^2 \to \infty$ and at $x \to 1$ [41]. The AdS/CFT correspondence has important implications for hadron phenomenology in the conformal limit, including an all-orders demonstration of counting rules [42, 43, 44] for hard exclusive processes [12], as well as determining essential aspects of hadronic light-front wavefunctions [41].

The Conformal Correspondence Principle [45, 46]: The recent investigations using the AdS/CFT correspondence has reawakened interest in the conformal features of QCD. QCD becomes scale free and conformally symmetric in the analytic limit of zero quark mass and zero β function [47]. This correspondence principle provides a new tool, the conformal template, which is very useful for theory analyses, such as the expansion polynomials for distribution amplitudes [48, 49, 50, 51], the non-perturbative wavefunctions which control exclusive processes at leading twist [52, 53].

The conformal template also can be used to derive commensurate relations [54, 55] which connect observables in QCD without scale or scheme ambiguity.

The classical Lagrangian of QCD for massless quarks is conformally symmetric. Since it has no intrinsic mass scale, the classical theory is invariant under the $SO(4,2)$ translations, boosts, and rotations of the Poincare group, plus the dilatations and other transformations of the conformal group. Scale invariance and therefore conformal symmetry is destroyed in the quantum theory by the renormalization procedure which introduces a renormalization scale as well as by quark masses. Conformal symmetry is thus broken in physical QCD; nevertheless, we can still recover the underlying features of the conformally invariant theory by evaluating any expression in QCD in the analytic limit of zero quark mass and zero β function:

$$\lim_{m_q \to 0, \beta \to 0} \mathcal{O}_{QCD} = \mathcal{O}_{\text{conformal QCD}} \ . \tag{3}$$

This conformal correspondence limit is analogous to Bohr's correspondence principle where one recovers predictions of classical theory from quantum theory in the limit of zero Planck constant. The contributions to an expression in QCD from its nonzero β-function can be systematically identified [56, 55, 57] order-by-order in perturbation theory using the Banks-Zaks procedure [58].

There are other important consequences of near-conformal behavior: the conformal approximation with zero β function can be used as template for QCD analyses [50, 49] such as the form of the expansion polynomials for distribution amplitudes [51, 59]. The "conformal correspondence principle" also dictates the form of the expansion basis for hadronic distribution amplitudes.

Commensurate Scale Relations: The near-conformal behavior of QCD is the basis for commensurate scale relations [54] which relate observables to each other without renormalization scale or scheme ambiguities [56]. An important example is the generalized Crewther relation [60]. In this method the effective charges of observables are related to each other in conformal gauge theory; the effects of the nonzero QCD $\beta-$ function are then taken into account using the BLM method [61] to set the scales of the respective couplings. The magnitude of the effective charge [62] defined from the ratio of elastic pion and photon-to-pion transition form factors $\alpha_s^{\text{exclusive}}(Q^2) = F_\pi(Q^2)/4\pi Q^2 F^2_{\gamma\pi^0}(Q^2)$ is connected to other effective charges and observables by commensurate scale relations. Its magnitude, $\alpha_s^{\text{exclusive}}(Q^2) \sim 0.8$ at small Q^2, is sufficiently large as to explain the observed magnitude of exclusive amplitudes such as the pion form factor using the asymptotic distribution amplitude. An analytic effective charge such as the pinch scheme [63] provides a method to unify the electroweak and strong couplings and forces.

Fixed Point Behavior: Although the QCD coupling decreases logarithmically at high virtuality due to asymptotic freedom, theoretical and phenomenological evidence is now accumulating that QCD couplings based on a physical observable, such as hadronic τ decay, becomes constant at small virtuality. It thus develops an infrared fixed point [64, 65, 66, 67, 68]. This is in contradiction to the usual assumption of

singular growth in the infrared. The near-constant behavior of effective couplings also suggests that QCD can be approximated as a conformal theory even at relatively small momentum transfer.

The Abelian Correspondence Principle: One can consider QCD predictions as functions of analytic variables of the number of colors N_C and flavors N_F. At $N_C \to \infty$ at fixed $N_C\alpha_s$, calculations in QCD greatly simplify since only planar diagrams enter. However, the $N_C \to 0$ limit is also very interesting. Remarkably, one can show at all orders of perturbation theory [69] that PQCD predictions reduce to those of an Abelian theory similar to QED at $N_C \to 0$ with $C_F\alpha_s$ and $\frac{N_F}{T_F C_F}$ held fixed, where $C_F = \frac{N_C^2-1}{2N_C}$ and $T_F = 1/2$. The resulting theory corresponds to the group $1/U(1)$ which means that light-by-light diagrams acquire a particular topological factor. The $N_C \to 0$ limit provides an important check on QCD analyses; QCD formulae and phenomena must match their Abelian analog. The renormalization scale is effectively fixed by this requirement. Commensurate scale relations obey the Abelian Correspondence principle, giving the correct Abelian relations between observables in the limit $N_C \to 0$.

2 Twenty-One Key Antiproton Experiments

Experiment is critical for testing QCD and unravelling its novel features. The advent of the new antiproton storage ring HESR to be constructed at GSI and the new *PANDA* detector open up a new range of perturbative and nonperturbative tests of QCD in exclusive and inclusive reactions. These include the formation of exotic hadrons and novel tests involving timelike generalized parton distributions, the effects of charm at threshold, transversity, and single-spin asymmetries. The interactions of antiprotons in nuclear targets allows tests of exotic nuclear phenomena such as color transparency, hidden color, reduced nuclear amplitudes, and the non-universality of nuclear antishadowing. I will also discuss the physics of the heavy-quark sea and the role of conformal symmetry in hard exclusive processes. Most of these key experiments can be performed with stored antiprotons of moderate energy $E^{\overline{p}}_{\rm lab} < 15$ GeV interacting in an internal target.

1. *Total Annihilation.* The antiproton and proton can annihilate into a multihadron inclusive state, a system potentially rich in gluonic matter. Specific predictions for the inclusive distributions can be made in soliton-anti-soliton models [70]. Skyrmion-anti-Skyrmion annihilation provides a fairly accurate description of low-energy baryon-antibaryon annihilation. A statistical approach may also be useful [71]. The production of charmonium states is particularly interesting in view of the anomalously large signal observed at Belle [72] for $e^+e^- \to J/\psi\eta_c$. The process $p\overline{p} \to c\bar{c}X$ where X is a glueball state could provide an important tagged source of gluonic excitations [73].

2. *Exotic Resonance Formation in $\overline{p}p$ Reactions.* The strongest hadronic interactions and thus the strongest opportunity to form resonances occurs when constituents have the same 4-velocity or rapidity. In the case of $\overline{p}p$ interactions, one can have total annihilation of the incident quarks and antiquarks into open or hidden charmed hadrons; one can have "diquark" anti-diquark $qq + \overline{q}\overline{q}$ annihilation into charm quarks. These then can coalesce with the remaining valence quarks to produce charmed hadrons or a $|\, q\overline{q}c\overline{c}\rangle$ "quartoquark" resonance. If a q and $\overline{q}$ annihilate to charm quarks, the remaining quarks can produce"hectoquark" state $|\, qq\overline{q}\overline{q}c\overline{c}\rangle$. One can have $c\overline{c}$ production where all of the incident quarks and antiquarks appear in the final state. In this last case, one can produce "octoquark" resonances $\left|\, uud\overline{uu}\overline{d}c\overline{c}\right\rangle$. Thus there can be several kinematic regimes where novel charmed hadrons can naturally appear. The octoquark is the analog of $J = 1, L = 1, S = 1$ $|\, uuduudc\overline{c}\rangle$ state postulated to cause the large A_{NN} at the charm threshold in transversely polarized pp collisions [74].

3. *Tests of Dimensional Counting Rules and Conformal Scaling for Hard Exclusive Processes* [42, 44, 75, 76]. The counting rule for $\overline{p}p$ annihilation into two hadrons, photons, or leptons is

$$\frac{d\sigma}{dt}(\overline{p}p \to AB) = \frac{|F_{AB}(t/s)|^2}{s^{4+n_A+n_B}}. \tag{4}$$

where n_I is the minimum number of Fock-state particles in each final-state hadron; in the case of leptons or photons, $n_I = 1$. For example, $n = 8$ for $\frac{d\sigma}{dt}(\overline{p}p \to K^+K^-)$ and $n = 7$ for timelike photoproduction $\frac{d\sigma}{dt}(\overline{p}p \to \pi^0\gamma)$ at fixed t/s or $\theta_{\rm CM}$. In the case of a multiparticle final state where all particles are produced at distinct $\theta^I_{\rm CM}$,

$$\Delta\sigma(\overline{p}p \to A, B, C, ...) \sim s^{-5-\sum_{I=A,B,C,...}(n_I-1)}. \tag{5}$$

For example, $\Delta\sigma(\overline{p}p \to K^+K^-\pi^0) \sim s^{-8}$. These rules can be derived from PQCD; they also follow from conformal symmetry and the LFWFs derived from AdS/CFT. The power-law predictions are modified by logarithmic corrections from the non-zero QCD β function and the evolution of the hadronic distribution amplitudes of each hadron. One also finds that Regge trajectories must become flat, approaching negative integers at large negative t [77]. This has recently been demonstrated within the context of AdS/CFT by Andreev and Siegel [78].

4. *Hadron helicity Conservation in Exclusive Processes* [79]. The helicity and the angular dependence of large-momentum-transfer exclusive processes such as $\overline{p}p \to AB$ can be used to test gluon spin and other basic elements of perturbative QCD. These processes isolate QCD hard-scattering subprocesses in situations where the helicities of all the interacting quarks are controlled. The

predictions can be summarized in terms of a general spin selection rule which states that the total hadron helicity is conserved:

$$\sum_{initial} \lambda_H = \sum_{final} \lambda_H, \tag{6}$$

up to corrections falling as an inverse power in the momentum transfer.

5. *Tests of Quark Interchange Dominance in Exclusive Processes.* The angular distributions $F_{AB}(t/s)$ appearing in the fixed-angle scaling laws are sensitive to the scattering mechanism as well as the shapes of the hadron distribution amplitudes. In the limit of large N_C, the dominant scattering amplitude derives from quark interchange [80, 77, 41]. For example, the dominant scattering mechanism for $K^+p \to K^+p$ derives from the exchange of the common u quark.

   The quark interchange amplitude [80] for $AB \to CD$ can be written as a convolution of the four light-front wavefunctions appearing in the process

$$\int d^2k_\perp dx \psi_A \times \psi_B \times \psi_C \times \psi_D \; [M_A^2 + M_B^2 - \mathcal{M}^2] \tag{7}$$

   where M is the invariant mass of the constituents. The complete expression is given in Ref. [80]. In the case of $K^+p \to K^+p$, the interchange amplitude scales as $1/ut^2$ and thus $d\sigma/dt(K^+p \to K^+p) \simeq 1/s^2u^2t^4$. This agrees with the observed scaling and angular dependence of the fixed- CM angle data. If the u-quark exchange mechanism is dominant, then one can predict the amplitude for $\overline{p}p \to K^+K^-$ via $s \leftrightarrow t$ crossing. Thus the crossed amplitude $\overline{p}p \to K^+K^-$ must scale as $1/ut^2$ and the cross section is $d\sigma/dt(\overline{p}p \to K^+K^-) \simeq 1/u^2s^6$.

6. *Anomalous Regge Behavior.* At fixed t and large $s >>> -t$, one can use the Regge expansion

$$M(\overline{p}p \to AB) = \sum_R \beta_R(t) s_R^\alpha(t) \zeta_R \tag{8}$$

   where $\alpha_R(t)$ parameterizes the Regge trajectory for spacelike t and $\zeta_R(t)$ is the signature factor which determines the phase of the amplitude. Remarkably, perturbative QCD and conformal scaling require that these trajectories approach negative integers at large $-t$ (-1 for meson exchange, -2 for baryon exchange in the t channel), rather than the conventional linear trajectories normally used in Regge theory [77]. The power behavior of $\beta_R(t)$ is also determined.

7. *Timelike Compton Scattering* [81, 82]: $\overline{p}p \to \gamma\gamma$. The scaling, normalization, and angular distribution of this fundamental process has been computed at lowest order in the PQCD factorization framework [83]. Conformal symmetry predicts the scaling $s^6 \frac{d\sigma}{dt}(\overline{p}p \to \gamma\gamma) = F(\theta_{cm})$ at large s and t. The ratio of the timelike Compton amplitude to the timelike proton form factor is important since uncertainties from the baryon coupling F_p to three quarks (the

same coupling which controls proton decay!) and the QCD coupling at timelike virtuality cancel out. This normalization thus can expose the importance of higher order corrections in α_s. The angular distributions of timelike Compton scattering including spin correlations are highly sensitive to the shape of the proton distribution amplitude $\phi_p(x_i, Q)$, the basic three quark wavefunction.

8. *Timelike Deeply Virtual Compton Scattering* $\overline{p}p \to \gamma^*\gamma$ *(DVCS).* At large photon virtuality, this amplitude is computable from the convolution of the $\overline{q}q \to \gamma^*\gamma$ amplitude with the timelike generalized parton distributions. Phase information can be obtained from the interference of the DVCS amplitude $\overline{p}p \to \ell^+\ell^-\gamma$ with the bremsstrahlung amplitude $\overline{p}\overline{p} \to \gamma^* \to \ell^+\ell^-\gamma$ derived from the timelike proton form factor which causes an $\ell^+\ell^-$ asymmetry. The handbag contribution to the DVCS amplitude can be computed from the overlap of proton light-front wavefunctions [84, 85] including contributions from Fock states with the same parton number $n = n'$, and states differing by the presence of an extra $q\overline{q}$: $n = n' + 2$.

9. *The* $J = 0$ *Fixed pole*: One of the most distinctive features of QCD is the presence of a $J = 0$ fixed Regge pole contribution to the Compton amplitude reflecting the fact that the two photons can act quasi-locally on the same quark [86]. This contribution can be observed in timelike DVCS: $\overline{p}p \to \gamma\gamma^*$ from its distinctive kinematic properties: the amplitude from the $J = 0$ term is independent of t at fixed s, independent of photon virtuality at fixed s.

10. *Time-like Proton Form Factors.* Leading-twist PQCD predictions for hard exclusive amplitudes [76] are written in a factorized form as the product of hadron distribution amplitudes $\phi_I(x_i, Q)$ for each hadron I convoluted with the hard scattering amplitude T_H obtained by replacing each hadron with collinear on-shell quarks with light-front momentum fractions $x_i = k_i^+/P^+$. The hadron distribution amplitudes are obtained by integrating the $n-$parton valence light-front wavefunctions:

$$\phi(x_i, Q) = \int^Q \Pi_{i=1}^{n-1} d^2k_{\perp i}\ \psi_{\rm val}(x_i, k_\perp). \tag{9}$$

Thus the distribution amplitudes are $L_z = 0$ projections of the LF wavefunction, and the sum of the spin projections of the valence quarks must equal the J_z of the parent hadron. Higher orbital angular momentum components lead to power-law suppressed exclusive amplitudes [76, 87]. Since quark masses can be neglected at leading twist in T_H, one has quark helicity conservation, and thus, finally, hadron-helicity conservation: the sum of initial hadron helicities equals the sum of final helicities. In particular, since the hadron-helicity violating Pauli form factor is computed from states with $\Delta L_z = \pm 1$, PQCD predicts $F_2(Q^2)/F_1(Q^2) \sim 1/Q^2$ [modulo logarithms]. A detailed analysis shows that

the asymptotic fall-off takes the form $F_2(Q^2)/F_1(Q^2) \sim \log^2 Q^2/Q^2$ [88]. One can also construct other models [89] incorporating the leading-twist perturbative QCD prediction which are consistent with the JLab polarization transfer data [90] for the ratio of proton Pauli and Dirac form factors. This analysis can also be extended to study the spin structure of scattering amplitudes at large transverse momentum and other processes which are dependent on the scaling and orbital angular momentum structure of light-front wavefunctions. Recently, Afanasev, Carlson, Chen, Vanderhaeghen, and I [91] have shown that the interfering two-photon exchange contribution to elastic electron-proton scattering, including inelastic intermediate states, can account for the discrepancy between Rosenbluth and Jefferson Lab spin transfer polarization data [90].

A crucial prediction of models for proton form factors is the relative phase of the timelike form factors, since this can be measured from the proton single spin symmetries in $e^+e^- \to p\overline{p}$ or $p\overline{p} \to \ell\overline{\ell}$ [92]. The Zemach radius of the proton is known to a precision of better than 2% from the comparison of hydrogen and muonium hyperfine splittings; this constraint needs to be incorporated into any analysis [93].

The annihilation process $\overline{p}p \to \ell^+\ell^-$ thus provides a primary test of proton structure. Its angular distribution allows a direct separation of the $G_E(s)$ and $G_M(s)$ timelike form factors. Carl Carlson, John Hiller, Dae Sung Hwang and I [92] have shown that measurements of the proton's polarization strongly discriminate between the analytic forms of models which fit the proton form factors in the spacelike region. In particular, the single-spin asymmetry normal to the scattering plane measures the relative phase difference between the timelike G_E and G_M form factors. The dependence on proton polarization in the timelike region is expected to be large in most models, of the order of several tens of percent. The continuation of the spacelike form factors to the timelike don=main $t = s > 4M_p^2$ is very sensitive to the analytic form of the form factors; in particular it is very sensitive to the form of the PQCD predictions including the corrections to conformal scaling. The forward-backward $\ell^+\ell^-$ asymmetry measures the interference of one-photon and two-photon contributions to $\overline{p}p \to \ell^+\ell^-$.

11. *Tests of Color Transparency.* The small transverse size fluctuations of a hadron wavefunction with a small color dipole moment will have minimal interactions in a nucleus [94, 37]. Color transparency can be tested in quasi-elastic antiproton-nucleus reactions such as $\overline{p}A \to \pi^+\pi^-(A-1)$ where the proton annihilates in the nucleus leaving a recoiling nucleus with one less proton. According to color transparency, at large $\mathcal{M}_{\pi^+\pi^-}$ the small size wavefunction fluctuations of the incident $\overline{p}$ and outgoing pions which enter the hard scattering exclusive $\overline{p}p \to \pi^+\pi^-$ amplitude will not be absorbed in the nucleus so that the ideal rate is proportional to the number Z of protons in the nucleus. In contrast, the standard nuclear physics prediction is the number $Z^{1/3}$ of protons on the

periphery of the nucleus.

12. *Intrinsic Charm* [95]. The probability for Fock states of a light hadron such as the proton to have an extra heavy quark pair decreases as $1/m_Q^2$ in non-Abelian gauge theory [96, 97]. The relevant matrix element is the cube of the QCD field strength $G^3_{\mu\nu}$. This is in contrast to abelian gauge theory where the relevant operator is $F^4_{\mu\nu}$ and the probability of intrinsic heavy leptons in QED bound state is suppressed as $1/m_\ell^4$. The intrinsic Fock state probability is maximized at minimal off shellness. The maximum probability occurs at $x_i = m^i_\perp / \sum_{j=1}^n m^j_\perp$; *i.e.*, when the constituents have equal rapidity. Thus the heaviest constituents have the highest momentum fractions and highest x. Intrinsic charm thus predicts that the charm structure function has support at large x_{bj} in excess of DGLAP extrapolations [95]; this is in agreement with the EMC measurements [98].

    Intrinsic charm allows charm production to occur close to it's kinematic threshold [99]. Charm and bottom production near threshold is sensitive to the multi-quark, gluonic, and hidden-color correlations of hadronic and nuclear wavefunctions in QCD since all of the target's constituents must act coherently within the small interaction volume of the heavy quark production subprocess. Although such multi-parton subprocess cross sections are suppressed by powers of $1/m_Q^2$, they have less phase-space suppression and can dominate the contributions of the leading-twist single-gluon subprocesses in the threshold regime. In fact, an anomalous signal was observed at CESR in J/ψ photoproduction near threshold [100]. Similarly, intrinsic charm predicts anomalously large rates for open and hidden charm in $\overline{p}p$ collisions such as $\overline{p}p \to \Lambda_C X$ and $\overline{p}p \to J/\psi X$ even at relatively small antiproton energies. The rate for threshold channels will be significantly enhanced in nuclear targets.

13. *Anomalous Deuteron Reactions and Hidden Color.* In general, the six-quark wavefunction of a deuteron is a mixture of five different color-singlet states [36]. The dominant color configuration at large distances corresponds to the usual proton-neutron bound state where transverse momenta are of order $\vec{k}^2 \sim 2M_d\epsilon_{BE}$. However, at small impact space separation, all five Fock color-singlet components eventually acquire equal weight, *i.e.*, the deuteron wavefunction evolves to 80% hidden color. At high Q^2 the deuteron form factor is sensitive to wavefunction configurations where all six quarks overlap within an impact separation $b_{\perp i} < \mathcal{O}(1/Q)$. The normalization of the deuteron form factor observed at large Q^2 [101], as well as the presence of two mass scales in the scaling behavior of the reduced deuteron form factor [102] $f_d(Q^2) = F_d(Q^2)/F^2(Q^2/4)$, suggests sizable hidden-color contributions such as $|(uud)_{8_C}(ddu)_{8_C}\rangle$ with probability of order 15% in the deuteron wavefunction [103]. See Fig. 1. Perturbative QCD and conformal symmetry can also be directly applied to exclusive antiproton-deuteron reactions, such as the fixed angle scaling $s^{12}d\sigma/dt(\overline{p}d \to \pi^- p)$ corresponding to

14 participating elementary fields. Such hard-scattering nuclear reactions are sensitive to the minimal six-quark hidden-color Fock states of the deuteron.

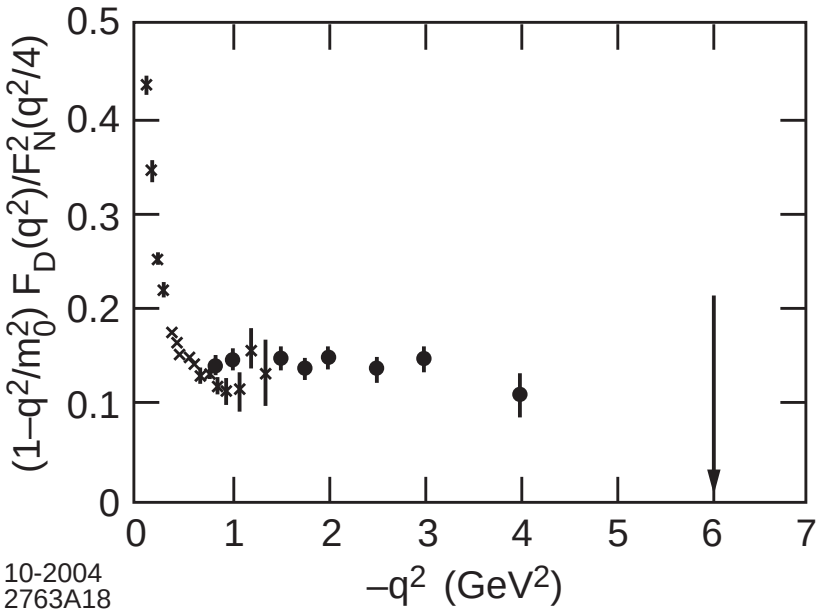

Figure 1: Reduced deuteron form factor testing the scaling predicted by perturbative QCD and conformal scaling. The data show two regimes: a fast-falling behavior at small Q^2 characteristic of normal nuclear binding, and a hard scattering regime with monopole fall-off controlled by the scale $m_0^2 = 0.28$ GeV^2. The latter contribution is attributable to non-nucleonic hidden-color components of the deuteron's six-quark Fock state. From Ref. [102].

14. *Transversity and the Drell-Yan reaction* [104]. The production of massive pairs in anti-proton–proton reactions $p\overline{p} \to \ell^+\ell^- X$ is the ideal prototype of a hard inclusive reaction. In particular, it provides the most direct test of the correlation between transversely-polarized quarks in a transversely polarized proton—via the A_{TT} correlation.

15. *Single-Spin asymmetries in Drell-Yan Processes* [33, 105]. Initial-state interactions between the annihilating antiquark of the $\overline{p}$ and the spectators of the target proton will produce a $T-$odd "Sivers effect" single-spin asymmetry proportional to the correlation $\vec{S}_p \cdot \vec{q} \times \vec{\overline{p}}$. Here S_p is the spin-vector of the target proton. The asymmetry is predicted to be equal but opposite in sign to the corresponding single-spin asymmetry $\vec{S}_p \cdot \vec{q} \times \vec{p}'$ in semi-inclusive $\gamma^* p \to p' X$ deep inelastic scattering. The same initial-state interactions which produce single-spin asymmetries also produce a dramatic $\cos 2\phi$ correlation of the lepton-pair plane and the $\vec{q} \to \vec{\overline{p}}$ plane [106].

16. *Diffractive Drell-Yan reactions.* The reaction $\overline{p}p \to \gamma^* p' X$, where the target nucleon remains intact and has a rapidity gap with the other final state hadrons, provides a novel look at the hard pomeron and its origin. The behavior of the Drell-Yan cross section at large x_F probes the $x \to 1$ behavior of the antiproton structure function. The power behavior is predicted by perturbative QCD counting rules [76, 107] and conformal arguments. In this regime DGLAP evolution is quenched [76] since the annihilating $\overline{q}$ is far off shell: $k^2 \sim -k_\perp^2/(1-x)$.

17. *Higher-Twist Processes.* Leading-twist perturbative QCD predicts a classic $1 + \cos^\theta$ distribution for the lepton angular distribution in the lepton pair rest frame. The data for pion-induced reactions shows significant deviations especially at large x_F for the lepton pair where higher-twist subprocesses such as $\pi q \to \gamma^* q$ are favored [108] and the pion itself enters the hard subprocess. The net result is a $\frac{\sin^2\theta}{Q^2}$ contribution which dominates the cross section at $x_F \to 1$. In the case of antiproton beams, higher-twist processes such as $(\overline{q}\overline{q})q \to \gamma^* \overline{q}$ arise from diquark correlations can be studied in detail in $\overline{p}p \to \gamma^* X$.

18. *Nuclear Antishadowing.* The Drell-Yan reaction $p\overline{A} \to \ell^+\ell^- X$ in nuclear targets provides an important measure of nuclear antishadowing. Recent work has shown that antishadowing is non-universal; it depends on the flavor of the individual quark components of the nuclear wavefunction. The shadowing and antishadowing of nuclear structure functions in the Gribov-Glauber picture is due respectively to the destructive and constructive interference of amplitudes arising from the multiple-scattering of quarks in the nucleus. The effective quark-nucleon scattering amplitude includes Pomeron and Odderon contributions from multi-gluon exchange as well as Reggeon quark-exchange contributions [38]. The coherence of these multiscattering nuclear processes leads to shadowing and antishadowing of the electromagnetic nuclear structure functions in agreement with measurements. Recently, Ivan Schmidt, Jian-Jun Yang, and I [39] have shown that this picture leads to substantially different antishadowing for charged and neutral current reactions, thus affecting the extraction of the weak-mixing angle $\sin^2\theta_W$. We find that part of the anomalous NuTeV result for $\sin^2\theta_W$ could be due to the non-universality of nuclear antishadowing for charged and neutral currents. Detailed measurements of the nuclear dependence of individual quark structure functions, including measurements of the Drell-Yan process in $\overline{p}A$ reactions, are thus needed to establish the distinctive phenomenology of shadowing and antishadowing and to make the NuTeV results definitive.

19. *Heavy Quark Asymmetries.* The binding of the strange quarks in the nucleon produces an asymmetry between the strange and antistrange distributions. This can be tested in the asymmetric production of charmed-strange hadrons. $\overline{p}p \to D_s X$ versus $\overline{p}p \to \overline{D}_s X$ or exclusive $\overline{p} \to D_s \overline{D}_s$ because of the coalescence of

the s or $\overline{s}$ arising from the $\left|\overline{u}\overline{d}\overline{d}\overline{s}s\right\rangle$ Fock state of the projectile antiproton.

20. Search for the Odderon. The interference of odderon and pomeron contributions leads to baryon-antibaryon asymmetries [109]. For example, the asymmetry in the fractional energy of charm versus anticharm or strange versus antistrange jets produced in high energy diffractive photoproduction is sensitive to the interference of the Odderon ($C = -$) and Pomeron ($C = +$) exchange amplitudes in QCD.

21. The Exclusive-Inclusive Connection. The Drell-Yan process provides and interesting arena for testing duality in QCD. In the exclusive limit of small M_X, $\overline{p}p \to \gamma^* X$ will approach the double-resonant regime: $\overline{p}p \to \gamma^* M^*$ where the massive system M^* could be a baryon-antibaryon system, a meson pair or even a single meson.

The following sections in these lectures expand on the physics issues underlying the above tests.

3 QCD on the Light Front

One of the central problems in particle physics is determining the structure of hadrons such as the proton and neutron in terms of their fundamental QCD quark and gluon degrees of freedom. The bound-state structure of hadrons plays a critical role in virtually every area of particle physics phenomenology. For example, in the case of the spacelike and timelike nucleon form factors, pion electroproduction $ep \to e'\pi^+ n$, and timelike Compton scattering $\overline{p}p \to \gamma\gamma$, the cross sections depend not only on the nature of the quark currents, but also on the coupling of the quarks to the initial and final hadronic states. Exclusive decay amplitudes such as $B \to K^*\gamma$, processes which are studied at B factories, depend not only on the underlying weak transitions between the quark flavors, but also the wavefunctions which describe how the B and K^* mesons are assembled in terms of their fundamental quark and gluon constituents. Unlike the leading-twist structure functions measured in deep inelastic scattering, such exclusive channels are sensitive to the structure of the hadrons at the amplitude level and to the coherence between the contributions of the various quark currents and multi-parton amplitudes.

Light-front Fock state wavefunctions $\psi_{n/H}(x_i, \vec{k}_{\perp i}, \lambda_i)$ encode the bound-state quark and gluon properties of hadrons, including their spin and flavor correlations, in the form of universal process- and frame- independent amplitudes. Because the generators of certain Lorentz boosts are kinematical, knowing the LFWFs in one frame allows one to obtain it in any other frame. LFWFs underlie virtually all areas of QCD phenomenology. The hadronic distribution amplitudes which control hard exclusive processes are computed from the valence Fock state LFWFs. Matrix elements of space-like local operators for the coupling of photons, gravitons, and the moments of

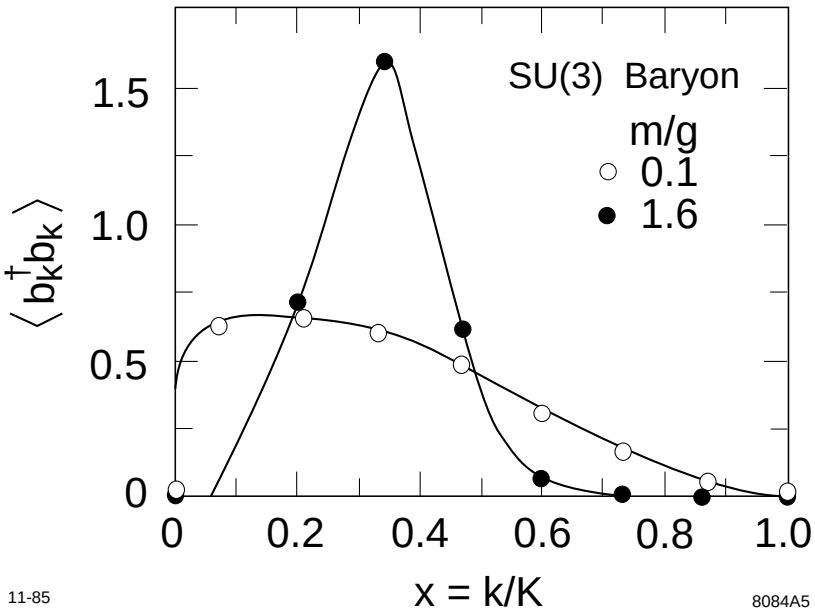

Figure 2: Valence contribution to the baryon structure function in QCD_{1+1}, as a function of the light-cone longitudinal momentum fraction. The gauge group is SU(3), m is the quark mass, and g is the gauge coupling. (From Ref. [18].)

deep inelastic structure functions all can be expressed as overlaps of light-front wavefunctions with the same number of Fock constituents. Similarly, the exclusive decays of heavy hadrons such as the B meson are computed from overlaps of LFWFs. The unintegrated parton distributions and generalized parton distributions measured in deeply virtual Compton scattering can be constructed from LFWFs. Hadronization phenomena such as the coalescence mechanism for leading heavy hadron production are computed from LFWF overlaps. Diffractive jet production provides another phenomenological window into the structure of LFWFs. However, some leading-twist phenomena such as the diffractive component of deep inelastic scattering, single spin asymmetries, nuclear shadowing and antishadowing cannot be computed from the LFWFs of hadrons in isolation.

Formally, the light-front expansion is constructed by quantizing QCD at fixed light-cone time [25] $\tau = t + z/c$ and forming the invariant light-front Hamiltonian: $H_{LF}^{QCD} = P^+P^- - \vec{P}_\perp^2$ where $P^\pm = P^0 \pm P^z$ [20]. The momentum generators P^+ and $\vec{P}_\perp$ are kinematical; *i.e.*, they are independent of the interactions. The generator $P^- = i\frac{d}{d\tau}$ generates light-cone time translations, and the eigen-spectrum of the Lorentz scalar H_{LF}^{QCD} gives the mass spectrum of the color-singlet hadron states in QCD together with their respective light-front wavefunctions. For example, the proton state satisfies $H_{LF}^{QCD} \mid \psi_p\rangle = M_p^2 \mid \psi_p\rangle$. The expansion of the proton eigensolution $\mid \psi_p\rangle$ on the color-singlet $B = 1$, $Q = 1$ eigenstates $\{ \mid n\rangle\}$ of the free Hamiltonian

$H_{LF}^{QCD}(g=0)$ gives the light-front Fock expansion:

$$\Big|\,\psi_p(P^+,\vec{P}_\perp)\Big\rangle = \sum_n \prod_{i=1}^{n} \frac{\mathrm{d}x_i\,\mathrm{d}^2\vec{k}_{\perp i}}{\sqrt{x_i}\,16\pi^3}\,16\pi^3$$
$$\times\,\delta\left(1-\sum_{i=1}^{n}x_i\right)\,\delta^{(2)}\left(\sum_{i=1}^{n}\vec{k}_{\perp i}\right)$$
$$\times\,\psi_{n/H}(x_i,\vec{k}_{\perp i},\lambda_i)\,\Big|\,n;\,x_iP^+,x_i\vec{P}_\perp+\vec{k}_{\perp i},\lambda_i\Big\rangle\,.$$

The light-cone momentum fractions $x_i = k_i^+/P^+$ and $\vec{k}_{\perp i}$ represent the relative momentum coordinates of the QCD constituents. The physical transverse momenta are $\vec{p}_{\perp i} = x_i\vec{P}_\perp + \vec{k}_{\perp i}$. The λ_i label the light-cone spin projections S^z of the quarks and gluons along the quantization direction z. The physical gluon polarization vectors $\epsilon^\mu(k,\ \lambda=\pm1)$ are specified in light-cone gauge by the conditions $k\cdot\epsilon=0,\ \eta\cdot\epsilon=\epsilon^+=0$. Light-front quantization in the doubly-transverse light-cone gauge [110, 111] has a number of advantages, including explicit unitarity, a physical Fock expansion, exact representations of current matrix elements, and the decoupling properties needed to prove factorization theorems in high momentum transfer inclusive and exclusive reactions.

The matrix elements of the light-front Hamiltonian are illustrated in Fig. 3. Light-front four-point instantaneous gluon and quark interactions appear when one eliminates the dependent quark and gluon fields using the QCD equation of motion in light-cone gauge $A^+=0$. This is the analog of the Coulomb interactions which appear in a gauge theory Hamiltonian when quantized in radiation gauge.

The solutions of $H_{LF}^{QCD}\,|\,\psi_p\rangle = M_p^2\,|\,\psi_p\rangle$ are independent of P^+ and $\vec{P}_\perp$; thus given the eigensolution Fock projections $\langle n;x_i,\vec{k}_{\perp i},\lambda_i|\psi_p\rangle = \psi_n(x_i,\vec{k}_{\perp i},\lambda_i)$, the wavefunction of the proton is determined in any frame [76]. In contrast, in equal-time quantization, a Lorentz boost always mixes dynamically with the interactions, so that computing a wavefunction in a new frame requires solving a nonperturbative problem as complicated as the Hamiltonian eigenvalue problem itself. The LFWFs $\psi_{n/H}(x_i,\vec{k}_{\perp i},\lambda_i)$ are properties of the hadron itself; they are thus universal and process independent.

One can also define the light-front Fock expansion using a covariant generalization of light-front time: $\tau = x\cdot\omega$. The four-vector ω, with $\omega^2=0$, determines the orientation of the light-front plane. The freedom to choose ω provides an explicitly covariant formulation of light-front quantization [26]: all observables such as matrix elements of local current operators, form factors, and cross sections are light-front invariants and thus must be independent of ω_μ. In recent work, Dae Sung Hwang, John Hiller, Volodya Karmonov, and I [89] have studied the analytic structure of LFWFs using the explicitly Lorentz-invariant formulation of the front form. Eigensolutions of the Bethe-Salpeter equation have specific angular momentum as specified by the Pauli-Lubanski vector. The corresponding LFWF for an n-particle Fock state evaluated at

Figure 3: Graphical Representation of QCD light-front Hamiltonian interactions in the Light-Front Fock Space. The figure illustrates the matrix elements between Fock states from the three-point and four-point interactions of the theory plus the contributions from instantaneous gluon and quark exchange. From Ref. [20].

equal light-front time $\tau = \omega \cdot x$ can be obtained by integrating the Bethe-Salpeter solutions over the corresponding relative light-front energies. The resulting LFWFs $\psi_n^I(x_i, k_{\perp i})$ are functions of the light-cone momentum fractions $x_i = k_i \cdot \omega / p \cdot \omega$ and the invariant mass squared of the constituents $M_0^2 = (\sum_{i=1}^n k_i^\mu)^2 = \sum_{i=1}^n [\frac{k_\perp^2 + m^2}{x}]_i$, each multiplying spin-vector and polarization tensor invariants which can involve ω^μ. They are eigenstates of the Karmanov–Smirnov kinematic angular momentum operator [112]. Thus LFWFs satisfy all Lorentz symmetries of the front form, including boost invariance, and they are proper eigenstates of angular momentum.

In principle, one can solve for the LFWFs directly from the fundamental theory using methods such as discretized light-front quantization (DLCQ), the transverse lattice, lattice gauge theory moments, or Bethe–Salpeter techniques. DLCQ has been remarkably successful in determining the entire spectrum and corresponding LFWFs in 1+1 field theories, including supersymmetric examples. Reviews of nonperturbative light-front methods may be found in references [20, 26, 113, 114]. One can also project the known solutions of the Bethe–Salpeter equation to equal light-front time, thus producing hadronic light-front Fock wave functions. A potentially important method is to construct the $q\overline{q}$ Green's function using light-front Hamiltonian theory, with DLCQ boundary conditions and Lippmann-Schwinger resummation. The zeros of the resulting resolvent projected on states of specific angular momentum J_z can then generate the meson spectrum and their light-front Fock wavefunctions. The DLCQ properties and boundary conditions allow a truncation of the Fock space while

retaining the kinematic boost and Lorentz invariance of light-front quantization. For a recent review of light-front methods and references, see Ref. [114].

Even without explicit solutions, much is known about the explicit form and structure of LFWFs. They can be matched to nonrelativistic Schrodinger wavefunctions at soft scales. LFWFs at large $k_\perp$ and $x_i \to 1$ are constrained at high momenta by arguments based on conformal symmetry, the operator product expansion, or perturbative QCD. The pattern of higher Fock states with extra gluons is given by ladder relations. The structure of Fock states with nonzero orbital angular momentum is also constrained.

4 Light-Front Wavefunctions and QCD Phenomenology

Given the light-front wavefunctions, one can compute the unintegrated parton distributions in x and $k_\perp$ which underlie generalized parton distributions for nonzero skewness. As shown by Diehl, Hwang, and myself [84], one can give a complete representation of virtual Compton scattering $\gamma^* p \to \gamma p$ at large initial photon virtuality Q^2 and small momentum transfer squared t in terms of the light-cone wavefunctions of the target proton. One can then verify the identities between the skewed parton distributions $H(x,\zeta,t)$ and $E(x,\zeta,t)$ which appear in deeply virtual Compton scattering and the corresponding integrands of the Dirac and Pauli form factors $F_1(t)$ and $F_2(t)$ and the gravitational form factors $A_q(t)$ and $B_q(t)$ for each quark and antiquark constituent. We have illustrated the general formalism for the case of deeply virtual Compton scattering on the quantum fluctuations of a fermion in quantum electrodynamics at one loop.

The integrals of the unintegrated parton distributions over transverse momentum at zero skewness provide the helicity and transversity distributions measurable in polarized deep inelastic experiments [76]. For example, the polarized quark distributions at resolution Λ correspond to

$$
\begin{aligned}
& q_{\lambda_q/\Lambda_p}(x,\Lambda) = \\
& \times \sum_{n,q_a} \int \prod_{j=1}^{n} dx_j d^2k_{\perp j} \sum_{\lambda_i} |\psi^{(\Lambda)}_{n/H}(x_i, \vec{k}_{\perp i}, \lambda_i)|^2 \\
& \times \delta\left(1 - \sum_i^n x_i\right) \delta^{(2)}\left(\sum_i^n \vec{k}_{\perp i}\right) \delta(x - x_q) \\
& \times \delta_{\lambda_a,\lambda_q} \Theta(\Lambda^2 - \mathcal{M}_n^2) \ ,
\end{aligned}
$$

where the sum is over all quarks q_a which match the quantum numbers, light-cone momentum fraction x, and helicity of the struck quark.

As shown by Raufeisen and myself [115], one can construct a "light-front density matrix" from the complete set of light-front wavefunctions which is a Lorentz scalar.

One can also define a light-front partition function Z_{LF} as an outer product of light-front wavefunctions. The deeply virtual Compton amplitude and generalized parton distributions can then be computed as the trace $Tr[Z_{LF}\mathcal{O}]$, where $\mathcal{O}$ is the appropriate local operator [115]. This partition function formalism can be extended to multi-hadronic systems and systems in statistical equilibrium to provide a Lorentz-invariant description of relativistic thermodynamics [115]. This form can be used at finite temperature to give a boost invariant formulation of thermodynamics. At zero temperature the light-front density matrix is directly connected to the Green's function for quark propagation in the hadron as well as deeply virtual Compton scattering. In addition, moments of transversity distributions and off-diagonal helicity convolutions are defined from the density matrix of the light-cone wavefunctions. The light-front wavefunctions also specify the multi-quark and gluon correlations of the hadron. For example, the distribution of spectator particles in the final state which could be measured in the proton fragmentation region in deep inelastic scattering at an electron-proton collider or in the Drell-Yan process $\overline{p}p \to \ell^+\ell^- X$ which can be studied in antiproton collisions at GSI are in principle encoded in the light-front wavefunctions.

Matrix elements of local operators such as spacelike proton form factors can be computed simply from the overlap integrals of light front wave functions in analogy to nonrelativistic Schrödinger theory. Thus given the $\psi^{(\Lambda)}_{n/H}$, one can construct any spacelike electromagnetic, electroweak, or gravitational form factor or local operator product matrix element of a composite or elementary system from the diagonal overlap of the LFWFs [116]. Exclusive semi-leptonic B-decay amplitudes involving timelike currents such as $B \to A\ell\overline{\nu}$ can also be evaluated exactly in the light-front formalism [117]. In this case, the timelike decay matrix elements require the computation of both the diagonal matrix element $n \to n$ where parton number is conserved and the off-diagonal $n+1 \to n-1$ convolution such that the current operator annihilates a $q\overline{q'}$ pair in the initial B wavefunction. This term is a consequence of the fact that the time-like decay $q^2 = (p_\ell + p_{\overline{\nu}})^2 > 0$ requires a positive light-cone momentum fraction $q^+ > 0$. Conversely for space-like currents, one can choose $q^+ = 0$, as in the Drell-Yan-West representation of the space-like electromagnetic form factors.

One can also compute the generalized parton distributions which appear the deeply virtual Compton amplitude (DVCS) in the handbag approximation from overlap of light-front wavefunctions [84, 85]. An interesting aspect of DVCS is the prediction from QCD of a $J = 0$ fixed Regge pole contribution to the real part of the Compton amplitude which has constant energy $s^0 F(t)$ dependence at any momentum transfer t or photon virtuality [118, 119]. This unique contribution is due to the quasi-local coupling of two photons to the quark current coming from the quark Z-graph in time-ordered perturbation theory or, equivalently, the instantaneous quark propagator arising in light-front quantization.

The relationship of QCD processes to the hadron LFWFs is illustrated in Figs. 4 and 5.

Other applications include two-photon exclusive reactions, and diffractive dissociation into jets. The universal light-front wave functions and distribution amplitudes control hard exclusive processes such as form factors, deeply virtual Compton scattering, high momentum transfer photoproduction, and two-photon processes.

The light-front Fock representation thus provides an exact formulation of current matrix elements of local and bi-local operators. In contrast, in equal-time Hamiltonian theory, one must evaluate connected time-ordered diagrams where the gauge particle or graviton couples to particles associated with vacuum fluctuations. Thus even if one knows the equal-time wavefunction for the initial and final hadron, one cannot determine the current matrix elements. In the case of the covariant Bethe-Salpeter formalism, the evaluation of the matrix element of the current requires the calculation of an infinite number of irreducible diagram contributions. One can also prove that the anomalous gravitomagnetic moment $B(0)$ vanishes for any composite system [120]. This property follows directly from the Lorentz boost properties of the light-front Fock representation and holds separately for each Fock state component.

One of the central issues in the analysis of fundamental hadron structure is the presence of non-zero orbital angular momentum in the bound-state wave functions. The evidence for a "spin crisis" in the Ellis-Jaffe sum rule signals a significant orbital contribution in the proton wave function [121, 122]. The Pauli form factor of nucleons is computed from the overlap of LFWFs differing by one unit of orbital angular momentum $\Delta L_z = \pm 1$. Thus the fact that the anomalous moment of the proton is nonzero requires nonzero orbital angular momentum in the proton wavefunction [116]. In the light-front method, orbital angular momentum is treated explicitly; it includes the orbital contributions induced by relativistic effects, such as the spin-orbit effects normally associated with the conventional Dirac spinors.

5 Perturbative QCD and Exclusive Processes

There are a number of fundamental tests of QCD based on exclusive reactions. There has been considerable progress analyzing exclusive and diffractive reactions at large momentum transfer from first principles in QCD. Rigorous statements can be made on the basis of asymptotic freedom and factorization theorems which separate the underlying hard quark and gluon subprocess amplitude from the nonperturbative physics of the hadronic wavefunctions. The leading-power contribution to exclusive hadronic amplitudes such as quarkonium decay, heavy hadron decay, and scattering amplitudes where hadrons are scattered with large momentum transfer can often be factorized as a convolution of distribution amplitudes $\phi_H(x_i, \Lambda)$ and hard-scattering quark/gluon scattering amplitudes T_H integrated over the light-cone momentum fractions of the valence quarks [76]:

$$\mathcal{M}_{\rm Hadron} \;=\; \int \prod \phi_H^{(\Lambda)}(x_i, \lambda_i)\, T_H^{(\Lambda)} dx_i \; . \tag{10}$$

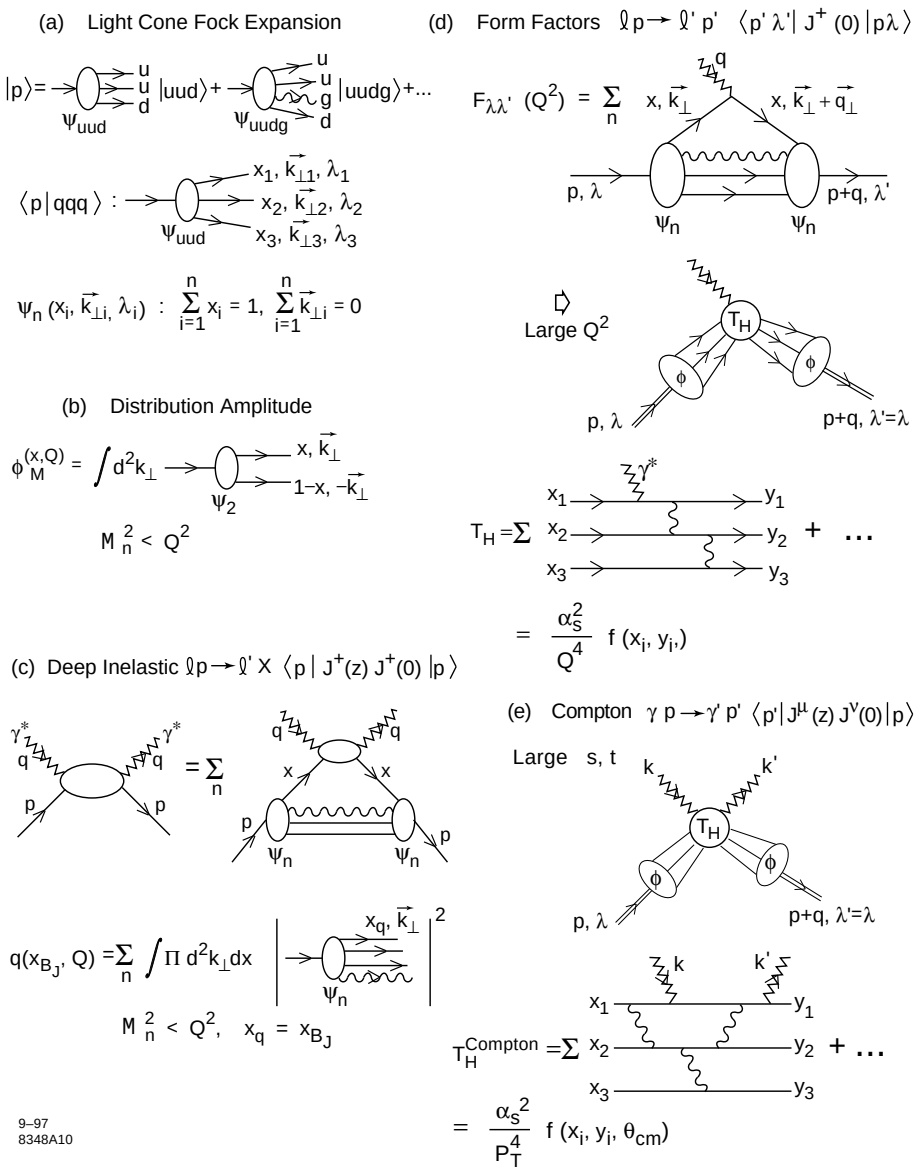

Figure 4: Representation of QCD hadronic processes in the light-cone Fock expansion. (a) The valence uud and higher Fock $uudg$ contributions to the light-cone Fock expansion for the proton. (b) The distribution amplitude $\phi(x,Q)$ of a meson expressed as an integral over its valence light-cone wavefunction restricted to $q\bar{q}$ invariant mass less than Q. (c) Representation of deep inelastic scattering and the quark distributions $q(x,Q)$ as probabilistic measures of the light-cone Fock wavefunctions. The sum is over the Fock states with invariant mass less than Q. (d) Exact representation of spacelike form factors of the proton in the light-cone Fock basis. The sum is over all Fock components. At large momentum transfer the leading-twist contribution factorizes as the product of the hard scattering amplitude T_H for the scattering of the valence quarks collinear with the initial to final direction convoluted with the proton distribution amplitude. (e) Leading-twist factorization of the Compton amplitude at large momentum transfer.

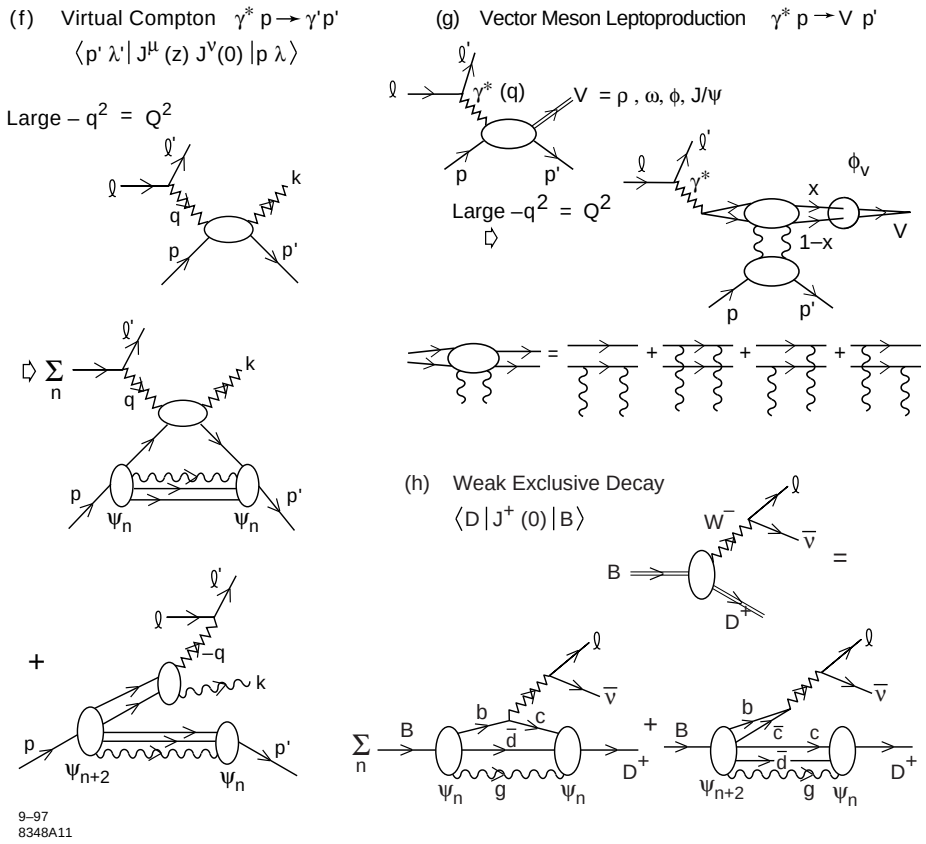

Figure 5: (f) Representation of deeply virtual Compton scattering in the light-cone Fock expansion at leading twist. Both diagonal $n \to n$ and off-diagonal $n+2 \to n$ contributions are required. (g) Diffractive vector meson production at large photon virtuality Q^2 and longitudinal polarization. The high energy behavior involves two gluons in the t channel coupling to the compact color dipole structure of the upper vertex. The bound-state structure of the vector meson enters through its distribution amplitude. (h) Exact representation of the weak semileptonic decays of heavy hadrons in the light-cone Fock expansion. Both diagonal $n \to n$ and off-diagonal pair annihilation $n+2 \to n$ contributions are required.

Here $T_H^{(\Lambda)}$ is the underlying quark-gluon subprocess scattering amplitude in which each incident and final hadron is replaced by valence quarks with collinear momenta $k_i^+ = x_i p_H^+$, $\vec{k}_{\perp i} = x_i \vec{p}_{\perp H}$. The invariant mass of all intermediate states in T_H is evaluated above the separation scale $\mathcal{M}_n^2 > \Lambda^2$. The essential part of the hadronic wavefunction is the distribution amplitude [76], defined as the integral over transverse momenta of the valence (lowest particle number) Fock wavefunction; *e.g.* for the pion

$$\phi_\pi(x_i, Q) \equiv \int d^2k_\perp \, \psi^{(Q)}_{q\bar{q}/\pi}(x_i, \vec{k}_{\perp i}, \lambda) \tag{11}$$

where the separation scale Λ can be taken to be order of the characteristic momentum transfer Q in the process. It should be emphasized that the hard scattering amplitude T_H is evaluated in the QCD perturbative domain where the propagator virtualities are above the separation scale.

The leading power fall-off of the hard scattering amplitude as given by dimensional counting rules follows from the nominal scaling of the hard-scattering amplitude: $T_H \sim 1/Q^{n-4}$, where n is the total number of fields (quarks, leptons, or gauge fields) participating in the hard scattering [44, 75]. Thus the reaction is dominated by subprocesses and Fock states involving the minimum number of interacting fields. In the case of $2 \to 2$ scattering processes, this implies

$$\frac{d\sigma}{dt}(AB \to CD) = F_{AB\to CD}(t/s)/s^{n-2} \tag{12}$$

where $n = N_A + N_B + N_C + N_D$ and n_H is the minimum number of constituents of H.

In the case of form factors, the dominant helicity conserving amplitude has the nominal power-law falloff $F_H(t) \sim (1/t)^{n_H - 1}$, The complete predictions from PQCD modify the nominal scaling by logarithms from the running coupling and the evolution of the distribution amplitudes. In some cases, such as large angle $pp \to pp$ scattering, there can be "pinch" contributions [123] when the scattering can occur from a sequence of independent near-on shell quark-quark scattering amplitudes at the same CM angle. After inclusion of Sudakov suppression form factors, these contributions also have a scaling behavior close to that predicted by constituent counting.

The constituent counting rules were originally derived in 1973 [44, 75] before the development of QCD in anticipation that the underlying theory of hadron physics would be renormalizable and close to a conformal theory. The factorized structure of hard exclusive amplitudes in terms of a convolution of valence hadron wavefunctions times a hard-scattering quark scattering amplitude was also proposed [44]. Upon the discovery of the asymptotic freedom in QCD, there was a systematical development of the theory of hard exclusive reactions, including factorization theorems, counting rules, and evolution equations for the hadronic distribution amplitudes [124, 125, 52, 126].

In a remarkable recent development, Polchinski and Strassler have shown how one can map features of gravitational theories in higher dimensions (AdS_5) to phenomenological properties of physical QCD in ordinary 3+1 space-time [12]. The AdS/CFT

correspondence connecting superstring theory to superconformal gauge theory has important implications for hadron phenomenology in the conformal limit, including an all-orders demonstration of counting rules for hard exclusive processes as well as determining essential aspects of hadronic light-front wavefunctions.

The distribution amplitudes which control leading-twist exclusive amplitudes at high momentum transfer can be related to the gauge-invariant Bethe-Salpeter wavefunction at equal light-cone time $\tau = x^+$. The logarithmic evolution of the hadron distribution amplitudes $\phi_H(x_i, Q)$ with respect to the resolution scale Q can be derived from the perturbatively-computable tail of the valence light-cone wavefunction in the high transverse momentum regime. The DGLAP evolution of quark and gluon distributions can also be derived in an analogous way by computing the variation of the Fock expansion with respect to the separation scale. Other key features of the perturbative QCD analyses are: (a) evolution equations for distribution amplitudes which incorporate the operator product expansion, renormalization group invariance, and conformal symmetry [76, 48, 127, 128, 59]; (b) hadron helicity conservation which follows from the underlying chiral structure of QCD [79]; (c) color transparency, which eliminates corrections to hard exclusive amplitudes from initial and final state interactions at leading power and reflects the underlying gauge theoretic basis for the strong interactions [37] and (d) hidden color degrees of freedom in nuclear wavefunctions, which reflect the color structure of hadron and nuclear wavefunctions [36]. There have also been recent advances eliminating renormalization scale ambiguities in hard-scattering amplitudes via commensurate scale relations [54] which connect the couplings entering exclusive amplitudes to the α_V coupling which controls the QCD heavy quark potential.

Exclusive processes such as $\overline{p}p \to \overline{p}p$, $\overline{p}p \to K^+K^-$ and $\overline{p}p \to \gamma\gamma$ provide a unique window for viewing QCD processes and hadron dynamics at the amplitude level [81, 53]. New tests of theory and comprehensive measurements of hard exclusive amplitudes can also be carried out for electroproduction at Jefferson Laboratory and in two-photon collisions at CLEO, Belle, and BaBar [82]. Hadronic exclusive processes are closely related to exclusive hadronic B decays, processes which are essential for determining the CKM phases and the physics of CP violation. The universal light-front wavefunctions which control hard exclusive processes such as form factors, deeply virtual Compton scattering, high momentum transfer photoproduction, and two-photon processes, are also required for computing exclusive heavy hadron decays [129, 130, 131, 132], such as $B \to K\pi$, $B \to \ell\nu\pi$, and $B \to Kp\overline{p}$ [133]. The same physics issues, including color transparency, hadron helicity rules, and the question of dominance of leading-twist perturbative QCD mechanisms enter in both realms of physics.

6 The Pion Form Factor

The pion spacelike form factor provides an important illustration of the perturbative QCD formalism. The proof of factorization begins with the exact Drell-Yan-West representation [134, 135, 116] of the current in terms of the light-cone Fock wavefunctions (see Section 7.) The integration over the momenta of the constituents of each wavefunction can be divided into two domains $\mathcal{M}_n^2 < \Lambda^2$ and $\mathcal{M}_n^2 > \Lambda^2$, where $\mathcal{M}_n^2$ is the invariant mass of the n-particle state. Λ plays the role of a separation scale. In practice, it can be taken to be of order of the momentum transfer.

Consider the contribution of the two-particle Fock state. The argument of the final state pion wavefunction is $k_\perp + (1-x)q_\perp$. First take $k_\perp$ small. At high momentum transfer where

$$\mathcal{M}^2 \sim \frac{(1-x)^2 q_\perp^2}{x(1-x)} = \frac{Q^2(1-x)}{x} > \Lambda^2, \tag{13}$$

one can iterate the equation of motion for the valence light-front wavefunction using the one gluon exchange kernel. Including all of the hard scattering domains, one can organize the result into the factorized form:

$$F_\pi(Q^2) = \int_0^1 dx \int_0^1 dy \phi_\pi(y,\Lambda) T_H(x,y,Q^2) \phi_\pi(x,\Lambda), \tag{14}$$

where T_H is the hard-scattering amplitude $\gamma^*(q\overline{q}) \to (q\overline{q})$ for the production of the valence quarks nearly collinear with each meson, and $\phi_M(x,\Lambda)$ is the distribution amplitude for finding the valence q and $\overline{q}$ with light-cone fractions of the meson's momentum, integrated over invariant mass up to Λ. The process independent distribution amplitudes contain the soft physics intrinsic to the nonperturbative structure of the hadrons. Note that T_H is non-zero only if $\frac{(1-x)Q^2}{x} > \Lambda^2$ and $\frac{(1-y)Q^2}{y} > \Lambda^2$. In this hard-scattering domain, the transverse momenta in the formula for T_H can be ignored at leading power, so that the structure of the process has the form of hard scattering on collinear quark and gluon constituents: $T_H(x,y,Q^2) = \frac{16\pi C_F \alpha_s(Q^{*2})}{(1-x)(1-y)Q^2}\,(1+\mathcal{O}(\alpha_s))$ and thus [124, 125, 52, 76, 126, 136, 137, 138, 139]

$$F_\pi(Q^2) = \frac{16\pi C_F \alpha_s(Q^{*2})}{Q^2} \int_0^{\widehat{x}} dx \frac{\phi_\pi(x,\Lambda)}{(1-x)} \int_0^{\widehat{y}} dy \frac{\phi_\pi(y,\Lambda)}{(1-y)}, \tag{15}$$

to leading order in $\alpha_s(Q^{*2})$ and leading power in $1/Q$. Here $C_F = 4/3$ and Q^* can be taken as the BLM scale [140]. The endpoint regions of integration $1-x < \frac{\Lambda^2}{Q^2} = 1-\widehat{x}$ and $1-y < \frac{\Lambda^2}{Q^2} = 1-\widehat{y}$ are to be explicitly excluded in the leading-twist formula. However, since the integrals over x and y are convergent, one can formally extend the integration range to $0 < x < 1$ and $0 < y < 1$ with an error of higher twist. This is only done for convenience; the actual domain only encompasses the off-shell regime. The contribution from the endpoint regions of integration, $x \sim 1$ and $y \sim 1$, are power-law and Sudakov suppressed and thus contribute corrections at higher order

in $1/Q$ [125, 52, 76]. The contributions from non-valence Fock states and corrections from fixed transverse momentum entering the hard subprocess amplitude are higher twist, *i.e.*, power-law suppressed. Loop corrections involving hard momenta give next-to-leading-order (NLO) corrections in α_s.

It is sometimes assumed that higher twist terms in the LC wave function, such as those with $L_z \neq 0$, have flat distributions at the $x \to 0, 1$ endpoints. This is difficult to justify since it would correspond to bound state wavefunctions which fall-off in transverse momentum but have no fall-off at large k_z. After evolution to $Q^2 \to \infty$, higher twist distributions can evolve eventually to constant behavior at $x = 0, 1$; however, the wavefunctions are in practice only being probed at moderate scales. In fact, if the higher twist terms are evaluated in the soft domain, then there is no evolution at all. A recent analysis by Beneke [141] indicates that the $1/Q^4$ contribution to the pion form factor is only logarithmically enhanced even if the twist-3 term is flat at the endpoints. It is also possible that contributions from the twist three $q\bar{q}g$ light-front wavefunctions may well cancel even this enhancement.

Thus perturbative QCD can unambiguously predict the leading-twist behavior of exclusive amplitudes. These contributions only involve the truncated integration domain of x and $k_\perp$ momenta where the quark and gluon propagators and couplings are perturbative; by definition the soft regime is excluded. The central question is then whether the PQCD leading-twist prediction can account for the observed leading power-law fall-off of the form factors and other exclusive processes. Assuming the pion distribution amplitude is close to its asymptotic form, one can predict the normalization of exclusive amplitudes such as the spacelike pion form factor $Q^2 F_\pi(Q^2)$. Next-to-leading order predictions are available which incorporate higher order corrections to the pion distribution amplitude as well as the hard scattering amplitude [127, 142, 143, 144]. The natural renormalization scheme for the QCD coupling in hard exclusive processes is $\alpha_V(Q)$, the effective charge defined from the scattering of two infinitely-heavy quark test charges. Assuming $\alpha_V(Q^*) \simeq 0.4$ at the BLM scale Q^*, the QCD LO prediction appears to be smaller by approximately a factor of 2 compared to the presently available data extracted from pion electroproduction experiments [140]. However, the extrapolation from spacelike t to the pion pole in electroproduction may be unreliable in the same sense that lattice gauge theory extrapolations to $m_\pi^2 \to 0$ are known to be nonanalytic. Thus it is not clear that there is an actual discrepancy between perturbative QCD and experiment. It would be interesting to develop predictions for the transition form factor $F_{q\bar{q}\to\pi}(t, q^2)$ which is in effect what is measured in electroproduction.

It is interesting to compare the calculation of a meson form factor in QCD with the calculation of the form factor of a bound state in QED. The analog to a soft wavefunction is the Schrödinger-Coulomb solution $\psi_{1s}(\vec{k}) \propto (1 + \vec{p}^2/(\alpha m_{\rm red})^2)^{-2}$, and the full wavefunction, which incorporates transversely polarized photon exchange, differs by a factor $(1 + \vec{p}^2/m_{\rm red}^2)$. Thus the leading-twist dominance of form factors in QED occurs at relativistic scales $Q^2 > m_{\rm red}^2$ [53].

7 Perturbative QCD Calculation of Baryon Form Factors

The baryon form factor at large momentum transfer provides another important example of the application of perturbative QCD to exclusive processes. Away from possible special points in the x_i integrations (which are suppressed by Sudakov form factors) baryon form factors can be written to leading order in $1/Q^2$ as a convolution of the connected hard-scattering amplitude T_H with the baryon distribution amplitudes. An example of a perturbative QCD contribution to F_2 is illustrated in Fig. 6 The Q^2-evolution of the baryon distribution amplitude can be derived from the operator product expansion of three quark fields or from the gluon exchange kernel. Taking into account the evolution of the baryon distribution amplitude, the nucleon magnetic form factors at large Q^2, has the form [76, 52, 79]

$$G_M(Q^2) \to \frac{\alpha_s^2(Q^2)}{Q^4} \sum_{n,m} b_{nm} \left(\log \frac{Q^2}{\Lambda^2}\right)^{\gamma_n^B + \gamma_n^B} \left[1 + \mathcal{O}\left(\alpha_s(Q^2), \frac{m^2}{Q^2}\right)\right] \quad . \tag{16}$$

where the γ_n^B are computable anomalous dimensions [145] of the baryon three-quark wave function at short distance, and the b_{mn} are determined from the value of the distribution amplitude $\phi_B(x, Q_0^2)$ at a given point Q_0^2 and the normalization of T_H. Asymptotically, the dominant term has the minimum anomalous dimension. The contribution from the endpoint regions of integration, $x \sim 1$ and $y \sim 1$, at finite $k_\perp$ is Sudakov suppressed [125, 52, 76]; however, the endpoint region may play a significant role in phenomenology.

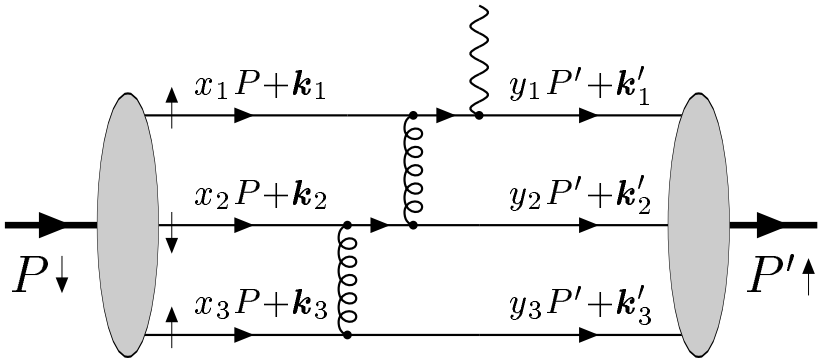

Figure 6: A typical leading QCD diagram contributing to the nucleon form factors. From Ref. [88] .

The proton form factor appears to scale at $Q^2 > 5$ GeV^2 according to the PQCD predictions. See Fig. 7. Nucleon form factors are approximately described phenomenologically by the well-known dipole form $G_M(Q^2) \simeq 1/(1 + Q^2/0.71 \text{ GeV}^2)^2$ which behaves asymptotically as $G_M(Q^2) \simeq (1/Q^4)(1 - 1.42 \text{ GeV}^2/Q^2 + \cdots)$. This

suggests that the corrections to leading twist in the proton form factor and similar exclusive processes involving protons become important in the range $Q^2 < 1.4$ GeV^2.

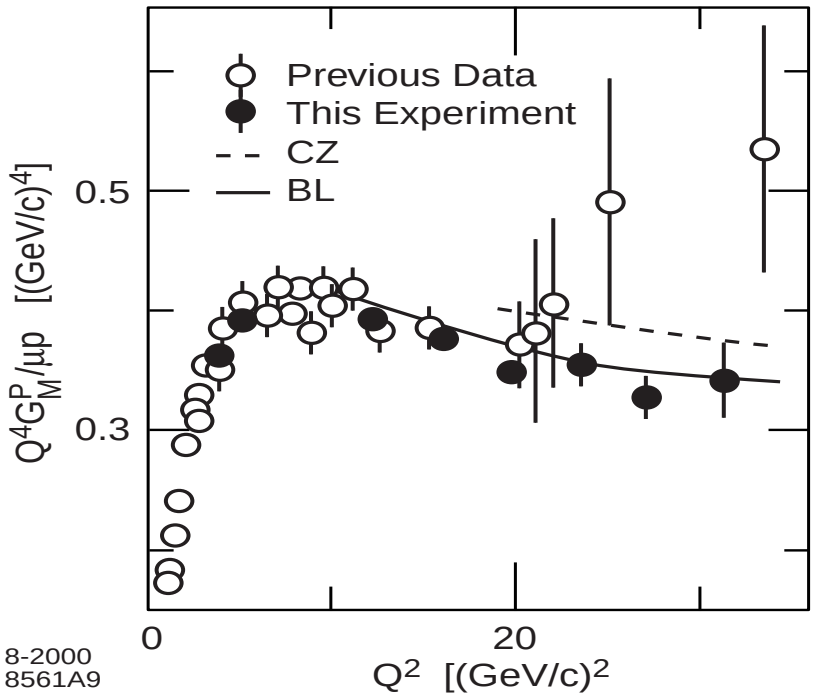

Figure 7: Predictions for the normalization and sign of the proton form factor at high Q^2 using perturbative QCD factorization and QCD sum rule predictions for the proton distribution amplitude (From Ji *et al.* [146]) The curve labelled BL has arbitrary normalization and incorporates the fall-off of two powers of the running coupling. The dotted line is the QCD sum rule prediction of given by Chernyak and Zhitnitsky [147, 148]. The results are similar for the model distribution amplitudes of King and Sachrajda [153], and Gari and Stefanis [154].

The shape of the distribution amplitude controls the normalization of the leading-twist prediction for the proton form factor. If one assumes that the proton distribution amplitude has the asymptotic form: $\phi_N = Cx_1x_2x_3$, then the convolution with the leading order form for T_H gives zero! If one takes a non-relativistic form peaked at $x_i = 1/3$, the sign is negative, requiring a crossing point zero in the form factor at some finite Q^2. The broad asymmetric distribution amplitude advocated by Chernyak and Zhitnitsky [147, 148] gives a more satisfactory result. If one assumes a constant value of $\alpha_s = 0.3$, and $f_N = 5.3 \times 10^{-3}$GeV^2, the leading order prediction is below the data by a factor of ≈ 3. However, since the form factor is proportional to $\alpha_s^2 f_N^2$, one can obtain agreement with experiment by a simple renormalization of the parameters. For example, if one uses the central value of Ioffe's determination $f_N = 8 \times 10^{-3}$GeV^2, then good agreement is obtained [149]. The normalization of

the proton distribution amplitude is also important for estimating the proton decay rate [150]. The most recent lattice results [151] suggest a significantly larger normalization for the required proton matrix elements, 3 to 5 times larger than earlier phenomenological estimates. One can also use PQCD to predict ratios of various baryon and isobar form factors assuming isospin or $SU(3)$-flavor symmetry for the basic wave function structure. Results for the neutral weak and charged weak form factors assuming standard $SU(2) \times U(1)$ symmetry can also be derived [152].

A useful technique for obtaining the solutions to the baryon evolution equations is to construct completely antisymmetric representations as a polynomial orthonormal basis for the distribution amplitude of multi-quark bound states. In this way. one obtains a distinctive classification of nucleon (N) and Delta (Δ) wave functions and the corresponding Q^2 dependence which discriminates N and Δ form factors. Braun and collaborators have shown how one can use conformal symmetry to classify the eigensolutions of the baryon distribution amplitude [59]. They identify a new 'hidden' quantum number which distinguishes components in the $\lambda = 3/2$ distribution amplitudes with different scale dependence. They are able to find analytic solutions of the evolution equation for $\lambda = 3/2$ and $\lambda = 1/2$ baryons where the two lowest anomalous dimensions for the $\lambda = 1/2$ operators (one for each parity) are separated from the rest of the spectrum by a finite 'mass gap'. These special states can be interpreted as baryons with scalar diquarks. Their results may support Carlson's solution [155] to the puzzle that the proton to Δ form factor falls faster [156] than other $p \to N^*$ amplitudes if the Δ distribution amplitude has a symmetric $x_1 x_2 x_3$ form.

In a remarkable development, Pobylitsa *et al.* [157] have shown how to compute transition form factors linking the proton to nucleon-pion states which have minimal invariant mass W. A new soft pion theorem for high momentum transfers allows one to compute the three quark distribution amplitudes for the near threshold pion states from a chiral rotation. The new soft pion results are in a good agreement with the SLAC electroproduction data for $W^2 < 1.4$ GeV^2 and $7 < Q^2 < 30.7$ GeV^2. This approach can be tested in antiproton collisions in reactions such as $\overline{p}p \to \overline{p}p\pi^0$ where the proton and pion have small invariant mass.

8 Timelike Proton Form Factors

The form factors of hadrons as measured in both the spacelike and timelike domains provide fundamental information on the structure and internal dynamics of hadrons. Recent measurements [158] of the electron-to-proton polarization transfer in $\overrightarrow{e}^- p \to e^- \overrightarrow{p}$ scattering at Jefferson Laboratory show that the ratio of Sachs form factors [159] $G_E^p(q^2)/G_M^p(q^2)$ is monotonically decreasing with increasing $Q^2 = -q^2$, in strong contradiction with the G_E/G_M scaling determined by the traditional Rosenbluth separation method. Recently, Afanasev, Carlson, Chen, Vanderhaeghen, and I [91] have shown that the interfering two-photon exchange contribution to elastic electron-proton scattering, including inelastic intermediate states, can account for

the discrepancy between Rosenbluth and Jefferson Lab spin transfer polarization data [90]. The Rosenbluth method thus in fact is not reliable because of its sensitivity to the two-photon exchange amplitudes [160, 161]. The polarization transfer method [158, 162] is relatively insensitive to such corrections.

The same data which indicate that G_E for protons falls faster than G_M at large spacelike Q^2 require in turn that F_2/F_1 falls more slowly than $1/Q^2$. The conventional expectation from dimensional counting rules [44] and perturbative QCD [125] is that the Dirac form factor F_1 should fall with a nominal power $1/Q^4$, and the ratio of the Pauli and Dirac form factors, F_2/F_1, should fall like $1/Q^2$, at high momentum transfers. The Dirac form factor agrees with this expectation in the range Q^2 from a few GeV^2 to the data limit of 31 GeV^2. However, the Pauli/Dirac ratio is not observed to fall with the nominal expected power, and the experimenters themselves have noted that the data is well fit by $F_2/F_1 \propto 1/Q$ in the momentum transfer range 2 to 5.6 GeV^2.

The new Jefferson Laboratory results make it critical to carefully identify and separate the timelike G_E and G_M form factors by measuring the center-of-mass angular distribution and by measuring the polarization of the proton in $e^+e^- \to p\overline{p}$ or $\overline{p}p \to \ell^+\ell^-$ reactions. The advent of high luminosity e^+e^- colliders at Beijing, Cornell, and Frascati provide the opportunity to make such measurements, both directly and via radiative return. The new GSI antiproton facility with a polarized target will make measurements of the single spin-dependence of $\overline{p}p \to \ell^+\ell^-$ feasible.

Although the spacelike form factors of a stable hadron are real, the timelike form factors have a phase structure reflecting the final-state interactions of the outgoing hadrons. In general, form factors are analytic functions $F_i(q^2)$ with a discontinuity for timelike momentum above the physical threshold $q^2 > 4M^2$. The analytic structure and phases of the form factors in the timelike regime are thus connected by dispersion relations to the spacelike regime [163, 164, 165]. The analytic form and phases of the timelike amplitudes are also sensitive to the resonances in the unphysical region $0 < q^2 < 4M^2$ below the physical threshold [163] in the $J^{PC} = 1^{--}$ channel, including gluonium states and di-baryon structures.

At very large center-of-mass energies, perturbative QCD factorization predicts diminished final interactions in $e^+e^- \to H\overline{H}$, since the hadrons are initially produced with small color dipole moments. This principle of QCD color transparency [166] is also an essential feature [167] of hard exclusive B decays [168, 130], and thus needs to be tested experimentally.

There have been a number of explanations and theoretically motivated fits of the F_2/F_1 data. Belitsky, Ji, and Yuan [169] have shown that factors of $\log(Q^2)$ arise from a careful QCD analysis of the form factors. The perturbative QCD form $Q^2F_2/F_1 \sim \log^2 Q^2$, which has logarithmic factors multiplying the nominal power-law behavior, fits the large-Q^2 spacelike data well. See Fig. 8. Others [170, 171] claim to find mechanisms that modify the traditionally expected power-law behavior with fractional powers of Q^2, and they also give fits which are in accord with the data in

the experimental range. Asymptotic behaviors of the ratio F_2/F_1 for general light-front wave functions are investigated in [89]. Each of the model forms predicts a specific fall-off and phase structure of the form factors from $s \leftrightarrow t$ crossing to the timelike domain. A fit with the dipole polynomial or nominal dimensional counting rule behavior would predict no phases in the timelike regime.

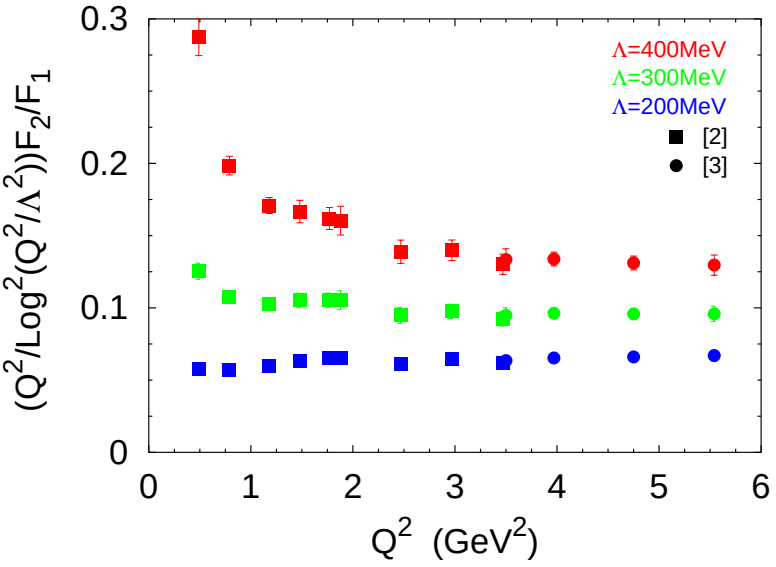

Figure 8: JLab data plotted in terms of the leading PQCD scaling. The lower, middle, and upper data points correspond to $\Lambda = 200, 300, 400$, respectively. From Ref. [88].

9 Single-Spin Asymmetry and the Phase of Timelike Form Factors

As noted by Dubnickova, Dubnicka, and Rekalo, and by Rock [172], the existence of the $T-$odd single-spin asymmetry normal to the scattering plane in baryon pair production $e^-e^+ \to B\overline{B}$ requires a nonzero phase difference between the G_E and G_M form factors. The phase of the ratio of form factors G_E/G_M of spin-1/2 baryons in the timelike region can thus be determined from measurements of the polarization of one of the produced baryons. As discussed below, Carlson, Hiller, Hwang and I have shown that measurements of the proton polarization in $e^+e^- \to p\overline{p}$ strongly discriminate between the analytic forms of models which have been suggested to fit the proton G_E/G_M data in the spacelike region [92].

The center-of-mass angular distribution provides the analog of the Rosenbluth method for measuring the magnitudes of various helicity amplitudes. The differential cross section for $e^-e^+ \to B\overline{B}$ when B is a spin-1/2 baryon is given in the center-of-

mass frame by

$$\frac{d\sigma}{d\Omega} = \frac{\alpha^2\beta}{4q^2}\ D\ , \tag{17}$$

where $\beta = \sqrt{1-4m_B^2/q^2}$ and D is given by

$$D = |G_M|^2\left(1+\cos^2\theta\right) + \frac{1}{\tau}\,|G_E|^2\sin^2\theta\ ; \tag{18}$$

where

$$\begin{aligned} G_M &= F_1 + F_2\ , \\ G_E &= F_1 + \tau F_2\ , \end{aligned} \tag{19}$$

and $\tau \equiv q^2/4m_B^2 > 1$.

The complex phases of the form factors in the timelike region make it possible for a single outgoing baryon to be polarized in $e^-e^+ \to B\overline{B}$ even without polarization in the initial state. The corresponding effect in the initial state produces a polarization correlation in $\overline{p}p \to \ell^+\ell^-$. This correlation can be measured at GSI if the target or beam baryon is polarized.

There are three polarization observables, corresponding to polarizations in three directions, called longitudinal, sideways, and normal but often denoted z, x, and y, respectively. Longitudinal (z) when discussing the final state means parallel to the direction of the outgoing or in going baryon. Sideways (x) means perpendicular to the direction of the baryon but in the scattering plane. Normal (y) means normal to the scattering plane, in the direction of $\vec{k}\times\vec{p}$ where $\vec{k}$ is the electron momentum and $\vec{p}$ is the baryon momentum, with x, y, and z forming a right-handed coordinate system. The polarization $\mathcal{P}_y$ does not require polarization of a lepton and is [172]

$$\mathcal{P}_y = \frac{\sin 2\theta\,\mathrm{Im}G_E^*G_M}{D\sqrt{\tau}} = \frac{(\tau-1)\sin 2\theta\,\mathrm{Im}F_2^*F_1}{D\sqrt{\tau}}\ . \tag{20}$$

The other two polarizations require measurement of the lepton polarization and are discussed in detail in Ref. [92]. Any model which fits the spacelike form factor data with an analytic function can be continued to the timelike region. Spacelike form factors are usually written in terms of $Q^2 = -q^2$. The correct relation for analytic continuation can be obtained by examining denominators in loop calculations in perturbation theory. The connection is $Q^2 \to q^2e^{-i\pi}$, or

$$\ln Q^2 = \ln(-q^2) \to \ln q^2 - i\pi\ . \tag{21}$$

If the spacelike F_2/F_1 is fit by a rational function of Q^2, then the form factors will be relatively real in the timelike region also. However, one in general gets a complex result from the continuation.

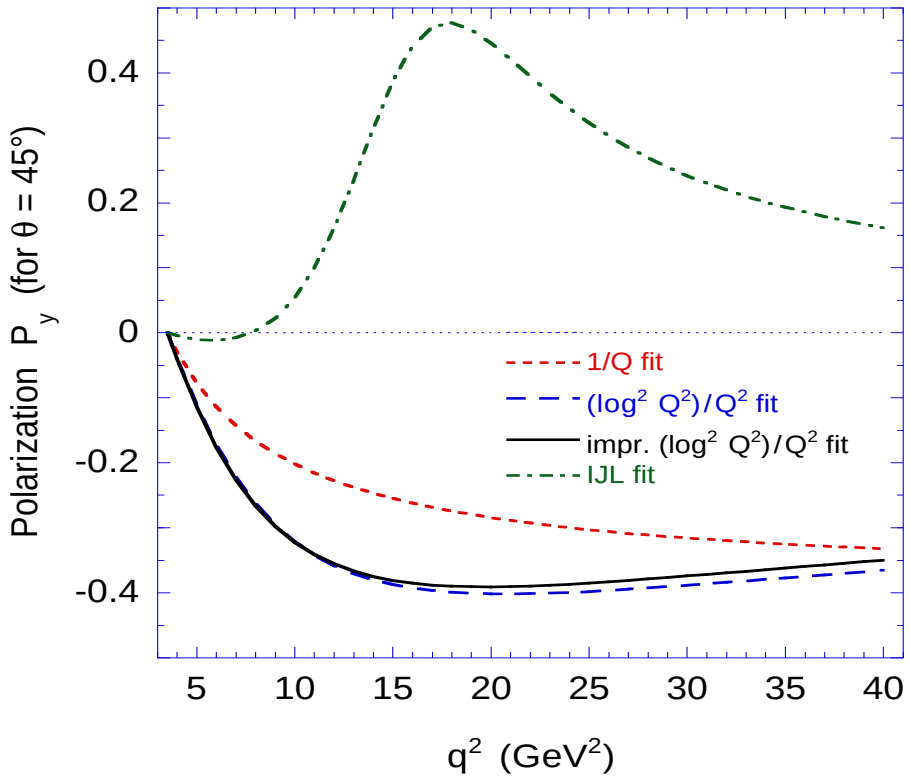

Figure 9: Predicted polarization $\mathcal{P}_y$ in the timelike region for selected form factor fits described in the text. The plot is for $\theta = 45°$. The four curves are for an $F_2/F_1 \propto 1/Q$ fit; the $(\log^2 Q^2)/Q^2$ fit of Belitsky *et al.* [88]; an improved $(\log^2 Q^2)/Q^2$ fit; and a fit from Iachello *et al.* [173].

More sophisticated dispersion relation based continuations could give more reliable results, if there is data also in the timelike region to pin down the magnitudes there. So far, this is possible for the magnetic form factor alone [163], but not for both form factors.

The expression for polarization $\mathcal{P}_y$, Eq. (20), leads to results shown in Fig. 9. The polarizations are shown for four different fits to the spacelike data as referenced in the figure. The value of $\mathcal{P}_y$ should be the same for $e^+e^- \to p\overline{p}$ and $\overline{p}p \to \ell^+\ell^-$ up to an overall sign. The predicted polarizations are not small. Note that a purely polynomial fit to the spacelike data gives zero $\mathcal{P}_y$. The normal polarization $\mathcal{P}_y$ is a single-spin asymmetry and requires a phase difference between G_E and G_M. It is an example of how time-reversal-odd observables can be nonzero if final-state or initial-state interactions give interfering amplitudes different phases. Its analog in the spacelike case is zero.

10 Compton Scattering

Compton scattering is a key test of the perturbative QCD approach [174, 175, 83]. A detailed recalculation of the helicity amplitudes and differential cross section for proton Compton scattering at fixed angle has been carried out recently by Brooks and Dixon [83] at leading-twist and at leading order in α_s. They use contour deformations to evaluate the singular integrals in the light-cone momentum fractions arising from pinch contributions. The shapes and scaling behavior predicted by perturbative QCD agree well with the existing data [176]. In order to reduce uncertainties associated with α_s and the three-quark wave function normalization, Brooks and Dixon have normalized the Compton cross section using the proton elastic form factor. The theoretical predictions for the ratio of Compton scattering to electron-proton scattering is about an order of magnitude below existing experimental data. However, this discrepancy of a factor of 3 in the relative normalization of the amplitudes could be attributed to the fact that the number of diagrams contributing to the Compton amplitude at next-to-leading order (α_s^3) is much larger in Compton scattering compared to the proton form factor.

The Compton amplitude is predicted to have a real Regge contribution [118, 119]

$$M(\gamma p \to \gamma' p') = -2\epsilon \cdot \epsilon' \sum_q e_q^2 F_0(t) \tag{22}$$

which is constant in energy for any t. Thus unlike ordinary Regge exchange in which the Regge power varies with t, the $J = 0$ term is independent of t as well photon virtualities q_1^2, q_2^2 at fixed t. The spin-zero form factor $F_0^q(t)$ is the $1/x_q$ matrix element of the proton

$$F_0^q(t) = \left\langle p' \left| \frac{1}{x_q} \right| p \right\rangle \tag{23}$$

evaluated at spacelike momentum transfer $t = (p - p')^2$. This $C = +$ form factor is a new object: it is relevant to the non-spin-flip Higgs coupling to the proton. At large t, it falls as $\sim 1/t^2$. A similar Pauli-like contribution also enters the spin-flip Compton amplitude. This contribution can be observed in timelike DVCS: $\overline{p}p \to \gamma\gamma^*$ from its distinctive kinematic properties: the amplitude from the $J = 0$ term is independent of t at fixed s, independent of photon virtuality at fixed s.

In the case of QED with scalar leptons, the fixed-pole contribution to the Compton amplitude is due to the 4-point seagull interaction. In QCD it arises from the quark Z-graphs; in the LF-quantized theory, it comes from the quasi-local instantaneous quark exchange interaction for $\gamma q \to \gamma q$. It is analogous to Thompson scattering on the electrons of an atom:

$$M(\gamma A \to \gamma' A') = -2\sum e^2 \frac{M_A}{m_e} \epsilon \cdot \epsilon'. \tag{24}$$

In the case of hadrons in QCD $\left\langle \frac{1}{x_q} \right\rangle$ plays the role of $\frac{M_A}{m_e}$. The moment $\left\langle \frac{1}{x_q} \right\rangle$ is particularly interesting since, using the Feynman-Hellmann theorem at $t = 0$, it is precisely

the expression for the change in proton mass in the light-cone kinetic energy as one varies a given quark mass [177]:

$$\frac{\partial M_p^2}{\partial m_q^2} = \left\langle \frac{1}{x_q} \right\rangle . \tag{25}$$

The $J = 0$ contribution can be isolated in various ways. Damashek and Gilman found a signal in forward high energy Compton scattering using analyticity and the optical theorem [178]. They found that the phenomenological value for the $J = 0$ term in the forward Compton amplitude was surprisingly close to the value $\sum_q e_q^2 F_0^q(t) = 1$, the same result that one has from Thompson scattering on an elementary proton. Its role in large t real Compton scattering was studied in Ref. [118].

The $J = 0$ term also plays an important role in recent work [91] correcting Rosenbluth from two-photon exchange because it has a real phase and a π^2 enhancement.

A debate has continued on whether processes such as the pion and proton form factors and elastic Compton scattering $\gamma p \to \gamma p$ might be dominated by higher twist mechanisms until very large momentum transfers [179, 180, 181, 182, 183]. For example, if one assumes that the light-cone wavefunction of the pion has the form $\psi_{\rm soft}(x, k_\perp) = A \exp\left(-b \frac{k_\perp^2}{x(1-x)}\right)$, then the Feynman endpoint contribution to the overlap integral at small $k_\perp$ and $x \simeq 1$ will dominate the form factor compared to the hard-scattering contribution until very large Q^2. However, this form for $\psi_{\rm soft}(x, k_\perp)$ does not fall-off at all for $k_\perp = 0$ and $k_z \to -\infty$. A soft QCD wavefunction would be expected to be exponentially suppressed in this regime, as in the BHL model $\psi_n^{\rm soft}(x_i, k_{\perp i}) = A \exp\left(-b \sum_i^n [\frac{\vec{k}_\perp^2 + m^2}{x}]_i\right)$ [184]. The endpoint contributions are also suppressed by a QCD Sudakov form factor [185], reflecting the fact that a near-on-shell quark must radiate if it absorbs large momentum. If the endpoint contribution dominates proton Compton scattering, then both photons will interact on the same quark line in a local fashion and the amplitude is real, in strong contrast to the QCD predictions which have a complex phase structure. The perturbative QCD predictions [174, 175, 83] for the Compton amplitude phase can be tested in virtual Compton scattering by interference with Bethe-Heitler processes [86].

The "handbag" approximation to Compton scattering [182, 183] has been applied to $\gamma\gamma \to p\overline{p}$ and $\overline{p}p \to \gamma\gamma$ reactions at large energy [186]. In this case, one assumes that the process occurs via the exchange of a diquark with light-cone momentum fraction $x \sim 0$, so that the hard subprocess is $\overline{q}q \to \gamma\gamma$ where nearly on-shell quarks annihilate with the full energy of the baryons. The critical question is whether the proton wavefunction has significant support when the massive diquark has zero light-front momentum fraction, since the diquark light-cone kinetic energy and the bound state wavefunction become far-off shell $k_F^2 \sim -(m^2 + k_\perp^2)/x \to -\infty$ in this domain.

Measurements of timelike Compton scattering in $\gamma\gamma \to p\overline{p}$ and $\overline{p}p \to \gamma\gamma$ at large s and t are thus critical for settling these issues.

11 Hadron Helicity Conservation

Hadron helicity conservation (HHC) is a QCD selection rule concerning the behavior of helicity amplitudes at high momentum transfer, such as fixed CM scattering. Since the convolution of T_H with the light-cone wavefunctions projects out states with $L_z = 0$, the leading hadron amplitudes conserve hadron helicity [79, 187]. Thus the dominant amplitudes are those in which the sum of hadron helicities in the initial state equals the sum of hadron helicities in the final state; other helicity amplitudes are relatively suppressed by an inverse power in the momentum transfer.

In the case of electron-proton scattering, hadron helicity conservation states that the proton helicity-conserving form factor (which is proportional to G_M) dominates over the proton helicity-flip amplitude (proportional to $G_E/\sqrt{\tau}$) at large momentum transfer. Here $\tau = Q^2/4M^2, Q^2 = -q^2$. Thus HHC predicts $G_E(Q^2)/\sqrt{\tau}G_M(Q^2) \to 0$ at large Q^2. The new data from Jefferson Laboratory [188] which shows a decrease in the ratio $G_E(Q^2)/G_M(Q^2)$ is not itself in disagreement with the HHC prediction.

The leading-twist QCD motivated form $Q^4 G_M(Q^2) \simeq \text{const}/Q^4 \ln Q^2\Lambda^2$ provides a good guide to both the time-like and spacelike proton form factor data at $Q^2 > 5$ GeV^2 [189]. The Jefferson Laboratory data [188] appears to suggest $QF_2(Q^2)/F_1(Q^2) \simeq$ const, for the ratio of the proton's Pauli and Dirac form factors in contrast to the fall-off $Q^2F_2(Q^2)/F_1(Q^2) \simeq$ const (modulo logarithms) expected from PQCD. It should however be noted that a PQCD-motivated fit is not precluded. For example, the form [92]

$$\frac{F_2(Q^2)}{F_1(Q^2)} = \frac{\mu_A}{1 + (Q^2/c)\ln^b(1 + Q^2/a)} \tag{26}$$

with $\mu_A = 1.79$, $a = 4m_\pi^2 = 0.073$ GeV^2, $b = -0.5922$, $c = 0.9599$ GeV^2 which is consistent with leading-twist hadron helicity conservation also fits the data well. More recently, Belitsky, Ji and Yuan [88] have demonstrated that the perturbative QCD prediction has the asymptotic form $Q^2\frac{F_2(Q^2)}{F_1(Q^2)} \sim \log^2 Q^2$ and also fits the data well.

The study of time-like hadronic form factors using $\overline{p}p \to \ell^+\ell^-$ annihilation and e^+e^- colliding beams can provide very sensitive tests of HHC, since the virtual photon always has spin ± 1 along the lepton axis at high energies in the CM system. Angular momentum conservation implies that the virtual photon can "decay" with one of only two possible angular distributions in the center of momentum frame: $(1 + \cos^2\theta)$ for $|\lambda_A - \lambda_B| = 1$ and $\sin^2\theta$ for $|\lambda_A - \lambda_B| = 0$ where λ_A and λ_B are the helicities of the outgoing hadrons. Hadronic helicity conservation, as required by QCD, greatly restricts the possibilities. It implies that $\lambda_A + \lambda_B = 0$. Consequently, angular momentum conservation requires $|\lambda_A| = |\lambda_B| = l/2$ for baryons, and $|\lambda_A| = |\lambda_B| = 0$ for mesons; thus the angular distributions for any sets of hadron pairs are now completely determined at leading twist: $\frac{d\sigma}{d\cos\theta}(e^+e^- = B\overline{B}) \propto 1 + \cos^2\theta$ and $\frac{d\sigma}{d\cos\theta}(e^+e^- = M\overline{M}) \propto \sin^2\theta$. Verifying these angular distributions for vector mesons and other higher spin mesons and baryons would verify the vector nature of the gluon in QCD and the validity of

PQCD applications to exclusive reactions.

It is usually assumed that a heavy quarkonium state such as the J/ψ always decays to light hadrons via the annihilation of its heavy quark constituents to gluons. However, as Karliner and I [190] have shown, the transition $J/\psi \to \rho\pi$ can also occur by the rearrangement of the $c\bar{c}$ from the J/ψ into the $|\, q\bar{q}c\bar{c}\rangle$ intrinsic charm Fock state of the ρ or π. On the other hand, the overlap rearrangement integral in the decay $\psi' \to \rho\pi$ will be suppressed since the intrinsic charm Fock state radial wavefunction of the light hadrons will evidently not have nodes in its radial wavefunction. This observation provides a natural explanation of the long-standing puzzle why the J/ψ decays prominently to two-body pseudoscalar-vector final states in conflict with HHC, whereas the ψ' does not. If the intrinsic charm explanation is correct, then this mechanism will complicate the analysis of virtually all heavy hadron decays such as $J/\psi \to p\overline{p}$. In addition, the existence of intrinsic charm Fock states, even at a few percent level, provides new, competitive decay mechanisms for B decays which are nominally CKM-suppressed [191]. For example, the weak decays of the B-meson to two-body exclusive states consisting of strange plus light hadrons, such as $B \to \pi K$, are expected to be dominated by penguin contributions since the tree-level $b \to su\overline{u}$ decay is CKM suppressed. However, higher Fock states in the B wave function containing charm quark pairs can mediate the decay via a CKM-favored $b \to sc\bar{c}$ tree-level transition. The presence of intrinsic charm in the b meson can be checked by the observation of final states containing three charmed quarks, such as $B \to J/\psi D\pi$ [192].

12 Other Hard Exclusive Processes

There are a large number of measured exclusive reactions in which the empirical power law fall-off predicted by dimensional counting and PQCD appears to be accurate over a large range of momentum transfer. The approach to scaling of $s^7 d\sigma/dt(\gamma p \to \pi^+ n)$ shown in Fig. 10 appears to indicate that leading-twist PQCD is applicable at momentum transfers exceeding a few GeV. If anything, the scaling appears to work too well, considering that one expects logarithmic deviations due to the running of the QCD coupling and the logarithmic evolution of the hadron distribution amplitudes. The deviations from scaling at lower energies [194] are interesting and can be attributed to s-channel resonances or perhaps heavy quark threshold effects, merging into the fixed-angle scaling in a similar way as one observes the approach to leading-twist Bjorken-scaling behavior in deep inelastic scattering via quark-hadron duality [195].

The absence of significant corrections to leading-twist scaling suggests that the running coupling is effectively frozen at the kinematics relevant to the data. If higher-twist soft processes are conspiring to mimic leading-twist scaling $s^7 d\sigma/dt(\gamma p \to \pi^+ n)$, then we would have the strange situation of seeing two separate kinematic domains of s^7 scaling of the photoproduction cross section. It has been argued [180, 196] that the Compton amplitude is dominated by soft end-point contributions of the proton

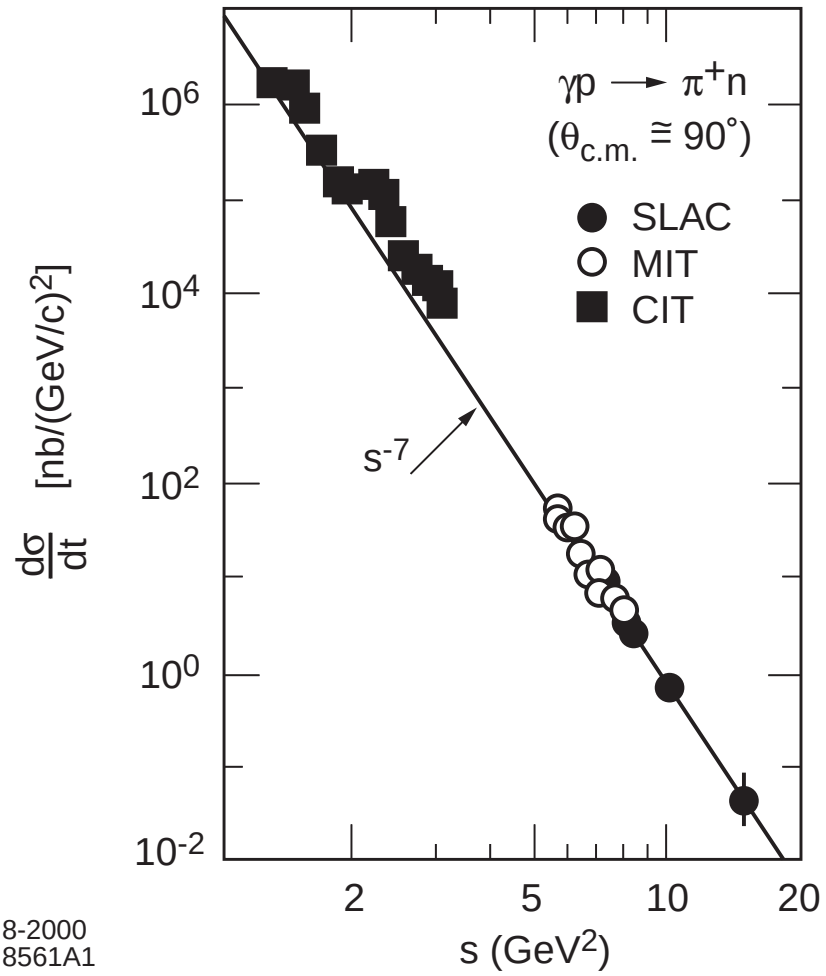

Figure 10: Comparison of photoproduction data with the dimensional counting power-law prediction. The data are summarized in Anderson *et al.* [193]

wavefunctions where the two photons both interact on a quark line carrying nearly all of the proton's momentum. However, a corresponding soft endpoint explanation of the observed $s^7 d\sigma/dt(\gamma p \to \pi^+ n)$ scaling of the pion photoproduction data is not apparent; there is no endpoint contribution which could explain the success of dimensional counting in large-angle pion photoproduction apparent in Fig. 10.

Exclusive two-photon processes where two photons annihilate into hadron pairs $\gamma\gamma \to H\overline{H}$ at high transverse momentum provide highly valuable probes of coherent effects in quantum chromodynamics. For example, in the case of exclusive final states at high momentum transfer and fixed θ_{cm} such as $\gamma\gamma \to p\overline{p}$ or meson pairs, photon-photon collisions provide a time-like microscope for testing fundamental scaling laws of PQCD and for measuring distribution amplitudes. Counting rules predict asymptotic fall-off $s^4 d\sigma/dt \sim f(t/s)$ for meson pairs and $s^6 d\sigma/dt \sim f(t/s)$ for baryon pairs. Hadron-helicity conservation predicts dominance of final states with $\lambda_H + \lambda_{\overline{H}} = 0$.

The angular dependence reflects the distribution amplitudes. One can also study $\gamma^*\gamma \to$ hadron pairs in $e^\pm e^-$ collisions as a function of photon virtuality, the time-like analog of deeply virtual Compton scattering which is sensitive to the two hadron distribution amplitude. One can also study the interference of the time-like Compton amplitude with the bremsstrahlung amplitude $e^\pm e \to BBe^\pm e^-$ where a time-like photon produces the pair. The $e^\pm$ asymmetry measures the relative phase of the time-like hadron form factor with that of the virtual Compton amplitude.

The PQCD predictions for the two-photon production of charged pions and kaons is insensitive to the shape of the meson distribution amplitudes. In fact, the ratio of the $\gamma\gamma \to \pi^+\pi^-$ and $e^+e^- \to \mu^+\mu^-$ amplitudes at large s and fixed θ_{CM} can be predicted since the ratio is nearly insensitive to the running coupling and the shape of the pion distribution amplitude:

$$\frac{\frac{d\sigma}{dt}(\gamma\gamma \to \pi^+\pi^-)}{\frac{d\sigma}{dt}(\gamma\gamma \to \mu^+\mu^-)} \sim \frac{4|F_\pi(s)|^2}{1-\cos^2\theta_{\rm c.m.}}. \tag{27}$$

The comparison of the PQCD prediction for the sum of $\pi^+\pi^-$ plus K^+K^- channels with CLEO data [197] is shown in Fig. 11. Results for separate pion and kaon channels have been given by the TPC/2γ collaboration [198]. The angular distribution of

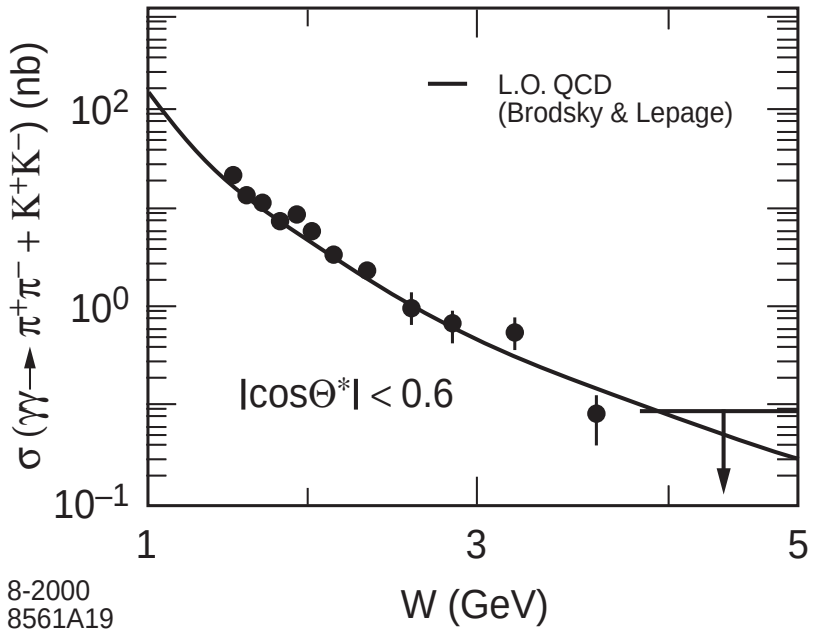

Figure 11: Comparison of the sum of $\gamma\gamma \to \pi^+\pi^-$ and $\gamma\gamma \to K^+K^-$ meson pair production cross sections with the perturbative QCD prediction [81] normalized to the timelike pion form factor. The data are from the CLEO collaboration [197].

meson pairs is also predicted by PQCD at large momentum transfer. The CLEO data

for charged pion and kaon pairs show a clear transition to the angular distribution predicted by PQCD for $W = \sqrt{s}_{\gamma\gamma} > 2$ GeV. Similarly in $\gamma\gamma \to p\overline{p}$ one can see a dramatic change in the fixed angle distribution as one enters the hard scattering domain. It is clearly important to measure the two-photon production of neutral pions and $\rho^+\rho^-$ cross sections in view of their strong sensitivity to the shape of meson distribution amplitudes. Furthermore, the ratio of $\pi^+\pi^-$ to $\pi^0\pi^0$ cross sections is highly sensitive to the production dynamics. The ratio $\sigma(\gamma\gamma \to \pi^0\pi^0)/\sigma(\gamma\gamma \to \pi^+\pi^-)$ at fixed angles is predicted to be very small in PQCD; in contrast, this ratio is of $\mathcal{O}$ 1 in soft handbag models.

An interesting contribution to $K^+p \to K^+p$ scattering comes from the exchange of the common u quark. The quark interchange amplitude for $A + B \to C + D$ can be written as a convolution of the four light-cone wavefunctions multiplied by a factor $\Delta^- = P_A^- + P_B^- - \sum_i k_i^-$, the inverse of the central propagator [80]. The interchange amplitude is consistent with constituent counting rule scaling, and often provides a phenomenologically accurate representation of the $\theta_{c.m.}$ angular distribution at large momentum transfer. For example, the angular distribution of processes such as $K^+p \to K^+p$ appear to follow the predictions based on quark interchange, *e.g.*, $T_H((u_1\overline{s})(u_2u_3d) \to (u_2\overline{s})(u_1u_3d)$ [80]. This mechanism also provides constraints on Regge intercepts $\alpha_R(t)$ for meson exchange trajectories at large momentum transfer [77]. An extensive review of this phenomenology is given in the review by Sivers *et al.* [199]

it is also interesting to study amplitudes where a nuclear wavefunction has to absorb large momentum transfer. For example, the helicity-conserving deuteron form factor is predicted to scale as $F_d(Q^2) \propto (Q^2)^{-5}$ reflecting the minimal six quark component of nuclear wavefunction. The deuteron form factor at high Q^2 is sensitive to wavefunction configurations where all six quarks overlap within an impact separation $b_{\perp i} < \mathcal{O}(1/Q)$. The leading power-law fall off predicted by QCD is $F_d(Q^2) = f(\alpha_s(Q^2))/(Q^2)^5$, where, asymptotically [102, 36], $f(\alpha_s(Q^2)) \propto \alpha_s(Q^2)^{5+2\gamma}$. In general, the six-quark wavefunction of a deuteron is a mixture of five different color-singlet states. The dominant color configuration at large distances corresponds to the usual proton-neutron bound state. However, at small impact space separation, all five Fock color-singlet components eventually acquire equal weight, *i.e.*, the deuteron wavefunction evolves to 80% "hidden color"[36]. The relatively large normalization of the deuteron form factor observed at large Q^2 hints at sizable hidden-color contributions [103].

Hidden color components can also play a predominant role in the reaction $\gamma d \to J/\psi pn$ at threshold if it is dominated by the multi-fusion process $\gamma gg \to J/\psi$. In the case of nuclear structure functions beyond the single nucleon kinematic limit, $1 < x_{bj} < A$, the nuclear light-cone momentum must be transferred to a single quark, requiring quark-quark correlations between quarks of different nucleons in a compact, far-off-shell regime. This physics is also sensitive to the part of the nuclear wavefunction which contains hidden-color components in distinction from a convolution of

separate color-singlet nucleon wavefunctions. One also sees the onset of the predicted perturbative QCD scaling behavior for exclusive nuclear amplitudes such as deuteron photodisintegration (Here $n = 1+6+3+3 = 13$.) $s^{11}\frac{d\sigma}{dt}(\gamma d \to pn) \sim$ constant at fixed CM angle. The measured deuteron form factor and the deuteron photodisintegration cross section appear to follow the leading-twist QCD predictions at large momentum transfers in the few GeV region [200, 201, 202]. A comparison of the data with the QCD predictions is shown in Fig. 12.

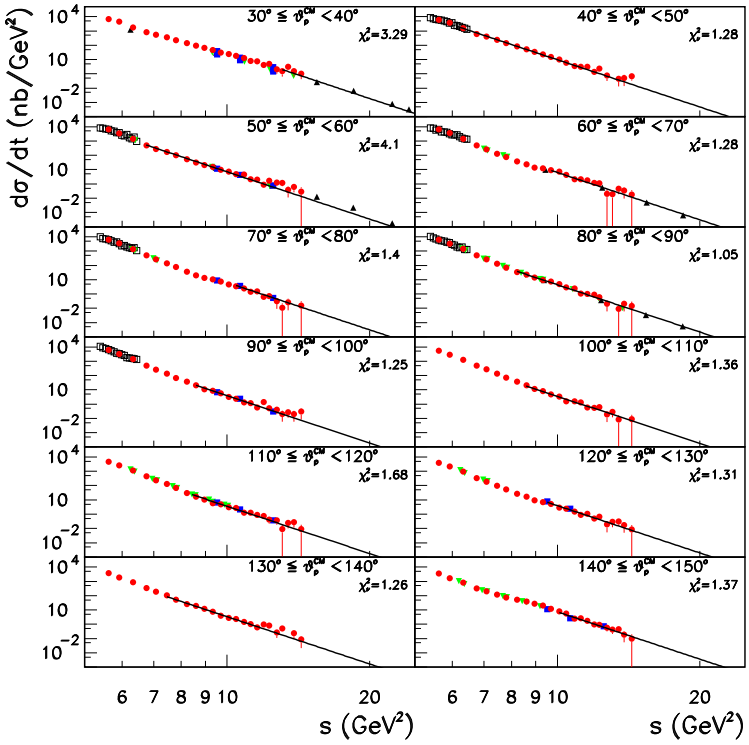

Figure 12: Fits of the cross sections $d\sigma/dt$ to s^{-11} for $P_T \geq P_T^{th}$ and proton angles between 30° and 150° (solid lines). Data are from CLAS (full/red circles), Mainz(open/black squares), SLAC (full-down/green triangles), JLab Hall A (full/blue squares) and Hall C (full-up/black triangles). Also shown in each panel is the χ^2_ν value of the fit. From Ref. [202].

In the case of the deuteron form factor, the proton and neutron share the deuteron's momentum equally to first approximation. Since the deuteron form factor contains the probability amplitudes for the proton and neutron to scatter from $p/2$ to $p/2+q/2$, it is natural to define the reduced deuteron form factor [102, 36]

$$f_d(Q^2) \equiv \frac{F_d(Q^2)}{F_{1N}\left(\frac{Q^2}{4}\right) F_{1N}\left(\frac{Q^2}{4}\right)} \,. \tag{28}$$

The effect of nucleon compositeness is removed from the reduced form factor. QCD then predicts the scaling

$$f_d(Q^2) \sim \frac{1}{Q^2}; \tag{29}$$

i.e. the same scaling law as a meson form factor. This scaling is consistent with experiment for $Q \gtrsim 1$ GeV. In fact as seen in Fig. 1, the deuteron reduced form factor contains two components: (1) a fast falling component characteristic of nuclear binding with probability 85%, and (2) a hard contribution falling as a monopole with a scale of order 0.5 GeV with probability 15%.

In the case of deuteron photodisintegration $\gamma d \to pn$ the amplitude requires the scattering of each nucleon at $t_N = t_d/4$. The perturbative QCD scaling is [203]

$$\frac{d\sigma}{d\Omega_{c.m.}}(\gamma d \to np) = \frac{1}{\sqrt{s(s-M_d^2)}} \frac{F_n^2(t_d/4)F_p^2(t_d/4)f_{red}^2(\theta_{c.m})}{p_\perp^2}. \tag{30}$$

The predicted scaling of the reduced photodisintegration amplitude $f_{red}(\theta_{c.m.}) \simeq$ const is also consistent with experiment [203, 200, 201]. See Fig. 13.

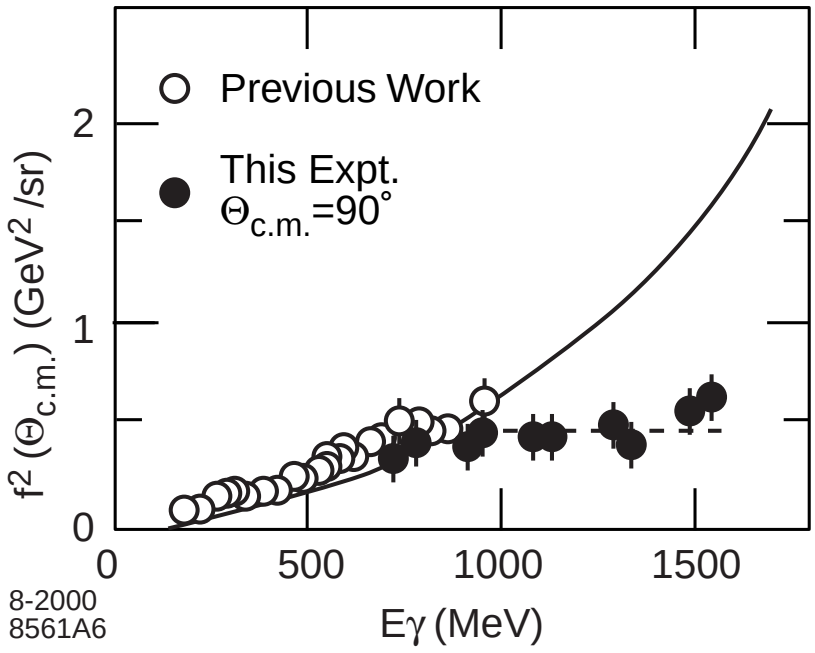

Figure 13: Comparison of deuteron photodisintegration data with the scaling prediction which requires $f^2(\theta_{cm})$ to be at most logarithmically dependent on energy at large momentum transfer. The data in are from Belz *et al.*[204] The solid curve is a nuclear physics prediction [205].

The observation of conformal scaling behavior [102] in exclusive deuteron processes such as deuteron photoproduction [202] and the deuteron form factor [101] is particularly interesting. For example, at high Q^2 the deuteron form factor is sensitive to

wavefunction configurations where all six quarks overlap within an impact separation $b_{\perp i} < \mathcal{O}(1/Q)$. In general, the six-quark wavefunction of a deuteron is a mixture of five different color-singlet states. The dominant color configuration at large distances corresponds to the usual proton-neutron bound state. However at small impact space separation, all five Fock color-singlet components eventually acquire equal weight, *i.e.*, the deuteron wavefunction evolves to 80% "hidden color." The derivation of the evolution equation for the deuteron distribution amplitude and its leading anomalous dimension γ is given in Ref. [36]. As emphasized in the introduction, the relatively large normalization of the deuteron form factor observed at large Q^2 [103], as well as the presence of two mass scales in the scaling behavior of the reduced deuteron form factor [102] $f_d(Q^2) = F_d(Q^2)/F^2(Q^2/4)$ suggests sizable hidden-color contributions in the deuteron wavefunction. See Fig. 1.

The postulate that the QCD coupling has an infrared fixed-point provides additional understanding of the applicability of conformal scaling and constituent counting rules to physical QCD processes [44, 75]. The general success of dimensional counting rules implies that the effective coupling $\alpha_V(Q^*)$ controlling the gluon exchange propagators in T_H are frozen in the infrared, since the effective momentum transfers Q^* exchanged by the gluons are often a small fraction of the overall momentum transfer [140]. In this case, the pinch contributions are suppressed by a factor decreasing faster than a fixed power [44]. The effective coupling $\alpha_\tau(s)$ extracted from τ decays displays a flat behavior at low mass scales [64].

The field of analyzable exclusive processes has been expanded to a wide range of QCD processes, such as electroweak decay amplitudes, highly virtual diffractive processes such as $\gamma^* p \to \rho p$ [206, 207], and semi-exclusive processes such as $\gamma^* p \to \pi^+ X$ [208] where the π^+ is produced in isolation at large p_T. An important new application is the recent analysis of hard exclusive B decays by Beneke *et al.* [129] and Keum *et al.* [130]

Deeply virtual Compton amplitude $\gamma^* p \to \gamma p$ has emerged as one of the most important exclusive QCD reactions [209, 210, 211, 212]. The process factorizes into a hard amplitude representing Compton scattering on the quark convoluted with the skewed parton distributions. The resulting amplitudes can be represented as diagonal and off-diagonal convolutions of light-cone wavefunctions, as in semileptonic B decay [84]. New sum rules can be constructed which correspond to gravitons coupling to the quarks of the proton [209]. It is possible that the handbag approximation to DVCS may be modified by corrections to the quark propagator similar to those which appear in the final state interaction corrections to deep inelastic scattering [34, 120]. In particular, one can expect that the propagator corrections will give single-spin asymmetries correlating the spin of the proton with the normal to the production plane in DVCS [31].

The hard diffraction of vector mesons $\gamma^* p \to V^0 p$ at high Q^2 and high energies for longitudinally polarized vector mesons factorizes into a skewed parton distribution convoluted with the hard scale $\gamma^* g \to g V^0$ amplitude, where the physics of the vector

meson is contained in its distribution amplitude [206, 127, 213]. The data appears consistent with the s, t and Q^2 dependence predicted by theory. Ratios of these processes for different mesons are sensitive to the ratio of $1/x$ moments of the V^0 distribution amplitudes.

The virtual two-photon annihilation process $\gamma^*\gamma \to$ hadrons, which is measurable in single-tagged $e^+e^- \to e^+e^-$hadrons events, provides a semi-local probe of even charge conjugation $C =^+$ hadron systems $\pi^0, \eta^0, \eta', \eta_c, \pi^+\pi^-$, etc. The $\gamma^*\gamma \to \pi^+\pi^-$ hadron pair process is related to virtual Compton scattering on a pion target by crossing. Hadron pair production is of particular interest since the leading-twist amplitude is sensitive to the $1/x - 1/(1-x)$ moment of the two-pion distribution amplitude coupled to two valence quarks [127, 214]. This type of measurement can also constrain the parameters of the effective chiral theory, which is needed for example to constrain the hadronic light-by-light contribution to the muon magnetic moment [215].

One can also study hard "semi-exclusive" processes [208] of the form $A + B \to C + Y$ which are characterized by a large momentum transfer between the particles A and C and a large rapidity gap between the final state particle C and the inclusive system Y. Such reactions are in effect generalizations of deep inelastic lepton scattering, providing novel currents which probe specific quark distributions of the target B at fixed momentum fraction and novel spin-dependent parton distributions.

13 Heavy Quark Components of the Proton Structure Function

In the simplest treatment of deep inelastic scattering, nonvalence quarks are produced via gluon splitting and DGLAP evolution. However, in a full theory heavy quarks are multiply-connected to the valence quarks [95]. For example, the asymmetry of the strange and anti-strange distributions in the nucleon is due to their different interactions with the other quark constituents. The probability for Fock states of a light hadron such as the proton to have an extra heavy quark pair decreases as $1/m_Q^2$ in non-Abelian gauge theory [96, 97]. The relevant matrix element is the cube of the QCD field strength $G^3_{\mu nu}$. This is in contrast to abelian gauge theory where the relevant operator is $F^4_{\mu\nu}$ and the probability of intrinsic heavy leptons in QED bound state is suppressed as $1/m_\ell^4$. The intrinsic Fock state probability is maximized at minimal off shellness. The maximum probability occurs at $x_i = m^i_\perp / \sum_{j=1}^n m^j_\perp$; *i.e.*, when the constituents have equal rapidity. Thus the heaviest constituents have the highest momentum fractions and highest x. Intrinsic charm thus predicts that the charm structure function has support at large x_{bj} in excess of DGLAP extrapolations [95]; this is in agreement with the EMC measurements [98]. It predicts leading charm hadron production and fast charmonium production in agreement with measurements [216]. The production cross section for the double charmed Ξ^+_{cc} baryon [217] and the production of double $J/\psi's$ appears to be consistent

with the dissociation and coalescence of double IC Fock states [218]. Intrinsic charm can also explain the $J/\psi \to \rho\pi$ puzzle [190]. It also affects the extraction of suppressed CKM matrix elements in B decays [191]. It is thus critical for new experiments (HERMES, HERA, COMPASS) to definitively establish the phenomenology of the charm structure function at large x_{bj}.

Since the intrinsic charm quarks have a relatively hard distribution in the nucleon, one expects enhanced open and hidden charm production near the kinematic threshold. This will be particularly interesting to study in the new GSI antiproton facility.

14 The Strange Quark Asymmetry

Although the strange and antistrange distributions in the nucleon are identical when they derive from gluon-splitting $g \to s\overline{s}$, this is not the case when the strange quarks are part of the intrinsic structure of the nucleon. There is a simple analog in QED: Consider the $\tau^{\pm}$ distributions in the (rare!) $|\, e^-\mu^+\tau^+\tau^-\rangle$ Fock state of muonium (μ^+e^-). The τ^- is attracted by Coulomb interactions to the high rapidity $\mu+$. Thus the τ^- will tend to have higher rapidity than the τ^+.

Similar effects will happen in QCD. If we use the diquark model $|\, p\rangle \sim \left|\, u_{3_c}(ud)_{\overline{3}_C}\right\rangle$, then the Q_{3_C} in the $\left|\, u(ud)Q\overline{Q}\right\rangle$ Fock state will be attracted to the heavy diquark and thus have higher rapidity than the $\overline{Q}$.

An alternative model is the $|\, K\Lambda\rangle$ fluctuation model for the $|\, uuds\overline{s}\rangle$ Fock state of the proton [28]. The s quark tends to have higher x.

The experimentally observed asymmetry [219] appears to be small but positive: $\int dx x[s(x)-\overline{s}(x)]$. The $\overline{s}(x)-s(x)$ asymmetry can be studied in detail in $p\overline{p}$ collisions by searching for antisymmetric forward-backward strange quark distributions in the $\overline{p}-p$ CM frame.

15 The Infrared Behavior of Effective QCD Couplings

It is often assumed that color confinement in QCD can be traced to the singular behavior of the running coupling in the infrared, *i.e.* "infrared slavery." For example, if $\alpha_s(q^2) \to 1/q^2$ at $q^2 \to 0$, then one-gluon exchange leads to a linear potential at large distances. However, theoretical [220, 221, 222, 223, 224] and phenomenological [225, 64, 65] evidence is now accumulating that the QCD coupling becomes constant at small virtuality; *i.e.*, $\alpha_s(Q^2)$ develops an infrared fixed point in contradiction to the usual assumption of singular growth in the infrared. Since all observables are related by commensurate scale relations, they all should have an IR fixed point [223]. A recent study of the QCD coupling using lattice gauge theory in Landau gauge in fact

shows an infrared fixed point [66]. This result is also consistent with Dyson-Schwinger equation studies of the physical gluon propagator [220, 221]. The relationship of these results to the infrared-finite coupling for the vector interaction defined in the quarkonium potential has recently been discussed by Badalian and Veselov [67].

One can define the fundamental coupling of QCD from virtually any physical observable [226]. Such couplings, called "effective charges", are all-order resummations of perturbation theory, so they correspond to the complete theory of QCD. Unlike the $\overline{\rm MS}$ coupling, a physical coupling is analytic across quark flavor thresholds [227, 228]. In particular, heavy particles will contribute to physical predictions even at energies below their threshold. This is in contrast to mathematical renormalization schemes such as $\overline{M}S$, where mass thresholds are treated as step functions. In addition, since the QCD running couplings defined from observables are bounded, integrations over effective charges are well defined and the arguments requiring renormalon resummations do apply. The physical couplings satisfy the standard renormalization group equation for its logarithmic derivative, $\mathrm{d}\alpha_{\rm phys}/\mathrm{d}\ln k^2 = \widehat{\beta}_{\rm phys}[\alpha_{\rm phys}(k^2)]$, where the first two terms in the perturbative expansion of $\widehat{\beta}_{\rm phys}$ are scheme-independent at leading twist; the higher order terms have to be calculated for each observable separately using perturbation theory.

Menke, Merino, and Rathsman [64] and I have considered a physical coupling for QCD which is defined from the high precision measurements of the hadronic decay channels of the $\tau^- \to \nu_\tau \mathrm{h}^-$. Let R_τ be the ratio of the hadronic decay rate to the leptonic rate. Then $R_\tau \equiv R_\tau^0 \left[1 + \frac{\alpha_\tau}{\pi}\right]$, where R_τ^0 is the zeroth order QCD prediction, defines the effective charge α_τ. The data for τ decays is well-understood channel by channel, thus allowing the calculation of the hadronic decay rate and the effective charge as a function of the τ mass below the physical mass. The vector and axial-vector decay modes which can be studied separately. Using an analysis of the τ data from the OPAL collaboration [68], we have found that the experimental value of the coupling $\alpha_\tau(s) = 0.621 \pm 0.008$ at $s = m_\tau^2$ corresponds to a value of $\alpha_{\overline{\rm MS}}(M_Z^2) = (0.117\text{-}0.122) \pm 0.002$, where the range corresponds to three different perturbative methods used in analyzing the data. This result is in good agreement with the world average $\alpha_{\overline{\rm MS}}(M_Z^2) = 0.117 \pm 0.002$. However, from the figure we also see that the effective charge only reaches $\alpha_\tau(s) \sim 0.9 \pm 0.1$ at $s = 1\,\mathrm{GeV}^2$, and it even stays within the same range down to $s \sim 0.5\,\mathrm{GeV}^2$. This result is in good agreement with the estimate of Mattingly and Stevenson [225] for the effective coupling $\alpha_R(s) \sim 0.85$ for $\sqrt{s} < 0.3\,\mathrm{GeV}$ determined from $\mathrm{e}^+\mathrm{e}^-$ annihilation, especially if one takes into account the perturbative commensurate scale relation, $\alpha_\tau(m_{\tau'}^2) = \alpha_R(s^*)$, where $s^* \simeq 0.10\, m_{\tau'}^2$. This behavior is not consistent with the coupling having a Landau pole, but rather shows that the physical coupling is close to constant at low scales, suggesting that physical QCD couplings are effectively constant or "frozen" at low scales.

Figure 14 shows a comparison of the experimentally determined effective charge $\alpha_\tau(s)$ with solutions to the evolution equation for α_τ at two-, three-, and four-loop order normalized at m_τ. At three loops the behavior of the perturbative solution

drastically changes, and instead of diverging, it freezes to a value $\alpha_\tau \simeq 2$ in the infrared. The infrared behavior is not perturbatively stable since the evolution of the coupling is governed by the highest order term. This is illustrated by the widely different results obtained for three different values of the unknown four loop term $\beta_{\tau,3}$ which are also shown. The values of $\beta_{\tau,3}$ used are obtained from the estimate of the four loop term in the perturbative series of R_τ, $K_4^{\overline{\rm MS}} = 25 \pm 50$ [229]. It is interesting to note that the central four-loop solution is in good agreement with the data all the way down to $s \simeq 1\,\mathrm{GeV}^2$.

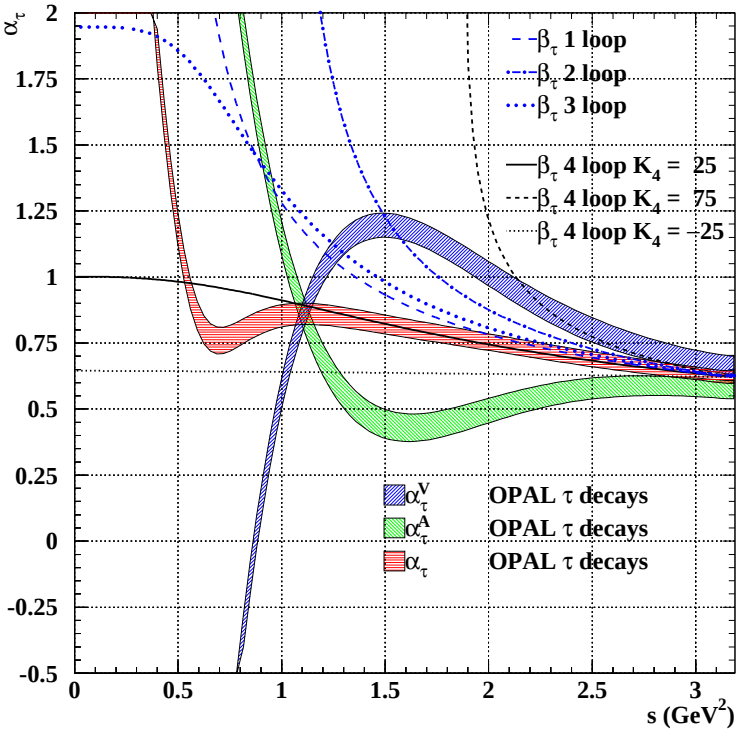

Figure 14: The effective charge α_τ for non-strange hadronic decays of a hypothetical τ lepton with $m_{\tau'}^2 = s$ compared to solutions of the fixed order evolution equation for α_τ at two-, three-, and four-loop order. The error bands include statistical and systematic errors.

The results for α_τ resemble the behavior of the one-loop "time-like" effective coupling [230, 231, 232]

$$\alpha_{\rm eff}(s) = \frac{4\pi}{\beta_0}\left\{\frac{1}{2} - \frac{1}{\pi}\arctan\left[\frac{1}{\pi}\ln\frac{s}{\Lambda^2}\right]\right\} \tag{31}$$

which is finite in the infrared and freezes to the value $\alpha_{\rm eff}(s) = 4\pi/\beta_0$ as $s \to 0$. It is

instructive to expand the "time-like" effective coupling for large s,

$$\begin{aligned}\alpha_{\rm eff}(s) &= \frac{4\pi}{\beta_0 \ln\left(s/\Lambda^2\right)}\left\{1 - \frac{1}{3}\frac{\pi^2}{\ln^2\left(s/\Lambda^2\right)} + \frac{1}{5}\frac{\pi^4}{\ln^4\left(s/\Lambda^2\right)} + \ldots\right\} \\ &= \alpha_{\rm s}(s)\left\{1 - \frac{\pi^2\beta_0^2}{3}\left(\frac{\alpha_{\rm s}(s)}{4\pi}\right)^2 + \frac{\pi^4\beta_0^4}{5}\left(\frac{\alpha_{\rm s}(s)}{4\pi}\right)^4 + \ldots\right\}. \qquad (32)\end{aligned}$$

This shows that the "time-like" effective coupling is a resummation of $(\pi^2\beta_0^2\alpha_{\rm s}^2)^n$-corrections to the usual running couplings. The finite coupling $\alpha_{\rm eff}$ given in Eq. (31) obeys standard PQCD evolution at LO. Thus one can have a solution for the perturbative running of the QCD coupling which obeys asymptotic freedom but does not have a Landau singularity.

The near constancy of the effective QCD coupling at small scales illustrates the near-conformal behavior of QCD. It helps explain the empirical success of dimensional counting rules for the power law fall-off of form factors and fixed angle scaling. As shown in the references [62, 233], one can calculate the hard scattering amplitude T_H for such processes [76] without scale ambiguity in terms of the effective charge α_τ or α_R using commensurate scale relations. The effective coupling is evaluated in the regime where the coupling is approximately constant, in contrast to the rapidly varying behavior from powers of $\alpha_{\rm s}$ predicted by perturbation theory (the universal two-loop coupling). For example, the nucleon form factors are proportional at leading order to two powers of $\alpha_{\rm s}$ evaluated at low scales in addition to two powers of $1/q^2$; The pion photoproduction amplitude at fixed angles is proportional at leading order to three powers of the QCD coupling. The essential variation from leading-twist counting-rule behavior then only arises from the anomalous dimensions of the hadron distribution amplitudes.

16 The Role of Conformal Symmetry in QCD Phenomenology

The classical Lagrangian of QCD for massless quarks is conformally symmetric. Since it has no intrinsic mass scale, the classical theory is invariant under the $SO(4,2)$ translations, boosts, and rotations of the Poincare group, plus the dilatations and other transformations of the conformal group. Scale invariance, and therefore conformal symmetry is destroyed in the quantum theory by the renormalization procedure which introduces a renormalization scale as well as by quark masses. Conversely, Parisi [47] has shown that perturbative QCD becomes a conformal theory for $\beta \to 0$ and zero quark mass. Conformal symmetry is thus broken in physical QCD; nevertheless, we can still recover the underlying features of the conformally invariant theory by evaluating any expression in QCD in the analytic limit of zero quark mass and

zero β function:

$$\lim_{m_q \to 0, \beta \to 0} \mathcal{O}_{QCD} = \mathcal{O}_{\text{conformal QCD}} \ . \tag{33}$$

This conformal correspondence limit is analogous to Bohr's correspondence principle where one recovers predictions of classical theory from quantum theory in the limit of zero Planck constant. The contributions to an expression in QCD from its nonzero β-function can be systematically identified [56, 55, 57] order-by-order in perturbation theory using the Banks-Zaks procedure [58].

There are a number of useful phenomenological consequences of near conformal behavior of QCD: the conformal approximation with zero β function can be used as template for QCD analyses [50, 49] such as the form of the expansion polynomials for distribution amplitudes [51, 59]. The near-conformal behavior of QCD is the basis for commensurate scale relations [54] which relate observables to each other without renormalization scale or scheme ambiguities [56, 55]. By definition, all contributions from the nonzero β function can be incorporated into the QCD running coupling $\alpha_s(Q)$ where Q represents the set of physical invariants. Conformal symmetry thus provides a template for physical QCD expressions. For example, perturbative expansions in QCD for massless quarks must have the form

$$\mathcal{O} = \sum_{n=0} C_n \alpha_s^n(Q_n^*) \tag{34}$$

where the C_n are identical to the expansion coefficients in the conformal theory, and Q_n^* is the scale chosen to resum all of the contributions from the nonzero β function at that order in perturbation theory. Since the conformal theory does not contain renormalons, the C_n do not have the divergent n growth characteristic of conventional PQCD expansions evaluated at a fixed scale.

17 The AFS/CFT Correspondence and Conformal Properties of Hadronic Light-Front Wavefunctions

As shown by Maldacena [11], there is a remarkable correspondence between large N_C supergravity theory in a higher dimensional anti-de Sitter space and supersymmetric QCD in 4-dimensional space-time. String/gauge duality provides a framework for predicting QCD phenomena based on the conformal properties of the AdS/CFT correspondence.

The AdS/CFT correspondence is based on the fact that the generators of conformal and Poincare transformations have representations on the five-dimensional anti-deSitter space AdS_5 as well as Minkowski spacetime. For example, Polchinski and Strassler [12] have shown that the power-law fall-off of hard exclusive hadron-hadron scattering amplitudes at large momentum transfer can be derived without the use

of perturbation theory by using the scaling properties of the hadronic interpolating fields in the large-r region of AdS space. Thus one can use the Maldacena correspondence to compute the leading power-law behavior of exclusive processes such as high-energy fixed-angle scattering of gluonium-gluonium scattering in supersymmetric QCD. The resulting predictions for hadron physics effectively coincide [12, 13, 14] with QCD dimensional counting rules for form factors and hard scattering amplitudes [42, 43, 44, 234]. Polchinski and Strassler [12] have also derived counting rules for deep inelastic structure functions at $x \to 1$ in agreement with perturbative QCD predictions [76, 107] as well as Bloom-Gilman exclusive-inclusive duality [235].

The supergravity analysis is based on an extension of classical gravity theory in higher dimensions and is nonperturbative. Thus analyses of exclusive processes [76] which were based on perturbation theory can be extended by the Maldacena correspondence to all orders. An important point is that the hard scattering amplitudes which are normally or order α_s^p in PQCD appear as order $\alpha_s^{p/2}$ in the supergravity predictions. This can be understood as an all-orders resummation of the effective potential [11, 236].

The superstring theory results are derived in the limit of a large N_C [237]. For gluon-gluon scattering, the amplitude scales as $1/N_C^2$. For color-singlet bound states of quarks, the amplitude scales as $1/N_C$. This large N_C-counting, in fact, corresponds to the quark interchange mechanism [80]. For example, for $K^+p \to K^+p$ scattering, the u-quark exchange amplitude scales approximately as $\frac{1}{u}\ \frac{1}{t^2}$, which agrees remarkably well with the measured large θ_{CM} dependence of the K^+p differential cross section [238]. This implies that the nonsinglet Reggeon trajectory asymptotes to a negative integer [77], in this case, $\lim_{-t\to\infty} \alpha_R(t) \to -1$.

De Teramond and I have extended the Polchinski-Strassler analysis to hadron-hadron scattering [41]. We have also shown how to compute the form and scaling of light-front hadronic wavefunctions using the AdS/CFT correspondence in quantum field theories which have an underlying conformal structure, such as $\mathcal{N} = 4$ superconformal QCD. For example, baryons are included in the theory by adding an open string sector in $AdS_5 \times S^5$ corresponding to quarks in the fundamental representation of the $SU(4)$ symmetry defined on S^5 and the fundamental and higher representations of $SU(N_C)$. The hadron mass scale is introduced by imposing boundary conditions at the AdS_5 coordinate $r = r_0 = \Lambda_{QCD} R^2$. The quantum numbers of the lowest Fock state of each hadron, including its internal orbital angular momentum and spin-flavor symmetry, are identified by matching the fall-off of the string wavefunction $\Psi(x, r)$ at the asymptotic $3+1$ boundary. Higher Fock states are identified with conformally invariant quantum fluctuations of the bulk geometry about the AdS background. The eigenvalues of the 10-dimensional Dirac and Rarita-Schwinger equations have also been used to determine the nucleon and Δ spectrum in conformal QCD. The results are in surprising agreement with the empirical spectra [239].

One can also use the scaling properties of the hadronic interpolating operator in the extended AdS/CFT space-time theory to determine the scaling of light-front

hadronic wavefunctions at high relative transverse momentum. De Teramond and I [41] have also shown how the angular momentum dependence of the light-front wavefunctions also follow from the conformal properties of the AdS/CFT correspondence. where g_s is the string scale and Λ_o represents the basic QCD mass scale. Quantum fluctuations of the strings in the AdS radial direction correspond to the quantum fluctuations of the hadron wavefunctions due to orbital angular momentum and radial nodes in the 3+1 theory.

The scaling and conformal properties of the AdS/CFT correspondence leads to a hard component of light-front wavefunctions of the form [41]:

$$\begin{aligned}\psi_{n/h}(x_i, \vec{k}_{\perp i}, \lambda_i, l_{zi}) &\sim \frac{(g_s\ N_C)^{\frac{1}{2}(n-1)}}{\sqrt{N_C}} \prod_{i=1}^{n-1} (k_{i\perp}^{\pm})^{|l_{zi}|} \\ &\times \left[\frac{\Lambda_o}{M^2 - \sum_i \frac{\vec{k}_{\perp i}^2 + m_i^2}{x_i} + \Lambda_o^2}\right]^{n+|l_z|-1}, \end{aligned} \tag{35}$$

where g_s is the string scale and Λ_o represents the basic QCD mass scale. The scaling predictions agree with perturbative QCD analyses [240, 76], but the AdS/CFT analysis is performed at strong coupling without the use of perturbation theory. The near-conformal scaling properties of light-front wavefunctions lead to a number of other predictions for QCD which are normally discussed in the context of perturbation theory, such as constituent counting scaling laws for structure functions at $x \to 1$, as well as the leading power fall-off of form factors and hard exclusive scattering amplitudes for QCD processes.

18 Applicability of PQCD and Conformal Symmetry to Hard Exclusive Processes

The PQCD/conformal symmetry predictions for hadron form factors are leading-twist predictions. The only mass parameter is the QCD scale, so the power-law predictions must be relevant—up to logarithms—even in the few GeV domain. Note also that the same PQCD couplings which enter hard exclusive reactions are tested in DGLAP evolution even at small Q^2. As noted above, the dimensional counting rules for form factors and exclusive processes have also been derived for conformal QCD using the AdS/CFT correspondence [12, 41].

In fact, there have been a remarkable number of empirical successes of PQCD predictions, including the scaling and angular dependence of $\gamma\gamma \to \pi^+\pi^-$, pion photoproduction, vector meson electroproduction, and the photon-to-pion transition form factor. A particularly dramatic example is deuteron photodisintegration which satisfies the predicted scaling law $[s^{11}\frac{d\sigma}{dt}(\gamma d \to pn) \sim \text{const}]$ at large $p_\perp$ and fixed CM angle [202] to remarkable high precision. Perturbative QCD predicts that only the

small compact part of the light-front wavefunctions enter exclusive hard scattering processes, and that these hadronic fluctuations have diminished interactions in a nuclear target [37]. Evidence for QCD color transparency has been observed for quasi-elastic photoproduction [241] and proton-proton scattering [242]. In general, the PQCD scaling behavior can be modulated by resonances and heavy quark threshold phenomena [74] which can cause dramatic spin correlations [243] as well as novel color transparency effects [37, 242]. The approach to scaling in pion photoproduction: $[s^7 \frac{d\sigma}{dt}(\gamma p \to n\pi^+) \sim \text{const}]$ and evidence for structure due to the strangeness threshold have recently been studied at Jefferson Laboratory [244].

Leading-order perturbative QCD predicts the empirical scaling of form factors and other hard exclusive amplitudes, but it typically underestimate the normalization. The normalization of theoretical prediction involves questions of the shape of the hadron distribution amplitudes, the proper scale for the running coupling [62] as well as higher order corrections. In fact, as noted above, in the AdS/CFT analysis, hard scattering amplitudes which are normally of order α_s^p in PQCD appear as order $\alpha_s^{p/2}$ in the nonperturbative theory [11, 236].

Further experimental studies, particularly measurements of $\overline{p}p$ annihilation into two hadrons at GSI, electroproduction at Jefferson Laboratory and the study of two-photon exclusive channels at CLEO and the B-factories have the potential of providing critical information on the hadron wavefunctions as well as testing the dominant dynamical processes at short distances.

19 Color Transparency

One of the most distinctive tests for the underlying gauge theory basis for the strong interactions is color transparency: the small transverse size fluctuations of a hadron wavefunction with a small color dipole moment have minimal interactions in a nucleus [94, 37]. Each hadron entering or emitted from a hard exclusive reaction initially emerges with high momentum and small transverse size $b_\perp$. A fundamental feature of gauge theory is that soft gluons decouple from the small color-dipole moment of the compact fast-moving color-singlet wavefunction configurations of the incident and final-state hadrons. The transversely compact color-singlet configurations can effectively persist over a distance of order $\ell_{\rm Ioffe} = \mathcal{O}(E_{\rm lab}/Q^2)$, the Ioffe coherence length. Thus if we study hard quasi-elastic processes in a nuclear target such as $eA \to e'p'(A-1)$ or $pA \to p'(A-1)$, the outgoing and ingoing hadrons will have minimal absorption in a nucleus. The diminished absorption of hadrons produced in hard exclusive reactions implies additivity of the nuclear cross section in nucleon number A and is the theoretical basis for the "color transparency" of hard quasi-elastic reactions [37, 245, 246]. In contrast, in conventional Glauber scattering, one predicts strong, nearly energy-independent initial and final state attenuation. Similarly, in hard diffractive processes such as $\gamma^*(Q^2)p \to \rho p$ [206], only the small transverse configurations $b_\perp \sim 1/Q$ of the longitudinally polarized vector meson distribution

amplitude are involved. Its hadronic interactions as it exits the nucleus will be minimal, and thus the $\gamma^*(Q^2)N \to \rho N$ reaction can occur coherently throughout a nuclear target in reactions without absorption or shadowing.

Color transparency has also been tested in large angle quasi-elastic $pA \to ppA-1$ scattering [247, 248, 249, 242] where only the small size fluctuations of the hadron wavefunction enters the hard exclusive scattering amplitude. There is evidence for the onset of color transparency in the regime $6 < s < 25$ GeV^2, indicating that small wavefunction configurations are indeed controlling this exclusive reaction at moderate momentum transfers. However at $p_{\rm lab} \simeq 12$ GeV, $E_{cm} \simeq 5$ GeV, color transparency dramatically fails. See Fig. 15. It is noteworthy that in the same energy range, the normal-normal spin asymmetry A_{NN} in elastic $pp \to pp$ scattering at $\theta_{cm} = 90^0$ increases dramatically to $A_{NN} \simeq 0.6$; it is about four times more probable that the protons scatter with helicity normal to the scattering plane than anti-normal [243].

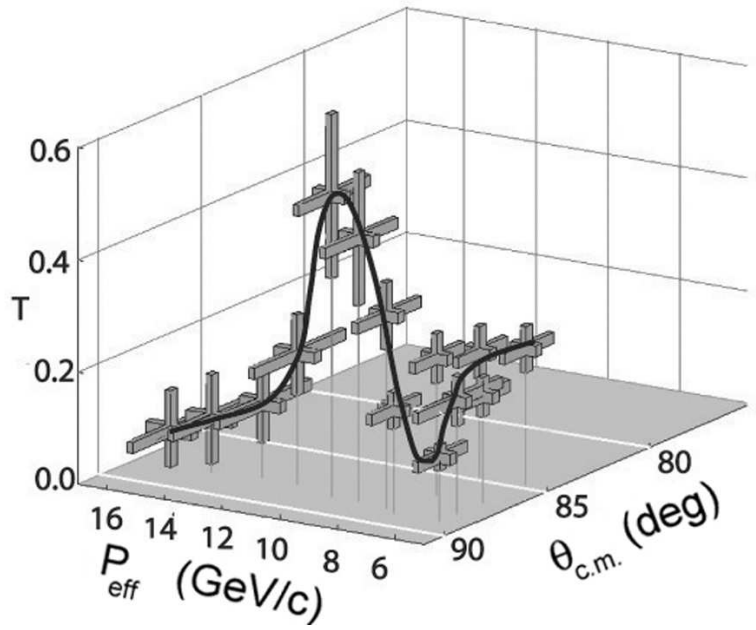

Figure 15: The dependence of Carbon transparency on effective incident beam momentum ($P_{\rm eff}$) and on center of mass scattering angle ($\theta_{\rm c.m.}$). The data are from the E850 C(p,2p) experiments [247, 248, 249, 242].

The unusual spin and color transparency effects seen in elastic proton-proton scattering at $E_{CM} \sim 5$ GeV and large angles could be related to the charm threshold and the effects of a $|uuduudc\bar{c}\rangle$ resonance which would appear as in the $J = L = S = 1$ pp partial wave [74, 250]. The intermediate state $|uuduudc\bar{c}\rangle$ has odd intrinsic parity and couples to the $J = S = 1$ initial state, thus strongly enhancing scattering when the incident projectile and target protons have their spins parallel and normal to the scattering plane. A similar enhancement of A_{NN} is observed at the strangeness

threshold. The physical protons coupling at the charm threshold will have normal Glauber interactions, thus explaining the anomalous change in color transparency observed at the same energy in quasi-elastic pp scattering. A crucial test of this hypothesis is the observation of open charm production near threshold with a cross section of order of 1μb [74, 250]. A similar cross section is expected for the second threshold for open charm production from $p\overline{p} \to$ charm $p\overline{p}$.

An alternative explanation of the color transparency and spin anomalies in pp elastic scattering has been postulated by Ralston, Jain, and Pire [251, 246]. The oscillatory effects in the large-angle $pp \to pp$ cross section and spin structure are postulated to be due to the interference of Landshoff pinch and perturbative QCD amplitudes. In the case of quasi-elastic reactions, the nuclear medium absorbs and filters out the non-compact pinch contributions, leaving the additive hard contributions unabsorbed. It is clearly important that these two alternative explanations be checked by experiment.

In general, one can expect strong effects whenever heavy quarks are produced at low relative velocity with respect to each other or the other quarks in the reaction since the QCD van der Waals interactions become maximal in this domain. The opening of the strangeness and charm threshold in intermediate states can become most apparent in large angle reactions such as pp scattering and pion photoproduction since the competing perturbative QCD amplitudes are power-suppressed. Charm and bottom production near threshold such as J/ψ photoproduction is also sensitive to the multi-quark, gluonic, and hidden-color correlations of hadronic and nuclear wavefunctions in QCD since all of the target's constituents must act coherently within the small interaction volume of the heavy quark production subprocess [99]. Although such multi-parton subprocess cross sections are suppressed by powers of $1/m_Q^2$, they have less phase-space suppression and can dominate the contributions of the leading-twist single-gluon subprocesses in the threshold regime.

20 Measuring Light-Front Wavefunctions in QCD and Testing Color Transparency using Diffractive Dissociation

Diffractive multi-jet production in heavy nuclei provides a novel way to measure the shape of light-front Fock state wave functions and test color transparency [37]. For example, consider the reaction [94, 252] $\pi A \to \mathrm{Jet}_1 + \mathrm{Jet}_2 + A'$ at high energy where the nucleus A' is left intact in its ground state. The transverse momenta of the jets balance so that $\vec{k}_{\perp i} + \vec{k}_{\perp 2} = \vec{q}_\perp < R^{-1}{}_A$. The light-cone longitudinal momentum fractions also need to add to $x_1 + x_2 \sim 1$ so that $\Delta p_L < R_A^{-1}$. The process can then occur coherently in the nucleus. Because of color transparency, the valence wave function of the pion with small impact separation will penetrate the nucleus

with minimal interactions, diffracting into jet pairs [94]. The $x_1 = x$, $x_2 = 1 - x$ dependence of the di-jet distributions will thus reflect the shape of the pion valence light-cone wave function in x; similarly, the $\vec{k}_{\perp 1} - \vec{k}_{\perp 2}$ relative transverse momenta of the jets gives key information on the derivative of the underlying shape of the valence pion wavefunction [252, 253]. The diffractive nuclear amplitude extrapolated to $t = 0$ should be linear in nuclear number A if color transparency is correct. The integrated diffractive rate should then scale as $A^2/R_A^2 \sim A^{4/3}$.

These predictions have been verified by the E791 experiment at Fermilab for 500 GeV incident pions on nuclear targets [254]. The high energy pion diffracts into dijets $\pi A \to q\bar{q}A'$ which balance in transverse momentum and leave the nucleus in its ground state [255]. The measured momentum fraction distribution of the jets is consistent with the shape of the pion asymptotic distribution amplitude, $\phi_\pi^{\rm asympt}(x) = \sqrt{3} f_\pi x(1-x)$ [256]. Data from CLEO [257] for the $\gamma\gamma^* \to \pi^0$ transition form factor also favor a form for the pion distribution amplitude close to the asymptotic solution to its perturbative QCD evolution equation [52, 258, 76].

These "self-resolving" diffractive processes thus provide direct experimental information on the light-cone wavefunctions of the photon and proton in terms of their QCD degrees of freedom, as well as the composition of nuclei in terms of their nucleon and mesonic degrees of freedom. When the hadronic jets have balancing but high transverse momentum, one studies the small size fluctuation of the incident pion. The forward diffractive amplitude is observed to grow in proportion to the total number of nucleons in the nucleus, in agreement with the color transparency prediction (see below), but in strong contrast to standard Glauber theory which predicts that only the front surface of the nucleus should be effective.

The diffractive dissociation of a hadron or nucleus can also occur via the Coulomb dissociation of a beam particle on an electron beam (*e.g.* at HERA or eRHIC) or on the strong Coulomb field of a heavy nucleus (*e.g.* at RHIC or nuclear collisions at the LHC) [259]. The amplitude for Coulomb exchange at small momentum transfer is proportional to the first derivative $\sum_i e_i \frac{\partial}{\vec{k}_{Ti}} \psi$ of the light-cone wavefunction, summed over the charged constituents. The Coulomb exchange reactions fall off less fast at high transverse momentum compared to pomeron exchange reactions since the light-cone wavefunction is effective differentiated twice in two-gluon exchange reactions. It is also interesting to study diffractive tri-jet production using proton beams $pA \to {\rm Jet}_1 + {\rm Jet}_2 + {\rm Jet}_3 + A'$ to determine the fundamental shape of the 3-quark structure of the valence light-cone wavefunction of the nucleon at small transverse separation [260].

There has been an important debate whether diffractive jet production faithfully measures the light-front wavefunctions of the projectile. Braun *et al.* [261] and Chernyak [262] have argued that one should systematically iterate the gluon exchange kernel from all sources, including final state interactions. Thus if the hard momentum exchange which produces the high transverse momentum di-jets occurs in the final state, then the x and $k_\perp$ distributions will reflect the gluon exchange kernel, not the pion's wavefunction. However, it should be noted that the measurements of pion

diffraction by the E791 experiment [256] are performed on a platinum target. Only the part of the pion wavefunction with small impact separation can give the observed color transparency; *i.e.*, additivity of the amplitude on nuclear number. Thus the nucleus automatically selects events where the jets are produced at high transverse momentum in the initial state before the pion reaches the nucleus [94].

The debate [263, 261, 262] concerning the nature of diffractive dijet dissociation also applies to the simpler analysis of diffractive dissociation via Coulomb exchange. The one-photon exchange matrix element can be identified with the spacelike electromagnetic form factor for $\pi \to q\overline{q}$; $\langle \pi; P-q|j^+(0)|q\overline{q}; P\rangle$. Here the state $|\, q\overline{q}\rangle$ is the eigenstate of the QCD Hamiltonian; it is effectively an 'out' state. If we choose the $q^+ = 0$ frame where $q^2 = -\vec{q}_\perp^{\,2}$, then the form factor is exactly the overlap integral in transverse momentum of the pion and $\overline{q}q$ LFWFs summed over Fock States. The form factor vanishes at $Q^2 = 0$ because it is the matrix element of the total charge operator and the pion and jet-jet eigenstates are orthogonal. The $n = 2$ contribution to the form factor is the convolution $\psi_\pi(x, k_\perp - (1-x)q_\perp)$ with $\psi_{\overline{q}q}(x, k_\perp)$. This can be expanded at small q^2 in terms of the transverse momentum derivatives of the pion wavefunction. The final-state wavefunction represents an outgoing wave of free quarks with momentum $y, \ell_\perp$ and $1-y, -\ell_\perp$. To first approximation, the wavefunction $\psi_{\overline{q}q}(x, k_\perp)$ peaks strongly at $x = y$ and $k_\perp = \ell_\perp$. Using this approximation, the form factor at small Q^2 is proportional to the derivative of the pion light-cone wavefunction $[e_q(1-x) - e_{\overline{q}}x]\frac{\partial}{dk_\perp}\psi_\pi(x, k_\perp)$ evaluated at $x = y$ and $k_\perp = \ell_\perp$. One can also consider corrections to the final state wavefunction from gluon exchange. However, the final quarks are already moving in the correct direction at zeroth order, so these corrections would be expected to be of higher order.

21 The Generalized Crewther Relation

A central principle of renormalization theory is that predictions which relate physical observables to each other cannot depend on theoretical conventions. For example, one can use any renormalization scheme, such as the modified minimal subtraction scheme, and any choice of renormalization scale μ to compute perturbative series relating observables A and B. However, all traces of the choices of the renormalization scheme and scale must disappear when one algebraically eliminates the $\alpha_{\overline{\rm MS}}(\mu)$ and directly relates A to B. This is the principle underlying "commensurate scale relations" (CSR) [264], which are general leading-twist QCD predictions relating physical observables to each other at their respective scales. An important example is the generalized Crewther relation [60]:

$$\left[1 + \frac{\alpha_R(s^*)}{\pi}\right]\left[1 - \frac{\alpha_{g_1}(Q^2)}{\pi}\right] = 1 \tag{36}$$

where the underlying form at zero β function is dictated by conformal symmetry [265]. Here $\alpha_R(s)/\pi$ and $-\alpha_{g_1}(Q^2)/\pi$ represent the entire radiative corrections to $R_{e^+e^-}(s)$

and the Bjorken sum rule for the $g_1(x, Q^2)$ structure function measured in spin-dependent deep inelastic scattering, respectively. The relation between s^* and Q^2 can be computed order by order in perturbation theory, as in the BLM method [61]. The ratio of physical scales guarantees that the effect of new quark thresholds is commensurate. Commensurate scale relations are renormalization-scheme independent and satisfy the group properties of the renormalization group. Each observable can be computed in any convenient renormalization scheme such as dimensional regularization. The $\overline{\rm MS}$ coupling can then be eliminated; it becomes only an intermediary [54]. In such a procedure there are no further renormalization scale (μ) or scheme ambiguities.

The generalized Crewther relation [60] can be derived by calculating the QCD radiative corrections to the deep inelastic sum rules and $R_{e^+e^-}$ in a convenient renormalization scheme such as the modified minimal subtraction scheme $\overline{\rm MS}$. One then algebraically eliminates $\alpha_{\overline{\rm MS}}(\mu)$. Finally, BLM scale-setting [61] is used to eliminate the β-function dependence of the coefficients. The form of the resulting relation between the observables thus matches the result which would have been obtained had QCD been a conformal theory with zero β function. The final result relating the observables is independent of the choice of intermediate $\overline{\rm MS}$ renormalization scheme.

The Crewther relation was originally derived assuming that the theory is conformally invariant; *i.e.*, for zero β function. In the physical case, where the QCD coupling runs, all non-conformal effects are resummed into the energy and momentum transfer scales of the effective couplings α_R and α_{g1}. The coefficients are independent of color and are the same in Abelian, non-Abelian, and conformal gauge theory. The non-Abelian structure of the theory is reflected in the expression for the scale Q^*.

Fits [225] to the experimental measurements of the R-ratio above the threshold for the production of $c\overline{c}$ bound states provide the empirical constraint: $\alpha_R(\sqrt{s} = 5.0\ {\rm GeV})/\pi \simeq 0.08 \pm 0.03$. The prediction for the effective coupling for the deep inelastic sum rules at the commensurate momentum transfer Q is then $\alpha_{g_1}(Q = 12.33 \pm 1.20\ {\rm GeV})/\pi \simeq \alpha_{\rm GLS}(Q = 12.33 \pm 1.20\ {\rm GeV})/\pi \simeq 0.074 \pm 0.026$. Measurements of the Gross-Llewellyn Smith sum rule have so far only been carried out at relatively small values of Q^2 [266, 267]; however, one can use the results of the theoretical extrapolation [268] of the experimental data presented in [269] to obtain $\alpha_{\rm GLS}^{\rm extrapol}(Q = 12.25\ {\rm GeV})/\pi \simeq 0.093 \pm 0.042$. This range overlaps with the prediction from the generalized Crewther relation. It is clearly important to have higher precision measurements to fully test this fundamental QCD prediction.

The ratio of commensurate scales Λ_{BA} is determined by the requirement that all terms involving the β function are incorporated into the arguments of the running couplings, as in the original BLM procedure [61]. Physically, the ratio of scales corresponds to the fact that the physical observables have different quark threshold and distinct sensitivities to fermion loops. More generally, the differing scales are in effect relations between mean values of the physical scales which appear in loop integrations. Commensurate scale relations are transitive; *i.e.*, given the relation

between effective charges for observables A and C and C and B, the resulting relation between A and B is independent of C. In particular, transitivity implies $\Lambda_{AB} = \Lambda_{AC} \times \Lambda_{CB}$. The shift in scales which gives conformal coefficients in effect pre-sums the large and strongly divergent terms in the PQCD series which grow as $n!(\beta_0\alpha_s)^n$, *i.e.*, the infrared renormalons associated with coupling-constant renormalization [270, 271, 272, 273].

Similarly, commensurate scale relations obey the "conformal correspondence principle": the CSRs reduce to correct conformal relations when N_C and N_F are tuned to produce zero β function. Thus conformal symmetry provides a *template* for QCD predictions, providing relations between observables which are present even in theories which are not scale invariant. All effects of the nonzero beta function are encoded in the appropriate choice of relative scales $\Lambda_{AB} = Q_A/Q_B$.

In the case of QED, the heavy lepton potential (in the limit of vanishing external charge) is conventionally used to define the effective charge $\alpha_{qed}(q^2)$. This definition, the Dyson Goldberger-Low effective charge, resums all lepton pair vacuum polarization contributions in the photon propagator, and it is analytic in the lepton masses. The scale of the QCD coupling is thus the virtuality of the exchanged photon. The extension of this concept to non-abelian gauge theories is non-trivial due to the self interactions of the gauge bosons which make the usual self-energy gauge dependent. However, by systematically implementing the Ward identities of the theory, one can project out the unique self-energy of each *physical* particle. This results in a gluonic self-energy which is gauge independent and which can be resummed to define an effective charge that is related through the optical theorem to differential cross sections. The algorithm for performing the calculation at the diagrammatic level is called the "pinch technique" [63, 274, 275, 276]. The generalization of the pinch technique to higher loops has recently been investigated [277, 278, 279, 280, 281, 282]. Binosi and Papavassiliou have shown the consistency of the pinch technique to all orders in perturbation theory, thus allowing a systematic application to the QCD and electroweak effective charges at higher orders. The pinch scheme is in fact used to define the evolution of the couplings in the electroweak theory. The pinch scheme thus provides an ideal scheme for QCD couplings as well.

22 Effective Charges and Unification

Recently Michael Binger and I have analyzed a supersymmetric grand unification model in the context of physical renormalization schemes [283]. Our essential assumption is that the underlying *forces* of the theory become unified at the unification scale. We have found a number of qualitative differences and improvements in precision over conventional approaches. There is no need to assume that the particle spectrum has any specific structure; the effect of heavy particles is included both below and above the physical threshold. Unlike mathematical schemes such as dimensional reduction, $\overline{DR}$, the evolution of the coupling is analytic and unification

is approached continuously rather than at a fixed scale. The effective charge formalism thus provides a template for calculating all mass threshold effects for any given grand unified theory. These new threshold corrections are important in making the measured values of the gauge couplings consistent with unification. A comparison with the conventional scheme based on $\overline{DR}$ dimensional regularization scheme is summarized in Fig. 16.

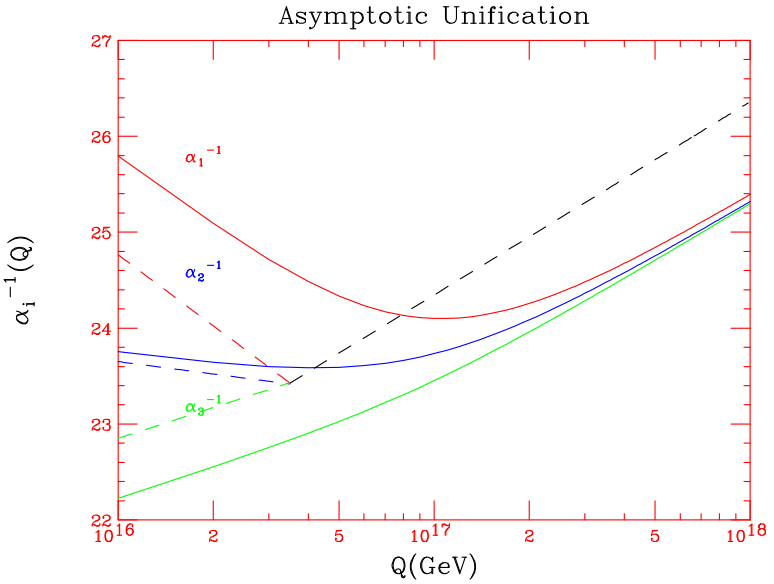

Figure 16: **Asymptotic Unification.** An illustration of strong and electroweak coupling unification in an $SU(5)$ supersymmetric model based on the pinch scheme effective charge. The solid lines are the analytic pinch scheme $\overline{PT}$ effective couplings, while the dashed lines are the $\overline{DR}$ couplings. For illustrative purposes, $a_3(M_Z)$ has been chosen so that unification occurs at a finite scale for $\overline{DR}$ and asymptotically for the $\overline{PT}$ couplings. Here $M_{SUSY} = 200$GeV is the mass of all light superpartners except the wino and gluino which have values $\frac{1}{2}mgx = M_{SUSY} = 2m_{wx}$.

23 Conclusions on Commensurate Scale Relations

Commensurate scale relations have a number of attractive properties:

1. The ratio of physical scales Q_A/Q_B which appears in commensurate scale relations reflects the relative position of physical thresholds, *i.e.* quark anti-quark pair production.

2. The functional dependence and perturbative expansion of the CSR are identical to those of a conformal scale-invariant theory where $\beta_A(\alpha_A) = 0$ and $\beta_B(\alpha_B) = 0$.

3. In the case of theories approaching fixed-point behavior $\beta_A(\overline{\alpha}_A) = 0$ and $\beta_B(\overline{\alpha}_B) = 0$, the commensurate scale relation relates both the ratio of fixed point couplings $\overline{\alpha}_A/\overline{\alpha}_B$ and the ratio of scales as the fixed point is approached.

4. Commensurate scale relations satisfy the Abelian correspondence principle [69]; *i.e.* the non-Abelian gauge theory prediction reduces to Abelian theory for $N_C \to 0$ at fixed $C_F\alpha_s$ and fixed N_F/C_F.

5. The perturbative expansion of a commensurate scale relation has the same form as a conformal theory, and thus has no $n!$ renormalon growth arising from the β-function. It is an interesting conjecture whether the perturbative expansion relating observables to observable are in fact free of all $n!$ growth. The generalized Crewther relation, where the commensurate relation's perturbative expansion forms a geometric series to all orders, has convergent behavior.

Virtually any perturbative QCD prediction can be written in the form of a commensurate scale relation, thus eliminating any uncertainty due to renormalization scheme or scale dependence.

24 Inclusive Reactions: Complications from Final-State Interactions

It is usually assumed—following the parton model—that the leading-twist structure functions measured in deep inelastic lepton-proton scattering are simply the probability distributions for finding quarks and gluons in the target nucleon. In fact, gluon exchange between the fast, outgoing quarks and the target spectators effects the leading-twist structure functions in a profound way, leading to diffractive leptoproduction processes, shadowing of nuclear structure functions, and target spin asymmetries. In particular, the final-state interactions from gluon exchange lead to single-spin asymmetries in semi-inclusive deep inelastic lepton-proton scattering which are not power-law suppressed in the Bjorken limit.

A new understanding of the role of final-state interactions in deep inelastic scattering has recently emerged [34]. The final-state interactions from gluon exchange between the outgoing quark and the target spectator system lead to single-spin asymmetries in semi-inclusive deep inelastic lepton-proton scattering at leading twist in perturbative QCD; *i.e.*, the rescattering corrections of the struck quark with the target spectators are not power-law suppressed at large photon virtuality Q^2 at fixed x_{bj} [31] See Fig. 17. The final-state interaction from gluon exchange occurring immediately after the interaction of the current also produces a leading-twist diffractive component to deep inelastic scattering $\ell p \to \ell' p' X$ corresponding to color-singlet exchange with the target system; this in turn produces shadowing and anti-shadowing of the nuclear structure functions [34, 38]. In addition, one can show that the pomeron structure

function derived from diffractive DIS has the same form as the quark contribution of the gluon structure function [35].

The final-state interactions occur at a light-cone time $\Delta\tau \simeq 1/\nu$ after the virtual photon interacts with the struck quark, producing a nontrivial phase. Thus none of the above phenomena is contained in the target light-front wave functions computed in isolation. In particular, the shadowing of nuclear structure functions is due to destructive interference effects from leading-twist diffraction of the virtual photon, physics not included in the nuclear light-front wave functions. Thus the structure functions measured in deep inelastic lepton scattering are affected by final-state rescattering, modifying their connection to light-front probability distributions. Some of these results can be understood by augmenting the light-front wave functions with a gauge link, but with a gauge potential created by an external field created by the virtual photon $q\bar{q}$ pair current [32]. The gauge link is also process dependent [33], so the resulting augmented LFWFs are not universal.

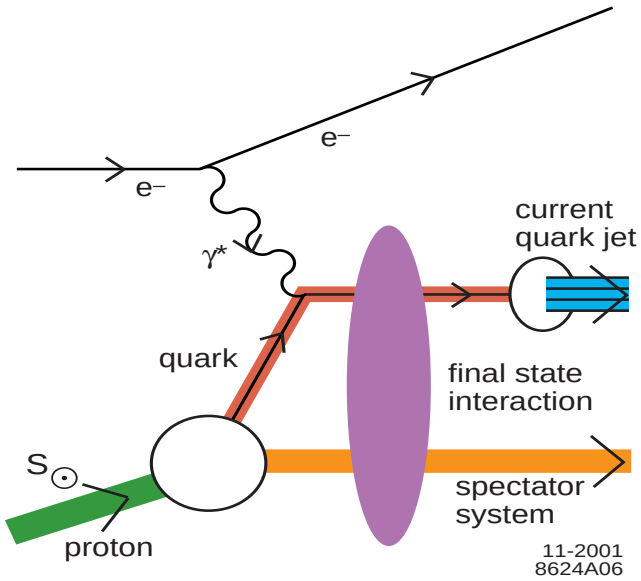

Figure 17: A final-state interaction from gluon exchange in deep inelastic lepton scattering. The difference of the QCD Coulomb-like phases in different orbital states of the proton produces a single proton spin asymmetry.

25 Single-Spin Asymmetries in Drell-Yan Processes

Single-spin asymmetries in hadronic reactions provide a remarkable window to QCD mechanisms at the amplitude level. In general, single-spin asymmetries measure the correlation of the spin projection of a hadron with a production or scattering plane [284]. Such correlations are odd under time reversal, and thus they can arise in

a time-reversal invariant theory only when there is a phase difference between different spin amplitudes. Specifically, a nonzero correlation of the proton spin normal to a production plane measures the phase difference between two amplitudes coupling the proton target with $J_p^z = \pm\frac{1}{2}$ to the same final-state. The calculation requires the overlap of target light-front wavefunctions with different orbital angular momentum: $\Delta L^z = 1$; thus a single-spin asymmetry (SSA) provides a direct measure of orbital angular momentum in the QCD bound state.

Consider the SSA produced in semi-inclusive deep inelastic scattering $\ell p^\uparrow \to \ell' \pi X$. In the target rest frame, such a single target spin correlation corresponds to the T-odd triple product $\vec{S}_p \cdot \vec{p}_\pi \times \vec{q}$. (The covariant form of this correlation is $\epsilon_{\mu\nu\sigma\tau} S_p^\mu p^\nu q^\sigma p_\pi^\tau$.) Significant asymmetries A_{UL} and A_{UT} of this type have in fact been observed for targets polarized parallel to or transverse to the lepton beam direction [285, 286].

Dae Sung Hwang and Ivan Schmidt [31] and I have shown that the QCD final-state interactions (gluon exchange) between the struck quark and the proton spectator system in semi-inclusive deep inelastic lepton scattering can produce single-spin asymmetries which survive in the Bjorken limit. Such effects are proportional to the matrix element of a higher-twist quark-quark-gluon correlator in the target hadron, and thus it has been assumed on dimensional grounds that any single-spin asymmetry arising from this source must be suppressed by a power of the momentum transfer Q in the Bjorken limit. However, another momentum scale enters into the semi-inclusive process—the transverse momentum $\vec{r}_\perp = \vec{p_{\pi}}_\perp - \vec{q}_\perp$ of the emitted pion relative to the photon direction, and we have shown that the power-law suppression due to the higher-twist quark-quark-gluon correlator takes the form of an inverse power of $r_\perp$ rather than Q.

Corrections from spin-one gluon exchange in the initial- or final-state of QCD processes are not suppressed at high energies because the coupling is vector-like. Therefore, as a consequence of the gauge coupling of QCD, single-spin asymmetries in semi-inclusive deep inelastic scattering survive in the Bjorken limit of large Q^2 at fixed x_{bj} and fixed $\vec{r}_\perp$. The resulting final-state phases are analogous to the "Coulomb" phases to the hard subprocess which arises from gauge interactions between outgoing charge particles in QED [287]. More specifically, we require the difference between the gauge interaction phases for the $J_p^z = \pm\frac{1}{2}$ amplitudes. The phases depend on the spin because the outgoing particles interact at different impact separation corresponding to their different relative orbital angular momentum.

In our paper [31], we explicitly evaluated the SSA for electroproduction for a specific model of a spin-half proton of mass M with charged spin-half and spin-0 constituents of mass m and λ, respectively, as in the QCD-motivated quark-diquark model of a nucleon. The basic leptoproduction reaction is then $\gamma^* p \to q(qq)_0$. Our analysis predicts a nonzero SSA for the target spin normal to the photon to quark-jet $\vec{S}_p \cdot \vec{p}_q \times \vec{q}$ which can be determined by using a jet variable such as thrust to determine the current quark direction; *i.e.*, we predict a SSA even without final-state jet hadronization. Our mechanism is thus distinct from a description of SSA based

on transversity and phased fragmentation functions.

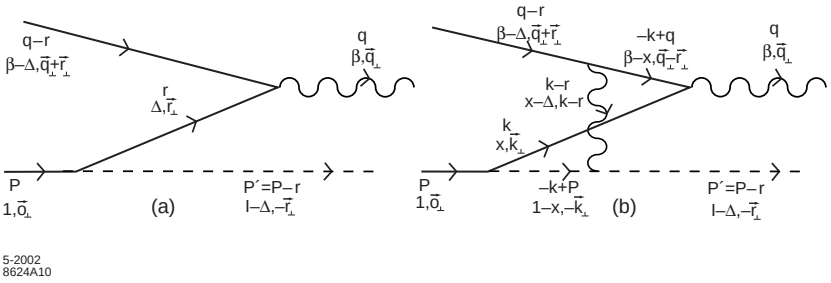

Figure 18: The initial-state interaction in the Drell-Yan process.

Recently Collins [288] has pointed out some important consequences of these results for SSA in deep inelastic scattering. In this treatment, the final-state interactions of the struck quark are incorporated into Wilson line path-ordered exponentials which augment the light-cone wavefunctions. [See also [289].] Since the final-state interactions appear at short light-cone times $\Delta x^+ = \mathcal{O}(1/\nu)$ after the virtual photon acts, they can be distinguished from hadronization processes which occur over long times. As first noted by Collins, initial-state interactions between the annihilating antiquark and the spectator system of the target can produce single-spin asymmetries in the Drell-Yan process.

Dae Sung Hwang, Ivan Schmidt and I [105] have extended our analysis to initial- and final-state QCD effects to predict single-spin asymmetries in hadron-induced hard QCD processes. Specifically, we shall consider the Drell-Yan (DY) type reactions [290] such as $\overline{p}p^{\uparrow} \to \ell^+\ell^- X$. Here the target particle is polarized normal to the production plane. The target spin asymmetry can be produced due to the initial-state gluon-exchange interactions between the interacting antiquark coming from one hadronic system and the spectator system of the other. This is shown in the diagram of Fig. 18. The importance of initial-state interactions in the theory of massive lepton pair production, $Q_\perp$ broadening, and energy loss in a nuclear target has been discussed in Refs. [291, 292, 293].

The orientation of the target spin $S_z = \pm 1/2$ corresponds to amplitudes differing by relative orbital angular momentum $\Delta L^z = 1$. The initial-state interaction from a gluon exchanged between the annihilating antiquark and target spectator system depends in detail on this relative orbital angular momentum. In contrast, the initial or final-state interactions due to the exchange of gauge particles between partons not participating in the hard subprocess do not contribute to the SSA. Such spectator-spectator interactions occur at large impact separation and are not sensitive to just one unit difference $\Delta L^z = 1$ of the orbital angular momentum of the target wavefunction.

Our mechanism thus depends on the interference of different amplitudes arising from the target hadron's wavefunction and is distinct from probabilistic measures

of the target such as transversity. It is also important to note that the target spin asymmetries which we compute in the DY and DIS processes require the same overlap of wavefunctions which enters the computation of the target nucleon's magnetic moment. In addition, by selecting different initial mesons in the DY process, we can isolate the flavor of the annihilating quark and antiquark. The flavor dependence of single-spin asymmetries thus has the potential to provide detailed information of the spin and flavor content of nucleons at the amplitude level.

As in our analysis of semi-inclusive DIS, we calculated the single-spin asymmetry in the Drell-Yan process induced by initial-state interactions by adopting an effective theory of a spin-$\frac{1}{2}$ proton of mass M with charged spin-$\frac{1}{2}$ and spin-0 constituents of mass m and λ, respectively, as in a quark-diquark model. We will take the initial particle to be just an antiquark. The result for specific meson projectiles such as $Mp^\uparrow \to \ell^+\ell^- X$ is then obtained by convolution with the antiquark distribution of the incoming meson. One can also incorporate target nucleon wavefunctions with a quark-vector diquark structure. In a more complete study, one should allow for a many-parton light-front Fock state wavefunction representation of the target. The results, however, are always normalized to the quark contribution to the proton anomalous moment, and thus are basically model-independent.

26 Crossing

There is a simple diagrammatic connection between the amplitude describing the initial-state interaction of the annihilating antiquark, which gives a single-spin asymmetry for the Drell-Yan process $\pi p^\uparrow \to \ell^+\ell^- X$, and the final-state rescattering amplitude of the struck quark, which gives the single-spin asymmetries in semi-inclusive deep inelastic leptoproduction $\ell p^\uparrow \to \ell' \pi X$. The crossing of the Feynman amplitude for $\gamma^*(\tilde{q})p(P) \to (\tilde{q}+r)(P-r)$ in DIS gives $(-\tilde{q}-r)p(P) \to \gamma^*(-\tilde{q})(P-r)$ for DY by reversing the four-vectors of the photon and quark lines. The outgoing quark with momentum $\tilde{q}+r$ in DIS becomes the incoming antiquark with momentum $-\tilde{q}-r$ in DY. We can use crossing of the Lorentz invariant amplitudes for DIS as a guide for obtaining the amplitudes for DY amplitude [294].

In general, one cannot use crossing to relate imaginary parts of amplitudes to each other, since under crossing, real and imaginary parts become connected. However, in our case, the relevant one-gluon exchange diagrams in DIS and DY are both purely imaginary at high energy, so their magnitudes are related by crossing. Thus a crucial test of our mechanism is an exact relation between the magnitude and flavor dependence of the SSA in the Drell-Yan reaction and the SSA in deep inelastic scattering. We thus predict the DY SSA of the proton spin with the normal to the antiquark to virtual photon plane: $\vec{S}_p \cdot \vec{p}_{\overline{q}} \times \vec{\tilde{q}}$. It is identical – up to a sign – to the SSA computed in DIS for $\vec{S}_p \cdot \vec{p}_q \times \vec{q}$.

The phase arising from the initial- and final-state interactions in QCD is analogous

to the Coulomb phase of Abelian QED amplitudes. The Coulomb phase depends on the product of charges and relative velocity of each ingoing and outgoing charged pair [287]. Thus the sign of the phase in DY and DIS are opposite because of the different color charge of the ingoing $\overline{3}_C$ antiquark in DY and the outgoing 3_C quark in DIS.

The asymmetry in the Drell-Yan process is thus the same as that obtained in DIS, with the appropriate identification of variables, but with the opposite sign. This has been stressed recently by Collins [288]. Therefore the single-spin asymmetry transverse to the production plane in the Drell-Yan process can be obtained from the results of our recent paper [31]:

$$\begin{aligned} \mathcal{P}_y &= -\frac{e_1 e_2}{8\pi} \frac{2\left(\Delta M + m\right) r^1}{\left[\left(\Delta M + m\right)^2 + \vec{r}_\perp^{\,2}\right]} \left[\vec{r}_\perp^{\,2} + \Delta(1-\Delta)(-M^2 + \frac{m^2}{\Delta} + \frac{\lambda^2}{1-\Delta})\right] \\ &\times \frac{1}{\vec{r}_\perp^{\,2}} \ln \frac{\vec{r}_\perp^{\,2} + \Delta(1-\Delta)(-M^2 + \frac{m^2}{\Delta} + \frac{\lambda^2}{1-\Delta})}{\Delta(1-\Delta)(-M^2 + \frac{m^2}{\Delta} + \frac{\lambda^2}{1-\Delta})} \,. \end{aligned} \tag{37}$$

Here $\Delta = \frac{q^2}{2P\cdot q} = \frac{q^2}{2M\nu}$ where ν is the energy of the lepton pair in the target rest frame. An explicit calculation is given in Ref. [105]. An illustration of the predictions for electroproduction is shown in Fig. 19.

The natural framework for the wavefunctions which appear in the SSA calculations is the light-front Fock expansion [76, 10]. In principle, the light-front wavefunctions for hadrons can be obtained by solving for the eigen-solutions of the light-front QCD Hamiltonian. Such wavefunctions are real and include all interactions up to a given light-front time. The final-state gluon exchange corrections which provide the SSA for semi-inclusive DIS occur immediately after the virtual photon strikes the active quark. Such interactions are not included in the light-front wavefunctions, just as Coulomb final-state interactions are not included in the Schrödinger bound state wavefunctions in QED. As noted above Collins [288] has argued that since the relevant rescattering interactions of the struck quark occur very close in light-cone time to the hard interaction, one can augment the light-front wavefunctions by a Wilson line factor which incorporates the effects of the final-state interactions in semi-inclusive DIS. However, such augmented wavefunctions are not universal and process independent; for example, in the case of the DY process, an incoming Wilson line of opposite phase must be used.

It should be emphasized that the same overlap of light-front wavefunctions with $\Delta L^z = 1$ which gives single-spin asymmetries also yields the Pauli form factor $F_2(t)$ and the generalized parton distribution $E(x,\zeta,t)$ entering deeply virtual Compton scattering [295, 296, 210, 85, 84]. Each quark of the target wavefunction appears additively, weighted linearly by the quark charge in the case of the Pauli form factor and weighted quadratically in the case of deep inelastic scattering, the Drell-Yan reaction and deeply virtual Compton scattering.

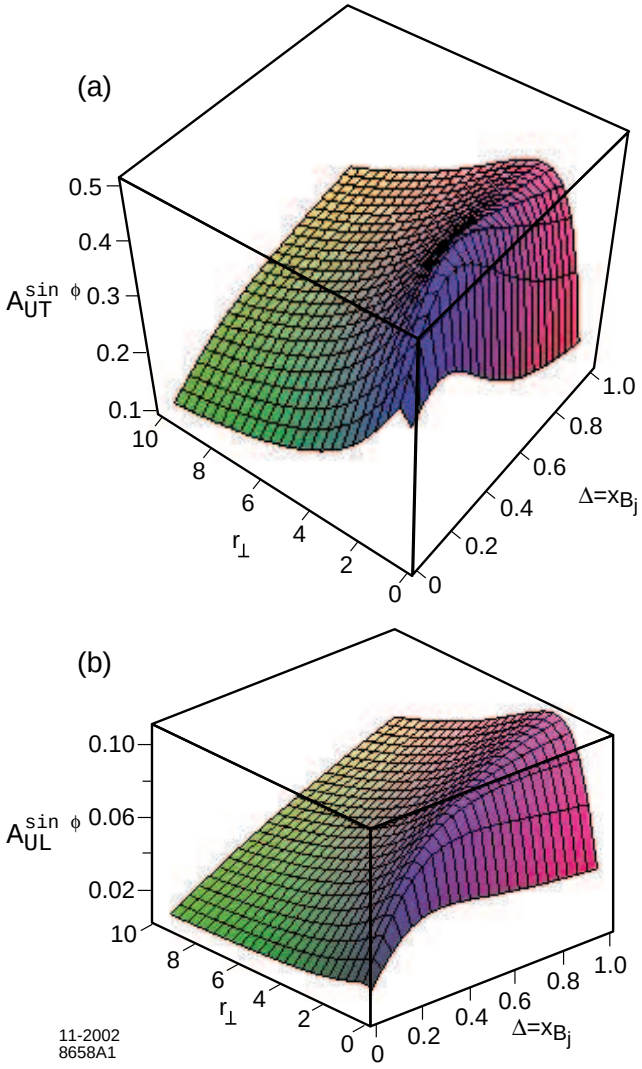

Figure 19: Model predictions for the target single-spin asymmetry $A_{UT}^{\sin\phi}$ for charged and neutral current deep inelastic scattering resulting from gluon exchange in the final state. Here $r_\perp$ is the magnitude of the transverse momentum of the outgoing quark relative to the photon or vector boson direction, and $\Delta = x_{bj}$ is the light-cone momentum fraction of the struck quark. The parameters of the model are given in the text. In (a) the target polarization is transverse to the incident lepton direction. The asymmetry in (b) $A_{UL}^{\sin\phi} = K A_{UT}^{\sin\phi}$ includes a kinematic factor $K = \frac{Q}{\nu}\sqrt{1-y}$ for the case where the target nucleon is polarized along the incident lepton direction. For illustration, we have taken $K = 0.26\sqrt{x}$, with $E_{lab} = 27.6$ GeV and $y = 0.5$.

Thus the same physical mechanism which produces a leading-twist single-spin asymmetry in semi-inclusive deep inelastic lepton scattering, also leads to a leading twist single-spin asymmetry in the Drell-Yan process. The initial-state interaction between the annihilating antiquark with the spectator of the target produces the required phase correlation. The equality in magnitude, but opposite sign, of the single-spin asymmetries in semi-inclusive DIS and the corresponding Drell-Yan processes is an important check of our mechanism.

It has been conventional to assume that the effects of initial- and final-state interactions are always power-law suppressed for hard processes in QCD. In fact, this is not in general correct, as can be seen from our analyses of leading-twist single-spin asymmetries in the Drell-Yan process and semi-inclusive deep inelastic scattering. The initial- and final-state interactions which survive in the scaling limit occur in light-cone time $\tau = \mathcal{O}(1/Q)$ immediately before or after the hard subprocess. Other initial- and final-state interactions, such as those between the spectator of the incident hadron and the spectator of the target hadron in the DY process, take place over long time scales, and they only provide inconsequential unitary phase corrections to the process. This is in accord with our intuition that interactions which occur at distant times cannot affect the primary reaction.

Our formalism can be adopted to single-spin asymmetries in more general hard inclusive reactions, such as $\overline{p}p^{\uparrow} \to \pi X$, where the pion is detected at high transverse momentum [297, 298]. In such cases, one must identify the relevant hard quark-gluon subprocess and analyze a set of gluon exchange corrections which connect the spectators of the polarized hadron with the active quarks and gluons participating in the hard subprocess. However, this type of final-state interaction cannot be readily identified as an augmented target wavefunction. It is also clear from our analyses that there are potentially important corrections to the hard quark propagator in hard exclusive subprocesses such as deeply virtual Compton scattering or exclusive meson electroproduction. These rescattering interactions of the propagating quark can provide new single-spin observables and will correct analyses based on the handbag approximation.

The empirical study of single-spin asymmetries in hard inclusive and exclusive processes thus provides a new window to the investigation of hadron spin, angular momentum, and flavor structure of hadrons.

27 The Origin of Nuclear Shadowing and Anti-shadowing

The Bjorken-scaling diffractive interactions on nucleons in a nucleus also lead to shadowing and anti-shadowing of the nuclear structure functions [34, 38]. The physics of nuclear shadowing in deep inelastic scattering can be most easily understood in the laboratory frame using the Glauber-Gribov picture [299, 300]. The virtual photon, W

or Z^0, produces a quark-antiquark color-dipole pair which can interact diffractively or inelastically on the nucleons in the nucleus. The destructive interference of diffractive amplitudes from pomeron exchange on the upstream nucleons then causes shadowing of the virtual photon interactions on the back-face nucleons [301, 302, 303, 304, 305, 306]. As emphasized by Ioffe [303], the coherence between processes which occur on different nucleons at separation L_A requires small Bjorken x_B : $1/Mx_B = 2\nu/Q^2 \geq L_A$. The coherence between different quark processes is also the basis of saturation phenomena in DIS and other hard QCD reactions at small x_B [307], and coherent multiple parton scattering has been used in the analysis of $p+A$ collisions in terms of the perturbative QCD factorization approach [308]. An example of the interference of one- and two-step processes in deep inelastic lepton-nucleus scattering illustrated in Fig. 20.

An important aspect of the shadowing phenomenon is that the diffractive contribution $\gamma^* N \to XN'$ to deep inelastic scattering (DDIS) where the nucleon N_1 in Fig. 20 remains intact is a constant fraction of the total DIS rate, confirming that it is a leading-twist contribution. The Bjorken scaling of DDIS has been observed at HERA [309, 310, 311]. As shown in Ref. [34], the leading-twist contribution to DDIS arises in QCD in the usual parton model frame when one includes the nearly instantaneous gluon exchange final-state interactions of the struck quark with the target spectators. The same final state interactions also lead to leading-twist single-spin asymmetries in semi-inclusive DIS [31]. Thus the shadowing of nuclear structure functions is also a leading-twist effect.

It was shown in Ref. [38] that if one allows for Reggeon exchanges which leave a nucleon intact, then one can obtain *constructive* interference among the multi-scattering amplitudes in the nucleus. A Bjorken-scaling contribution to DDIS from Reggeon exchange has in fact also been observed at HERA [310, 311]. The strength and energy dependence of the $C = +$ Reggeon $t-$channel exchange contributions to virtual Compton scattering is constrained by the Kuti-Weisskopf [312] behavior $F_2(x) \sim x^{1-\alpha_R}$ of the non-singlet electromagnetic structure functions at small x. The phase of the Reggeon exchange amplitude is determined by its signature factor. Because of this complex phase structure [38], one obtains constructive interference and *antishadowing* of the nuclear structure functions in the range $0.1 < x < 0.2$—a pronounced excess of the nuclear cross section with respect to nucleon additivity [313].

In the case where the diffractive amplitude on N_1 is imaginary, the two-step process has the phase $i \times i = -1$ relative to the one-step amplitude, producing destructive interference. (The second factor of i arises from integration over the quasi-real intermediate state.) In the case where the diffractive amplitude on N_1 is due to $C = +$ Reggeon exchange with intercept $\alpha_R(0) = 1/2$, for example, the phase of the two-step amplitude is $\frac{1}{\sqrt{2}}(1-i) \times i = \frac{1}{\sqrt{2}}(i+1)$ relative to the one-step amplitude, thus producing constructive interference and antishadowing.

The effective quark-nucleon scattering amplitude includes Pomeron and Odderon contributions from multi-gluon exchange as well as Reggeon quark-exchange contribu-

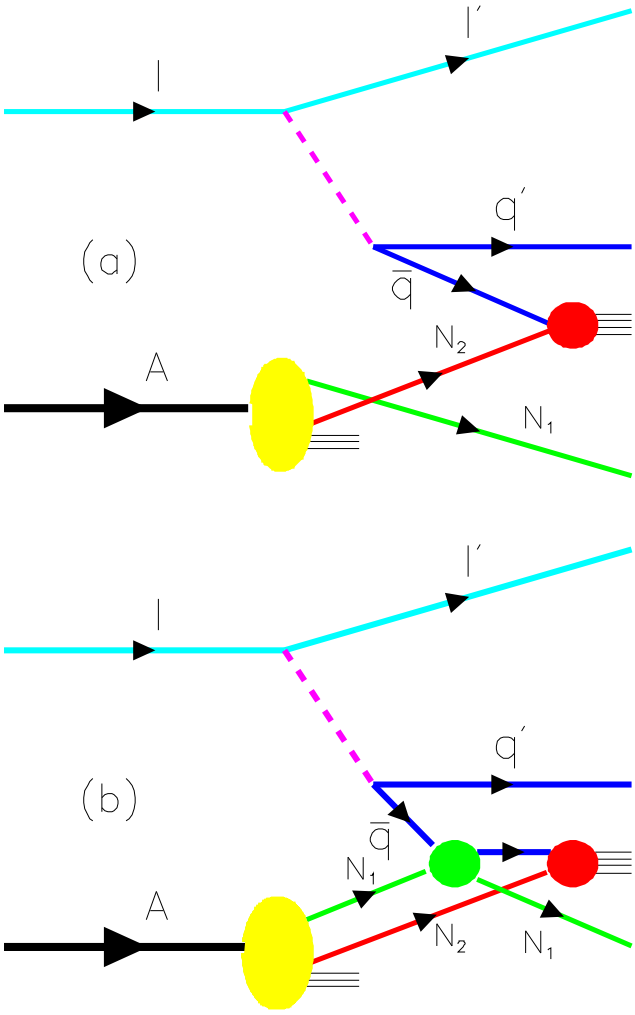

Figure 20: The one-step and two-step processes in DIS on a nucleus. If the scattering on nucleon N_1 is via pomeron exchange, the one-step and two-step amplitudes are opposite in phase, thus diminishing the $\overline{q}$ flux reaching N_2. This causes shadowing of the charged and neutral current nuclear structure functions.

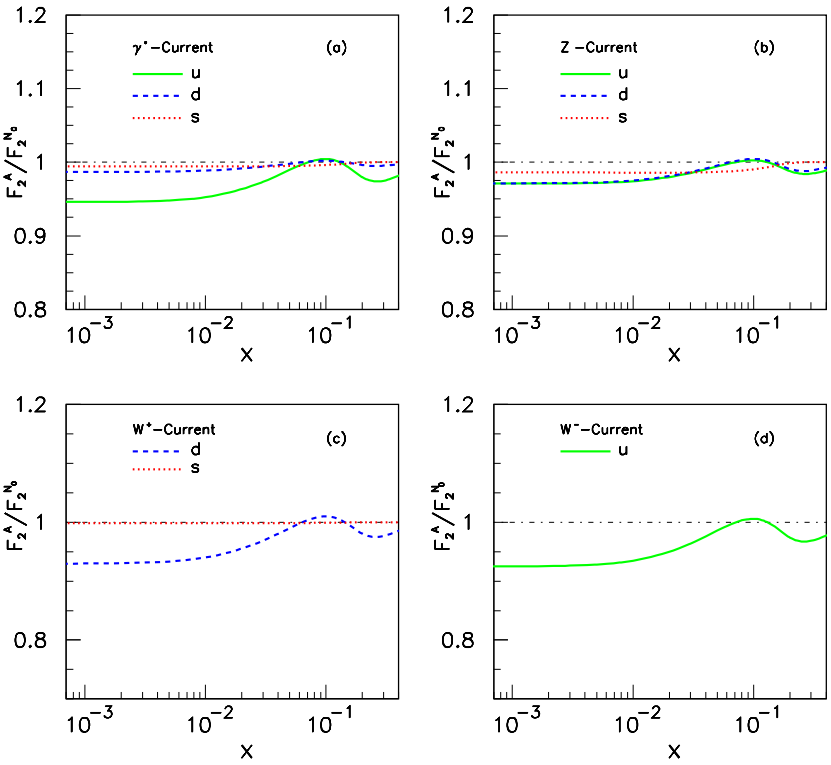

Figure 21: The quark contributions to the ratios of structure functions at $Q^2 = 1$ GeV^2. The solid, dashed and dotted curves correspond to the u, d and s quark contributions, respectively. This corresponds in our model to the nuclear dependence of the $\sigma(\overline{u}-A)$, $\sigma(\overline{d}-A)$, $\sigma(\overline{s}-A)$ cross sections, respectively. In order to stress the individual contribution of quarks, the numerator of the ratio $F_2^A/F_2^{N_0}$ shown in these two figures is obtained from the denominator by a replacement q^{N_0} into q^A for only the considered quark. As a result, the effect of antishadowing appears diminished.

tions [38]. The coherence of these multiscattering nuclear processes leads to shadowing and antishadowing of the electromagnetic nuclear structure functions in agreement with measurements. The Reggeon contributions to the quark scattering amplitudes depend specifically on the quark flavor; for example the isovector Regge trajectories couple differently to u and d quarks. The s and $\overline{s}$ couple to yet different Reggeons. This implies distinct anti-shadowing effects for each quark and antiquark component of the nuclear structure function. Ivan Schmidt, Jian-Jun Yang, and I [314] have shown that this picture leads to substantially different antishadowing for charged and neutral current reactions.

Figures 21–22 illustrate the individual quark q and anti-quark $\overline{q}$ contributions to the ratio of nuclear ^{56}Fe (structure functions $R = F_2^A/F_2^{N_0}$ in a model calculation where the Reggeon contributions are constrained by the Kuti-Weisskopf behavior [312] of the nucleon structure functions at small x_{bj}. Because the strange quark distribution

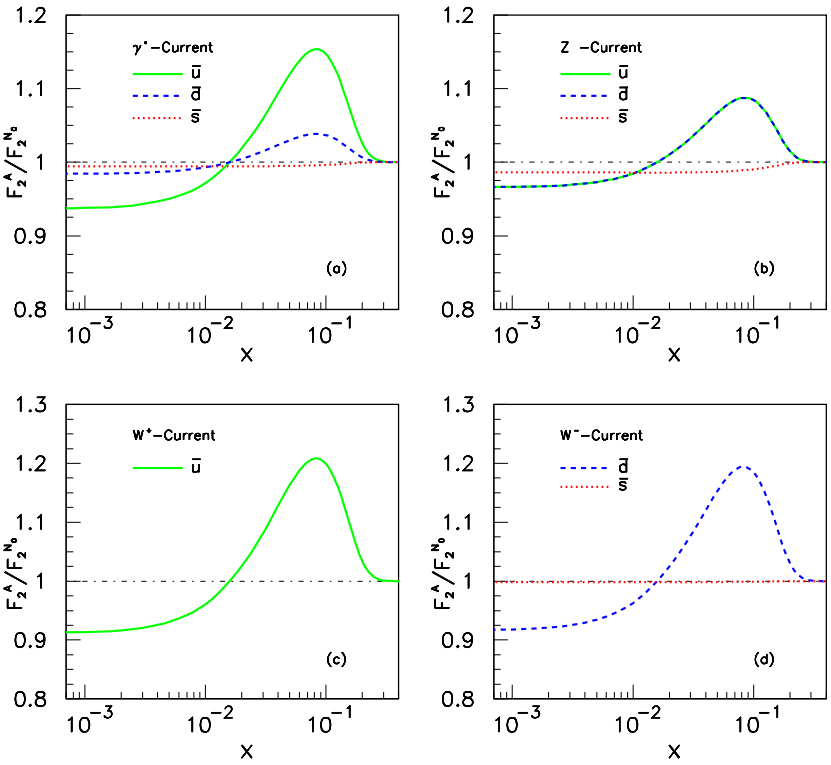

Figure 22: The anti-quark contributions to ratios of the structure functions at $Q^2 = 1$ GeV^2. The solid, dashed and dotted curves correspond to $\overline{u}$, $\overline{d}$ and $\overline{s}$ quark contributions, respectively. This corresponds in our model to the nuclear dependence of the $\sigma(u-A)$, $\sigma(d-A)$, $\sigma(s-A)$ cross sections, respectively. In order to stress the individual contribution of quarks, the numerator of the ratio $F_2^A/F_2^{N_0}$ shown in these two figures is obtained from the denominator by a replacement $\overline{q}^{N_0}$ into $\overline{q}^A$ for only the considered anti-quark.

is much smaller than u and d quark distributions, the strange quark contribution to the ratio is very close to 1 although s^A/s^{N_0} may significantly deviate from 1.

Our analysis leads to substantially different nuclear antishadowing for charged and neutral current reactions; in fact, the neutrino and antineutrino DIS cross sections are each modified in different ways due to the various allowed Regge exchanges. The non-universality of nuclear effects will modify the extraction of the weak-mixing angle $\sin^2\theta_W$, particularly because of the strong nuclear effects for the F_3 structure function. The shadowing and antishadowing of the strange quark structure function in the nucleus can also be considerably different than that of the light quarks. We thus find that part of the anomalous NuTeV result [315] for $\sin^2\theta_W$ could be due to the nonuniversality of nuclear antishadowing for charged and neutral currents. Our picture also implies non-universality for the nuclear modifications of spin-dependent structure functions. A new determination of $\sin^2\theta_W$ is also expected from the neutrino

scattering experiment NOMAD at CERN [316]. A systematic program of measurements of the nuclear effects in charged and neutral current reactions could also be carried out in high energy electron-nucleus colliders such as HERA and eRHIC, or by using high intensity neutrino beams [317].

Thus the antishadowing of nuclear structure functions depends in detail on quark flavor. Careful measurements of the nuclear dependence of charged, neutral, and electromagnetic DIS processes are thus needed to establish the distinctive phenomenology of shadowing and antishadowing and to make the NuTeV results definitive. It is also important to map out the shadowing and antishadowing of each quark component of the nuclear structure functions to illuminate the underlying QCD mechanisms. Such studies can be carried out in semi-inclusive deep inelastic scattering for the electromagnetic current at Hermes and at Jefferson Laboratory by tagging the flavor of the current quark. It is also important to measure antishadowing and test non-universality in antiproton reactions at GSI such as $\overline{p}A \to \ell^+\ell^- X$ as well in pion- and kaon-induced Drell-Yan reactions [318, 319].

28 Conclusions

New theoretical developments in QCD, together with a number of key experiments, have brought new perspectives to our understanding of dynamical aspects of the strong interactions.

Color transparency, as evidenced by the Fermilab measurements of diffractive dijet production, implies that a pion can interact coherently throughout a nucleus with minimal absorption, in dramatic contrast to traditional Glauber theory based on a fixed $\sigma_{\pi n}$ cross section. Color transparency gives direct validation of the gauge interactions of QCD.

The observation that $\simeq 10\%$ of the positron-proton deep inelastic cross section at HERA is diffractive points to the importance of final-state gauge interactions as well as a new perspective to the nature of the hard pomeron. The same interactions are responsible for nuclear shadowing and Sivers-type single-spin asymmetries in semi-inclusive deep inelastic scattering and in Drell-Yan reactions. These new observations are in contradiction to parton model and light-cone gauge based arguments that final state interactions can be ignored at leading twist. The modifications of the deep inelastic lepton-proton cross section due to final state interactions are consistent with color-dipole based scattering models and imply that the traditional identification of structure functions with the quark probability distributions computed from the wavefunctions of the target hadron computed in isolation must be modified.

Empirical evidence continues to accumulate that the strange-antistrange quark distributions are not symmetric in the proton, and that the proton wavefunction contains charm quarks with large light-cone momentum fractions x. The recent observation by SELEX that doubly-charmed quarks are produced at large x_F and small p_T in hadron-nucleus collisions is evidence for the diffractive dissociation of complex

off-shell Fock states of the projectile. These observations contradict the traditional view that sea quarks and gluons are always produced perturbatively via DGLAP evolution. The existence of intrinsic glue and charm has strong consequences for lepton-pair and open charm production Measurable with antiproton beams.

The dynamical origins of the antishadowing of nuclear structure functions in the domain $0.1 < x_{Bj} < 1$ is now becoming understood. An important conclusion is that antishadowing is nonuniversal – different for quarks and antiquarks and different for strange quarks versus light quarks. This has important consequences for antiproton–nucleus Drell-Yan and other inclusive reactions.

The most dramatic spin correlation ever observed is the large $4:1$ A_{NN} asymmetry measured in elastic proton-proton scattering at large CM angles at $\sqrt{s} \simeq 5$ Gev. If this effect is due to intermediate $uuduudc\bar{c}$ states—corresponding to the formation of "octoquark" resonances—then there should be comparable effects in elastic $\overline{p}p$ scattering.

Dimensional counting rules for hard exclusive processes have now been derived in the context of nonperturbative QCD using the AdS/CFT correspondence. The recent measurements of the predicted s^{11} scaling behavior in deuteron photodisintegration adds further evidence for the dominance of leading-twist quark-gluon subprocesses. Lowest-order perturbation theory appears to give the proper scaling, but not the magnitude of the measured hard exclusive cross sections, suggesting the importance of higher-order corrections or even a nonperturbative resummation. I have given evidence that the running coupling has constant fixed-point behavior, which together with BLM scale fixing, helps explains the near conformal scaling behavior of the fixed-CM angle cross sections. The angular distribution of hard exclusive processes is generally consistent with quark interchange, as predicted from large N_C considerations. Other important tests of hard exclusive processes can be carried out with antiproton beams, including timelike proton form factors. I have also noted the importance of testing for the presence of $J = 0$ behavior in two-photon reactions such as $\overline{p}p \to \gamma\gamma$ as a test of the near-local two-photon couplings to quarks.

A rigorous prediction of QCD is the "hidden color" of nuclear wavefunctions at short distances. I have noted that the two-scale behavior, as well as the large magnitude of the hard component of the reduced deuteron form factor at high Q^2, gives importance evidence for this essential feature of the non-Abelian theory. This points to the importance of studying hard $\overline{p}$ deuteron reactions.

I have emphasized several theoretical tools: light-front wavefunctions as a representation of hadrons at the amplitude level, the Abelian correspondence principle, and the conformal template. It is important to note that there is no renormalization scale ambiguity in QCD when one uses effective charges to define the perturbative expansions or when one related observable to observable, as in commensurate scale relations such as the generalized Crewther relation.

I have also discussed how the remarkable AdS/CFT duality, which has been established between supergravity string theory in 10 dimensions and conformal extensions

of QCD, is now providing to a new understanding of QCD at strong coupling and a new examination at its nearly-conformal structure.

The antiproton storage ring HESR to be constructed at GSI will open up a new range of perturbative and nonperturbative tests of QCD in exclusive and inclusive reactions. I have discussed 21 tests of QCD using antiproton beams which can illuminate these novel features of QCD. The proposed experiments include the formation of exotic hadrons, measurements of timelike generalized parton distributions, the production of charm at threshold, transversity measurements in Drell-Yan reactions, and searches for single-spin asymmetries. The interactions of antiprotons in nuclear targets will allow tests of exotic nuclear phenomena such as color transparency, hidden color, reduced nuclear amplitudes, and the non-universality of nuclear antishadowing.

Acknowedgements

I wish to thank Uli Weidner and his colleagues for hosting this outstanding Fermi School of Physics at Varenna. This talk is based on collaborations with Carl Carlson, Markus Diehl, Guy de Teramond, Rikard Enberg, John Hiller, Paul Hoyer, Dae Sung Hwang, Gunnar Ingelman, Volodya Karmanov, Sven Menke, Carlos Merino, Joerg Raufeisen, Johan Rathsman, and Ivan Schmidt.

References

[1] J. Greensite, Prog. Part. Nucl. Phys. **51**, 1 (2003) [arXiv:hep-lat/0301023].

[2] D. J. Gross and F. Wilczek, Phys. Rev. Lett. **30**, 1343 (1973).

[3] H. D. Politzer, Phys. Rev. Lett. **30**, 1346 (1973).

[4] E. Klempt, arXiv:hep-ex/0101031.

[5] K. Rajagopal and F. Wilczek, arXiv:hep-ph/0011333.

[6] D. H. Rischke, Prog. Part. Nucl. Phys. **52**, 197 (2004) [arXiv:nucl-th/0305030].

[7] D. J. Schwarz, Annalen Phys. **12**, 220 (2003) [arXiv:astro-ph/0303574].

[8] J. C. Collins, D. E. Soper and G. Sterman, Adv. Ser. Direct. High Energy Phys. **5**, 1 (1988).

[9] G. T. Bodwin, Phys. Rev. D **31**, 2616 (1985) [Erratum-ibid. D **34**, 3932 (1986)].

[10] S. J. Brodsky and G. P. Lepage, in: *Perturbative Quantum Chromodynamics*, edited by A. H. Mueller (World Scientific, Singapore 1989).

[11] J. M. Maldacena, *Adv. Theor. Math. Phys.* **2**, 231 (1998) [*Int. J. Theor. Phys.* **38**, 1113 (1999)] [arXiv:hep-th/9711200].

[12] J. Polchinski and M. J. Strassler, *Phys. Rev. Lett.* **88**, 031601 (2002) [arXiv:hep-th/0109174].

[13] R. C. Brower and C. I. Tan, *Nucl. Phys. B* **662**, 393 (2003) [arXiv:hep-th/0207144].

[14] O. Andreev, *Phys. Rev. D* **67**, 046001 (2003) [arXiv:hep-th/0209256].

[15] H. Fritzsch, M. Gell-Mann and H. Leutwyler, Phys. Lett. B **47**, 365 (1973).

[16] G. 't Hooft, Nucl. Phys. B **75**, 461 (1974).

[17] H. C. Pauli and S. J. Brodsky, Phys. Rev. D **32**, 1993 (1985).

[18] K. Hornbostel, S. J. Brodsky and H. C. Pauli, Phys. Rev. D **41**, 3814 (1990).

[19] M. Burkardt, Nucl. Phys. A **504**, 762 (1989).

[20] S. J. Brodsky, H. C. Pauli and S. S. Pinsky, Phys. Rept. **301**, 299 (1998) [arXiv:hep-ph/9705477].

[21] K. G. Wilson, Phys. Rept. **23**, 331 (1976).

[22] T. DeGrand, Int. J. Mod. Phys. A **19**, 1337 (2004) [arXiv:hep-ph/0312241].

[23] P. Maris and C. D. Roberts, Int. J. Mod. Phys. E **12**, 297 (2003) [arXiv:nucl-th/0301049].

[24] S. Dalley, arXiv:hep-ph/0409139.

[25] P. A. M. Dirac, Rev. Mod. Phys. **21**, 392 (1949).

[26] J. Carbonell, B. Desplanques, V. A. Karmanov, and J. F. Mathiot, Phys. Rep. **300**, 215 (1998) [arXiv:nucl-th/9804029].

[27] S. J. Brodsky, *Presented at Workshop on QCD Down Under, Barossa Valley and Adelaide, Australia, 10-19 Mar 2004.* arXiv:hep-ph/0408071.

[28] S. J. Brodsky and B. Q. Ma, Phys. Lett. B **381**, 317 (1996) [arXiv:hep-ph/9604393].

[29] J. D. Bjorken, Phys. Rev. **179**, 1547 (1969).

[30] E. D. Bloom *et al.*, Phys. Rev. Lett. **23**, 930 (1969).

[31] S. J. Brodsky, D. S. Hwang and I. Schmidt, Phys. Lett. B **530**, 99 (2002) [arXiv:hep-ph/0201296].

[32] A. V. Belitsky, X. Ji and F. Yuan, Nucl. Phys. B **656**, 165 (2003) [arXiv:hep-ph/0208038].

[33] J. C. Collins, Phys. Lett. B **536**, 43 (2002) [arXiv:hep-ph/0204004].

[34] S. J. Brodsky, P. Hoyer, N. Marchal, S. Peigne and F. Sannino, Phys. Rev. D **65**, 114025 (2002) [arXiv:hep-ph/0104291].

[35] S. J. Brodsky, R. Enberg, P. Hoyer and G. Ingelman, arXiv:hep-ph/0409119.

[36] S. J. Brodsky, C. R. Ji and G. P. Lepage, Phys. Rev. Lett. **51**, 83 (1983).

[37] S. J. Brodsky and A. H. Mueller, Phys. Lett. B **206**, 685 (1988).

[38] S. J. Brodsky and H. J. Lu, Phys. Rev. Lett. **64**, 1342 (1990).

[39] S. J. Brodsky, I. Schmidt and J. J. Yang, arXiv:hep-ph/0409279.

[40] G. P. Zeller *et al.* [NuTeV Collaboration], Phys. Rev. Lett. **88**, 091802 (2002) [Erratum-ibid. **90**, 239902 (2003)] [arXiv:hep-ex/0110059].

[41] S. J. Brodsky and G. F. de Teramond, Phys. Lett. B **582**, 211 (2004) [arXiv:hep-th/0310227].

[42] S. J. Brodsky and G. R. Farrar, *Phys. Rev. Lett.* **31**, 1153 (1973).

[43] V. A. Matveev, R. M. Muradian and A. N. Tavkhelidze, *Lett. Nuovo Cim.* **7**, 719 (1973).

[44] S. J. Brodsky and G. R. Farrar, *Phys. Rev. D* **11**, 1309 (1975).

[45] S. J. Brodsky, arXiv:hep-ph/0408069.

[46] S. J. Brodsky, SLAC-PUB-10206 *Invited talk at International Conference on Color Confinement and Hadrons in Quantum Chromodynamics - Confinement 2003, Wako, Japan, 21-24 Jul 2003*

[47] G. Parisi, *Phys. Lett. B* **39**, 643 (1972).

[48] S. J. Brodsky, Y. Frishman, G. P. Lepage and C. Sachrajda, Phys. Lett. **91B**, 239 (1980).

[49] S. J. Brodsky, P. Damgaard, Y. Frishman and G. P. Lepage, *Phys. Rev. D* **33**, 1881 (1986).

[50] S. J. Brodsky, Y. Frishman and G. P. Lepage, *Phys. Lett. B* **167**, 347 (1986).

[51] V. M. Braun, G. P. Korchemsky and D. Muller, Prog. Part. Nucl. Phys. **51**, 311 (2003) [arXiv:hep-ph/0306057].

[52]

[52] G. P. Lepage and S. J. Brodsky, Phys. Lett. B **87**, 359 (1979).

[53] S. J. Brodsky and G. P. Lepage, SLAC-PUB-4947 *In *A.H. Mueller, (ed): Perturbative Quantum Chromodynamics, 1989, p. 93-240,* and S. J. Brodsky, SLAC-PUB-8649 *In *Shifman, M. (ed.): At the frontier of particle physics, vol. 2* 1343-1444.*

[54] S. J. Brodsky and H. J. Lu, *Phys. Rev. D* **51**, 3652 (1995) [arXiv:hep-ph/9405218].

[55] J. Rathsman, in *Proc. of the 5th International Symposium on Radiative Corrections (RADCOR 2000)* ed. Howard E. Haber, arXiv:hep-ph/0101248.

[56] S. J. Brodsky, E. Gardi, G. Grunberg and J. Rathsman, Phys. Rev. D **63**, 094017 (2001) [arXiv:hep-ph/0002065].

[57] G. Grunberg, JHEP **0108**, 019 (2001) [arXiv:hep-ph/0104098].

[58] T. Banks and A. Zaks, Nucl. Phys. B **196**, 189 (1982).

[59] V. M. Braun, S. E. Derkachov, G. P. Korchemsky and A. N. Manashov, Nucl. Phys. **B553**, 355 (1999) [arXiv:hep-ph/9902375].

[60] S. J. Brodsky, G. T. Gabadadze, A. L. Kataev and H. J. Lu, Phys. Lett. **B372**, 133 (1996) [arXiv:hep-ph/9512367].

[61] S. J. Brodsky, G. P. Lepage and P. B. Mackenzie, *Phys. Rev. D* **28**, 228 (1983).

[62] S. J. Brodsky, C. R. Ji, A. Pang and D. G. Robertson, Phys. Rev. D **57**, 245 (1998) [arXiv:hep-ph/9705221].

[63] J. M. Cornwall, Phys. Rev. D **26**, 1453 (1982).

[64] S. J. Brodsky, S. Menke, C. Merino and J. Rathsman, *Phys. Rev. D* **67**, 055008 (2003) [arXiv:hep-ph/0212078].

[65] M. Baldicchi and G. M. Prosperi, *Phys. Rev. D* **66**, 074008 (2002) [arXiv:hep-ph/0202172].

[66] S. Furui and H. Nakajima, arXiv:hep-lat/0403021.

[67] A. M. Badalian and A. I. Veselov, arXiv:hep-ph/0407082.

[68] K. Ackerstaff *et al.* [OPAL Collaboration], *Eur. Phys. J. C* **7**, 571 (1999) [arXiv:hep-ex/9808019].

[69] Phys. Lett. B **417**, 145 (1998) [arXiv:hep-ph/9707543].

[70] J. R. Ellis and M. Karliner, New J. Phys. **4**, 18 (2002) [arXiv:hep-ph/0108259].

[71] J. D. Bjorken and S. J. Brodsky, Phys. Rev. D **1**, 1416 (1970).

[72] K. Abe *et al.* [Belle Collaboration], Phys. Rev. Lett. **89**, 142001 (2002) [arXiv:hep-ex/0205104].

[73] S. J. Brodsky, A. S. Goldhaber and J. Lee, Phys. Rev. Lett. **91**, 112001 (2003) [arXiv:hep-ph/0305269].

[74] S. J. Brodsky and G. F. de Teramond, Phys. Rev. Lett. **60**, 1924 (1988).

[75] V. A. Matveev, R. M. Muradian and A. N. Tavkhelidze, Lett. Nuovo Cim. **7**, 719 (1973).

[76] G. P. Lepage and S. J. Brodsky, *Phys. Rev. D* **22**, 2157 (1980).

[77] R. Blankenbecler, S. J. Brodsky, J. F. Gunion and R. Savit, Phys. Rev. D **8**, 4117 (1973).

[78] O. Andreev and W. Siegel, arXiv:hep-th/0410131.

[79] S. J. Brodsky and G. P. Lepage, Phys. Rev. D **24**, 2848 (1981).

[80] J. F. Gunion, S. J. Brodsky and R. Blankenbecler, Phys. Rev. D **8**, 287 (1973).

[81] S. J. Brodsky and G. P. Lepage, Phys. Rev. D **24**, 1808 (1981).

[82] For a review of QCD tests in photon-photon collisions see, S. J. Brodsky, in *Proc. of the e^+e^- Physics at Intermediate Energies Conference* ed. Diego Bettoni, eConf **C010430**, W01 (2001) [arXiv:hep-ph/0106294].

[83] T. C. Brooks and L. J. Dixon, Phys. Rev. D **62**, 114021 (2000) [arXiv:hep-ph/0004143].

[84] S. J. Brodsky, M. Diehl and D. S. Hwang, Nucl. Phys. B **596**, 99 (2001) [arXiv:hep-ph/0009254].

[85] M. Diehl, T. Feldmann, R. Jakob and P. Kroll, Nucl. Phys. B **596**, 33 (2001) [Erratum-ibid. B **605**, 647 (2001)] [arXiv:hep-ph/0009255].

[86] S. J. Brodsky, F. E. Close and J. F. Gunion, Phys. Rev. D **6**, 177 (1972).

[87]

[87] X. d. Ji, J. P. Ma and F. Yuan, Phys. Rev. Lett. **90**, 241601 (2003) [arXiv:hep-ph/0301141].

[88] A. V. Belitsky, X. D. Ji and F. Yuan, Phys. Rev. Lett. **91**, 092003 (2003) [arXiv:hep-ph/0212351].

[89] S. J. Brodsky, J. R. Hiller, D. S. Hwang and V. A. Karmanov, Phys. Rev. D **69**, 076001 (2004) [arXiv:hep-ph/0311218].

[90] M. K. Jones *et al.* [Jefferson Lab Hall A Collaboration], Phys. Rev. Lett. **84**, 1398 (2000) [arXiv:nucl-ex/9910005].

[91] Y. C. Chen, A. Afanasev, S. J. Brodsky, C. E. Carlson and M. Vanderhaeghen, arXiv:hep-ph/0403058.

[92] S. J. Brodsky, C. E. Carlson, J. R. Hiller and D. S. Hwang, Phys. Rev. D **69**, 054022 (2004) [arXiv:hep-ph/0310277].

[93] S. J. Brodsky, C. E. Carlson, J. R. Hiller and D. S. Hwang, arXiv:hep-ph/0408131.

[94] G. Bertsch, S. J. Brodsky, A. S. Goldhaber and J. F. Gunion, Phys. Rev. Lett. **47**, 297 (1981).

[95] S. J. Brodsky, P. Hoyer, C. Peterson and N. Sakai, Phys. Lett. B **93**, 451 (1980).

[96] M. Franz, V. Polyakov and K. Goeke, Phys. Rev. D **62**, 074024 (2000) [arXiv:hep-ph/0002240].

[97] S. J. Brodsky, J. C. Collins, S. D. Ellis, J. F. Gunion and A. H. Mueller, DOE/ER/40048-21 P4 *Proc. of 1984 Summer Study on the SSC, Snowmass, CO, Jun 23 - Jul 13, 1984*

[98] B. W. Harris, J. Smith and R. Vogt, Nucl. Phys. B **461**, 181 (1996) [arXiv:hep-ph/9508403].

[99] S. J. Brodsky, E. Chudakov, P. Hoyer and J. M. Laget, Phys. Lett. B **498**, 23 (2001) [arXiv:hep-ph/0010343].

[100] B. Gittelman, K. M. Hanson, D. Larson, E. Loh, A. Silverman and G. Theodosiou, Phys. Rev. Lett. **35**, 1616 (1975).

[101] R. G. Arnold *et al.*, Phys. Rev. Lett. **35**, 776 (1975).

[102] S. J. Brodsky and B. T. Chertok, Phys. Rev. D **14**, 3003 (1976).

[103] G. R. Farrar, K. Huleihel and H. y. Zhang, Phys. Rev. Lett. **74**, 650 (1995).

[104] M. Miyama, Nucl. Phys. Proc. Suppl. **79**, 620 (1999) [arXiv:hep-ph/9905559].

[105] S. J. Brodsky, D. S. Hwang and I. Schmidt, Nucl. Phys. B **642**, 344 (2002) [arXiv:hep-ph/0206259].

[106] D. Boer, S. J. Brodsky and D. S. Hwang, Phys. Rev. D **67**, 054003 (2003) [arXiv:hep-ph/0211110].

[107] S. J. Brodsky, M. Burkardt and I. Schmidt, Nucl. Phys. B **441**, 197 (1995) [arXiv:hep-ph/9401328].

[108] E. L. Berger and S. J. Brodsky, Phys. Rev. Lett. **42**, 940 (1979).

[109] S. J. Brodsky, J. Rathsman and C. Merino, Phys. Lett. B **461**, 114 (1999) [arXiv:hep-ph/9904280].

[110] E. Tomboulis, Phys. Rev. D **8**, 2736 (1973).

[111] P. P. Srivastava and S. J. Brodsky, Phys. Rev. D **64**, 045006 (2001) [arXiv:hep-ph/0011372].

[112] V. A. Karmanov and A. V. Smirnov, Nucl. Phys. A **546**, 691 (1992).

[113] S. Dalley, Nucl. Phys. B (Proc. Suppl.) **108**, 145 (2002).

[114] S. J. Brodsky, in *Nagoya 2002, Strong coupling gauge theories and effective field theories, 1-18.* [arXiv:hep-th/0304106].

[115] J. Raufeisen and S. J. Brodsky, arXiv:hep-th/0408108.

[116] S. J. Brodsky and S. D. Drell, Phys. Rev. D **22**, 2236 (1980).

[117] S. J. Brodsky and D. S. Hwang, Nucl. Phys. B **543**, 239 (1999) [arXiv:hep-ph/9806358].

[118] S. J. Brodsky, F. E. Close and J. F. Gunion, Phys. Rev. D **5**, 1384 (1972).

[119] S. J. Brodsky, F. E. Close and J. F. Gunion, Phys. Rev. D **8**, 3678 (1973).

[120] S. J. Brodsky, D. S. Hwang, B. Q. Ma and I. Schmidt, Nucl. Phys. B **593**, 311 (2001) [arXiv:hep-th/0003082].

[121] R. L. Jaffe and A. Manohar, Nucl. Phys. B **337**, 509 (1990).

[122] X. d. Ji, Nucl. Phys. Proc. Suppl. **119**, 41 (2003) [arXiv:hep-lat/0211016].

[123] P. V. Landshoff, Phys. Rev. D **10**, 1024 (1974).

[124] S. J. Brodsky and G. P. Lepage, SLAC-PUB-2294 *Workshop on Current Topics in High Energy Physics*, Cal Tech., Pasadena, Calif., Feb 13-17, 1979.

[125] G. P. Lepage and S. J. Brodsky, Phys. Rev. Lett. **43**, 545 (1979).

[126] A. V. Efremov and A. V. Radyushkin, Theor. Math. Phys. **42** (1980) 97;

[127] D. Muller, Phys. Rev. D **51**, 3855 (1995) [arXiv:hep-ph/9411338].

[128] P. Ball and V. M. Braun, Nucl. Phys. B **543**, 201 (1999) [arXiv:hep-ph/9810475].

[129] M. Beneke, G. Buchalla, M. Neubert and C. T. Sachrajda, Nucl. Phys. B **591**, 313 (2000) [arXiv:hep-ph/0006124].

[130] Y. Y. Keum, H. N. Li and A. I. Sanda, Phys. Rev. D **63**, 054008 (2001) [arXiv:hep-ph/0004173].

[131] A. Szczepaniak, E. M. Henley and S. J. Brodsky, Phys. Lett. B **243**, 287 (1990).

[132] A review of QCD analyses of exclusive B decays is given in S. J. Brodsky, Published in *Ise-Shima 2001, B physics and CP violation, 229-234* [arXiv:hep-ph/0104153].

[133] C. K. Chua, W. S. Hou and S. Y. Tsai, Phys. Rev. D **66**, 054004 (2002) [arXiv:hep-ph/0204185].

[134] S. D. Drell and T. Yan, Phys. Rev. Lett. **24**, 181 (1970).

[135] G. B. West, Phys. Rev. Lett. **24**, 1206 (1970).

[136] V. L. Chernyak, A. R. Zhitnitsky and V. G. Serbo, JETP Lett. **26**, 594 (1977).

[137] V. L. Chernyak, V. G. Serbo and A. R. Zhitnitsky, Sov. J. Nucl. Phys. **31**, 552 (1980).

[138] G. R. Farrar and D. R. Jackson, Phys. Rev. Lett. **43**, 246 (1979).

[139] A. Duncan and A. H. Mueller, Phys. Rev. **D21**, 1636 (1980).

[140] S. J. Brodsky, C. R. Ji, A. Pang and D. G. Robertson, Phys. Rev. D **57**, 245 (1998) [arXiv:hep-ph/9705221].

[141] M. Beneke, Nucl. Phys. Proc. Suppl. **111**, 62 (2002) [arXiv:hep-ph/0202056].

[142] D. Muller, D. Robaschik, B. Geyer, F. M. Dittes and J. Horejsi, Fortsch. Phys. **42**, 101 (1994) [arXiv:hep-ph/9812448].

[143] B. Melic, B. Nizic and K. Passek, Phys. Rev. D **60**, 074004 (1999) [arXiv:hep-ph/9802204].

[144] A. Szczepaniak, A. Radyushkin and C. Ji, Phys. Rev. **D57**, 2813 (1998) [arXiv:hep-ph/9708237].

[145] M. E. Peskin, Phys. Lett. **B88**, 128 (1979).

[146] C-R Ji, A. F. Sill and R. M. Lombard-Nelsen, Phys. Rev. **D36**, 165 (1987).

[147] V. L. Chernyak and I. R. Zhitnitsky, Nucl. Phys. **B246**, 52 (1984).

[148] V. L. Chernyak, A. A. Ogloblin and I. R. Zhitnitsky, Z. Phys. **C42**, 583 (1989).

[149] N. G. Stefanis, Eur. Phys. J. **C7**, 1 (1999) [arXiv:hep-ph/9911375].

[150] S. J. Brodsky, J. R. Ellis, J. S. Hagelin and C. T. Sachrajda, Nucl. Phys. B **238**, 561 (1984).

[151] Y. Kuramashi [JLQCD Collaboration], [arXiv:hep-ph/0103264].

[152] S. J. Brodsky, G. P. Lepage and S. A. Zaidi, Phys. Rev. **D23**, 1152 (1981).

[153] I. D. King and C. T. Sachrajda, Nucl. Phys. **B279**, 785 (1987).

[154] M. Gari and N. Stefanis, Phys. Lett. **B175**, 462 (1986), M. Gari and N. Stefanis, Phys. Lett. **187B**, 401 (1987).

[155] C. E. Carlson, Phys. Rev. **D34**, 2704 (1986).

[156] P. Stoler, Phys. Rept. **226**, 103 (1993).

[157] P. V. Pobylitsa, V. Polyakov and M. Strikman, Phys. Rev. Lett. **87**, 022001 (2001) [arXiv:hep-ph/0101279].

[158] M. K. Jones *et al.* [Jefferson Lab Hall A Collaboration], Phys. Rev. Lett. **84**, 1398 (2000). [arXiv:nucl-ex/9910005]. O. Gayou *et al.* [Jefferson Lab Hall A Collaboration], Phys. Rev. Lett. **88**, 092301 (2002). [arXiv:nucl-ex/0111010].

[159] R. G. Sachs, Phys. Rev. **126**, 2256 (1962); J. D. Walecka, Nuovo Cim. **11**, 821 (1959).

[160] P. A. M. Guichon and M. Vanderhaeghen, Phys. Rev. Lett. **91**, 142303 (2003) [arXiv:hep-ph/0306007].

[161] P. G. Blunden, W. Melnitchouk and J. A. Tjon, Phys. Rev. Lett. **91**, 142304 (2003) [arXiv:nucl-th/0306076].

[162] R. G. Arnold, C. E. Carlson, and F. Gross, Phys. Rev. C **23**, 363 (1981), and references cited therein.

[163] R. Baldini, S. Dubnicka, P. Gauzzi, S. Pacetti, E. Pasqualucci, and Y. Srivastava, Eur. Phys. J. C **11**, 709 (1999); R. Baldini *et al.*, *Proc. of the e^+e^- Physics at Intermediate Energies Conference* ed. Diego Bettoni, eConf **C010430**, T20 (2001) [hep-ph/0106006].

[164] For a discussion on the validity of continuing spacelike form factors to the timelike region, see, B. V. Geshkenbein, B. .L. Ioffe, and M. A. Shifman, Sov. J. Nucl. Phys. **20**, 66 (1975) [Yad. Fiz. **20**, 128 (1974)].

[165] See also R. Calabrese, in *Proc. of the e^+e^- Physics at Intermediate Energies Conference* ed. Diego Bettoni, eConf **C010430**, W07 (2001); H. W. Hammer, *ibid.*, W08 (2001) [arXiv:hep-ph/0105337]; Carl E. Carlson, *ibid.*, W09 (2001) [arXiv:hep-ph/0106290]; M. Karliner, *ibid.*, W10 (2001) [arXiv:hep-ph/0108106].

[166] S. J. Brodsky and A. H. Mueller, Phys. Lett. B **206**, 685 (1988).

[167] J. D. Bjorken, Nucl. Phys. Proc. Suppl. **11**, 325 (1989).

[168] M. Beneke, G. Buchalla, M. Neubert and C. T. Sachrajda, Nucl. Phys. B **606**, 245 (2001) [arXiv:hep-ph/0104110].

[169] A. V. Belitsky, X. Ji, and F. Yuan, Phys. Rev. Lett. **91**, 092003 (2003). arXiv:hep-ph/0212351.

[170] J. P. Ralston and P. Jain, Phys. Rev. D **69**, 053008 (2004) [arXiv:hep-ph/0302043].

[171] G. A. Miller and M. R. Frank, Phys. Rev. C **65**, 065205 (2002) [arXiv:nucl-th/0201021].

[172] A. Z. Dubnickova, S. Dubnicka, and M. P. Rekalo, Nuovo Cim. A **109**, 241 (1996); S. Rock, *Proc. of the e^+e^- Physics at Intermediate Energies Conference* ed. Diego Bettoni, eConf **C010430**, W14 (2001) [hep-ex/0106084].

[173] F. Iachello, A. D. Jackson, and A. Lande, Phys. Lett. B **43**, 191 (1973).

[174] A. S. Kronfeld and B. Nizic, Phys. Rev. **D44**, 3445 (1991).

[175] P. A. Guichon and M. Vanderhaeghen, Prog. Part. Nucl. Phys. **41**, 125 (1998) [arXiv:hep-ph/9806305].

[176] M. A. Shupe *et al.*, Phys. Rev. D **19**, 1921 (1979).

[177] W. I. Weisberger, Phys. Rev. D **5**, 2600 (1972).

[178] M. Damashek and F. J. Gilman, Phys. Rev. D **1**, 1319 (1970).

[179] N. Isgur and C. H. Llewellyn Smith, Phys. Lett. **B217**, 535 (1989).

[180] A. V. Radyushkin, Phys. Rev. **D58**, 114008 (1998) hep-ph/9803316.

[181] J. Bolz and P. Kroll, Z. Phys. **A356**, 327 (1996) hep-ph/9603289.

[182] M. Diehl, T. Feldmann, R. Jakob and P. Kroll, Eur. Phys. J. C **8**, 409 (1999) [arXiv:hep-ph/9811253].

[183] H. W. Huang, P. Kroll and T. Morii, Eur. Phys. J. C **23**, 301 (2002) [arXiv:hep-ph/0110208].

[184] G. P. Lepage, S. J. Brodsky, T. Huang and P. B. Mackenzie, and S. J. Brodsky, T. Huang and G. P. Lepage, *In *Banff 1981, Proceedings, Particles and Fields 2*, 143-199.*

[185] H. N. Li and G. Sterman, Nucl. Phys. B **381**, 129 (1992).

[186] C. Weiss, [arXiv:hep-ph/0206295].

[187] V. Chernyak, [arXiv:hep-ph/9906387].

[188] M. K. Jones [Jefferson Lab Hall A Collaboration], Nucl. Phys. A **699**, 124 (2002).

[189] M. Ambrogiani *et al.* [E835 Collaboration], Phys. Rev. D **60**, 032002 (1999).

[190] S. J. Brodsky and M. Karliner, Phys. Rev. Lett. **78**, 4682 (1997) [arXiv:hep-ph/9704379].

[191] S. J. Brodsky and S. Gardner, Phys. Rev. D **65**, 054016 (2002) [arXiv:hep-ph/0108121].

[192] C. H. Chang and W. S. Hou, Phys. Rev. D **64**, 071501 (2001).

[193] R. L. Anderson *et al.*, Phys. Rev. Lett. **30**, 627 (1973)

[194] H. J. Besch, F. Krautschneider, K. P. Sternemann and W. Vollrath, Z. Phys. C **16**, 1 (1982).

[195] W. Melnitchouk, Nucl. Phys. A **699**, 278 (2002) [arXiv:hep-ph/0106262].

[196] M. Diehl, P. Kroll and C. Vogt, Phys. Lett. B **532**, 99 (2002) [arXiv:hep-ph/0112274].

[197] V. Savinov, in *Proc. of the e^+e^- Physics at Intermediate Energies Conference* ed. Diego Bettoni, eConf **C010430**, W03 (2001) [arXiv:hep-ex/0106013].

[198] J. Boyer *et al.*, Phys. Rev. Lett. **56**, 207 (1980); TPC/Two Gamma Collaboration (H. Aihara *et al.*), Phys. Rev. Lett. **57**, 404 (1986).

[199] D. Sivers, S. J. Brodsky and R. Blankenbecler, Phys. Rept. **23**, 1 (1976).

[200] R. J. Holt, Phys. Rev. **C41**, 2400 (1990).

[201] C. Bochna *et al.* [E89-012 Collaboration], Phys. Rev. Lett. **81**, 4576 (1998) [arXiv:nucl-ex/9808001].

[202] P. Rossi *et al.* [CLAS Collaboration], arXiv:hep-ph/0405207.

[203] S. J. Brodsky and J. R. Hiller, Phys. Rev. **C28**, 475 (1983).

[204] J. E. Belz *et al.*, Phys. Rev. Lett. **74**, 646 (1995).

[205] T. S. Lee, CONF-8805140-10.

[206] S. J. Brodsky, L. Frankfurt, J. F. Gunion, A. H. Mueller and M. Strikman, Phys. Rev. **D50**, 3134 (1994), [arXiv:hep-ph/9402283].

[207] J. C. Collins, Phys. Rev. D **57**, 3051 (1998) [Erratum-ibid. D **61**, 019902 (2000)] [arXiv:hep-ph/9709499].

[208] S. J. Brodsky, M. Diehl, P. Hoyer and S. Peigne, Phys. Lett. B **449**, 306 (1999) [arXiv:hep-ph/9812277].

[209] X. Ji, Phys. Rev. **D55**, 7114 (1997), [arXiv:hep-ph/9609381].

[210] A. V. Radyushkin, Phys. Rev. **D56**, 5524 (1997) [hep-ph/9704207].

[211] M. Diehl, T. Feldmann, R. Jakob and P. Kroll, Phys. Lett. **B460**, 204 (1999) [arXiv:hep-ph/9903268].

[212] M. Diehl, T. Feldmann, R. Jakob and P. Kroll, Eur. Phys. J. **C8**, 409 (1999), [arXiv:hep-ph/9811253].

[213] J. C. Collins, L. Frankfurt and M. Strikman, Phys. Rev. **D56**, 2982 (1997) [arXiv:hep-ph/9611433].

[214] M. Diehl, T. Gousset, and B. Pire, [arXiv:hep-ph/0003233].

[215] M. Ramsey-Musolf and M. B. Wise, Phys. Rev. Lett. **89**, 041601 (2002) [arXiv:hep-ph/0201297].

[216] J. C. Anjos, J. Magnin and G. Herrera, Phys. Lett. B **523**, 29 (2001) [arXiv:hep-ph/0109185].

[217] A. Ocherashvili *et al.* [SELEX Collaboration], arXiv:hep-ex/0406033.

[218] R. Vogt and S. J. Brodsky, Phys. Lett. B **349**, 569 (1995) [arXiv:hep-ph/9503206].

[219] B. Portheault, arXiv:hep-ph/0406226.

[220] L. von Smekal, R. Alkofer and A. Hauck, Phys. Rev. Lett. **79**, 3591 (1997) [arXiv:hep-ph/9705242].

[221] D. Zwanziger, Phys. Rev. D **69**, 016002 (2004) [arXiv:hep-ph/0303028].

[222] D. M. Howe and C. J. Maxwell, Phys. Lett. B **541**, 129 (2002) [arXiv:hep-ph/0204036].

[223] D. M. Howe and C. J. Maxwell, Phys. Rev. D **70**, 014002 (2004) [arXiv:hep-ph/0303163].

[224] S. Furui and H. Nakajima, arXiv:hep-lat/0309166.

[225] A. C. Mattingly and P. M. Stevenson, Phys. Rev. D **49**, 437 (1994) [arXiv:hep-ph/9307266].

[226] G. Grunberg, *Phys. Lett.* **B95**, 70 (1980) [Erratum-ibid. **B110**, 501 (1982)]. G. Grunberg, *Phys. Rev.* **D29**, 2315 (1984).

[227] S. J. Brodsky, M. S. Gill, M. Melles and J. Rathsman, *Phys. Rev. D* **58**, 116006 (1998) [arXiv:hep-ph/9801330].

[228] S. J. Brodsky, M. Melles and J. Rathsman, *Phys. Rev. D* **60**, 096006 (1999) [arXiv:hep-ph/9906324].

[229] F. Le Diberder and A. Pich, Phys. Lett. **B289**, 165 (1992).

[230] M. Beneke and V. M. Braun, Phys. Lett. B **348**, 513 (1995) [arXiv:hep-ph/9411229].

[231] P. Ball, M. Beneke and V. M. Braun, *Nucl. Phys.* **B452**, 563 (1995) [arXiv:hep-ph/9502300].

[232] Y. L. Dokshitzer, G. Marchesini and B. R. Webber, *Nucl. Phys.* **B469**, 93 (1996) [arXiv:hep-ph/9512336].

[233] B. Melic, B. Nizic and K. Passek, Phys. Rev. D **65**, 053020 (2002) [arXiv:hep-ph/0107295].

[234] S. J. Brodsky, Published in *Newport News 2002, Exclusive processes at high momentum transfer 1-33.* [arXiv:hep-ph/0208158.]

[235] E. D. Bloom and F. J. Gilman, Phys. Rev. D **4**, 2901 (1971).

[236] S. J. Rey and J. T. Yee, *Eur. Phys. J. C* **22**, 379 (2001) [arXiv:hep-th/9803001].

[237] G. 't Hooft, *Nucl. Phys. B* **72**, 461 (1974).

[238] D. W. Sivers, S. J. Brodsky and R. Blankenbecler, *Phys. Rept.* **23**, 1 (1976).

[239] G. F. de Teramond and S. J. Brodsky, arXiv:hep-th/0409074.

[240] X. D. Ji, F. Yuan and J. P. Ma, *Phys. Rev. Lett.* **90**, 241601 (2003).

[241] D. Dutta *et al.* [Jefferson Lab E940104 Collaboration], Phys. Rev. C **68**, 021001 (2003) [arXiv:nucl-ex/0305005].

[242] J. Aclander *et al.*, Phys. Rev. C **70**, 015208 (2004) [arXiv:nucl-ex/0405025].

[243] R. Court *et al.*, Phys. Rev. Lett. **57**, 507 (1986).

[244] L. Y. Zhu [Jefferson Lab E94-104 Collaboration], arXiv:nucl-ex/0409018.

[245] L. L. Frankfurt and M. I. Strikman, Phys. Rept. **160**, 235 (1988).

[246] P. Jain, B. Pire and J. P. Ralston, Phys. Rept. **271**, 67 (1996) [arXiv:hep-ph/9511333].

[247] A. S. Carroll *et al.*, Phys. Rev. Lett. **61**, 1698 (1988).

[248] Y. Mardor *et al.*, Phys. Lett. **B437**, 257 (1998) [arXiv:nucl-ex/9710002].

[249] A. Leksanov *et al.*, Phys. Rev. Lett. **87**, 212301 (2001) [arXiv:hep-ex/0104039].

[250] G. F. de Teramond, R. Espinoza and M. Ortega-Rodriguez, Phys. Rev. **D58**, 034012 (1998) [arXiv:hep-ph/9708202].

[251] J. P. Ralston and B. Pire, Phys. Rev. Lett. **57**, 2330 (1986).

[252] L. Frankfurt, G. A. Miller and M. Strikman, Found. Phys. **30**, 533 (2000) [arXiv:hep-ph/9907214].

[253] N. N. Nikolaev, W. Schafer and G. Schwiete, Phys. Rev. D **63**, 014020 (2001) [arXiv:hep-ph/0009038].

[254] E. M. Aitala *et al.* [E791 Collaboration], Phys. Rev. Lett. **86**, 4773 (2001) [arXiv:hep-ex/0010044].

[255] D. Ashery, Comments Nucl. Part. Phys. **2**, A235 (2002).

[256] E. M. Aitala *et al.* [E791 Collaboration], Phys. Rev. Lett. **86**, 4768 (2001) [arXiv:hep-ex/0010043].

[257] J. Gronberg *et al.* [CLEO Collaboration], Phys. Rev. D **57**, 33 (1998) [arXiv:hep-ex/9707031].

[258] A. V. Efremov and A. V. Radyushkin, Theor. Math. Phys. **42**, 97 (1980) [Teor. Mat. Fiz. **42**, 147 (1980)].

[259] S. Brodsky, M. Diehl, P. Hoyer, and S. Peigne, unpublished.

[260] L. Frankfurt, G. A. Miller, and M. Strikman, Phys. Lett. **B304**, 1 (1993), [arXiv:hep-ph/9305228].

[261] V. M. Braun, D. Y. Ivanov, A. Schafer and L. Szymanowski, Nucl. Phys. B **638**, 111 (2002) [arXiv:hep-ph/0204191].

[262] V. L. Chernyak, [arXiv:hep-ph/0206144].

[263] I. P. Ivanov, N. N. Nikolaev, W. Schafer, B. G. Zakharov and V. R. Zoller, arXiv:hep-ph/0207045.

[264] S. J. Brodsky and H. J. Lu, arXiv:hep-ph/9506322.

[265] R. J. Crewther, Phys. Rev. Lett. **28**, 1421 (1972).

[266] CCFR Collaboration, W.C. Leung, *et al.*, Phys. Lett. **B317**, 655 (1993).

[267] CCFR and NuTeV Collaboration, presented by D. Harris at XXX Recontre de Moriond, 1995, presented by J. H. Kim at the European Conference on High Energy Physics, Brussels, July 1995.

[268] A. L. Kataev, A.V. Sidorov, Phys. Lett. **B331**, 179 (1994).

[269] CCFR Collaboration, P.Z. Quinta, *et al.*, Phys. Rev. Lett. **71**, 1307 (1993).

[270] G. 't Hooft, in the Proceedings of the International School, Erice, Italy, 1977, edited by A. Zichichi, Subnuclear Series Vol. 15 (Plenum, New York, 1979).

[271] A. H. Mueller, Phys. Lett. **B308**, 355 (1993).

[272] H. J. Lu, Phys. Rev. **D45**, 1217 (1992).

[273] M. Beneke and V. M. Braun, Phys. Lett. **B348**, 513 (1995).

[274] G. Degrassi and A. Sirlin, Phys. Rev. D **46**, 3104 (1992).

[275] N.J. Watson. Nucl. Phys. B **494**, 388-432 (1997).

[276] J. Papavassiliou, E. de Rafael, N.J. Watson. Nucl. Phys. B **503**, 79 (1997). hep-ph/9612237.

[277] N. J. Watson, Nucl. Phys. Proc. Suppl. **74**, 341 (1999) [arXiv:hep-ph/9812203].

[278] N.J. Watson. Nucl. Phys. B **552**, 461 (1999). hep-ph/9812202.

[279] J. Papavassiliou. Phys. Rev. Lett. **84**, 2782 (2000). hep-ph/9912336.

[280] D. Binosi and J. Papavassiliou, Phys. Rev. D **66**, 111901 (2002). hep-ph/0208189.

[281] D. Binosi and J. Papavassiliou, Nucl. Phys. Proc. Suppl. **121**, 281 (2003). hep-ph/0209016.

[282] D. Binosi, arXiv:hep-ph/0401182.

[283] M. Binger and S. J. Brodsky, Phys. Rev. D **69**, 095007 (2004) [arXiv:hep-ph/0310322].

[284] D. W. Sivers, Phys. Rev. D **43**, 261 (1991).

[285] HERMES Collaboration, A. Airapetian et al., Phys. Rev. Lett. **84**, 4047 (2000); Phys. Rev. D **64**, 097101 (2001).

[286] A. Bravar, for the SMC Collaboration, Nucl. Phys. B (Proc. Suppl.) **79**, 520 (1999).

[287] S. Weinberg, Phys. Rev. **140**, B516 (1965).

[288] J. C. Collins, Phys. Lett. B **536**, 43 (2002). [arXiv:hep-ph/0204004].

[289] X. d. Ji and F. Yuan, interactions?," arXiv:hep-ph/0206057.

[290] S. D. Drell and T. M. Yan, Phys. Rev. Lett. **25**, 316 (1970) [Erratum-ibid. **25**, 902 (1970)].

[291] G. T. Bodwin, S. J. Brodsky and G. P. Lepage, Phys. Rev. Lett. **47**, 1799 (1981).

[292] G. T. Bodwin, S. J. Brodsky and G. P. Lepage, Phys. Rev. D **39**, 3287 (1989).

[293] S. J. Brodsky, A. Hebecker and E. Quack, Phys. Rev. D **55**, 2584 (1997).

[294] A. Brandenburg, V. V. Khoze and D. Muller, Phys. Lett. B **347**, 413 (1995).

[295] D. Muller, D. Robaschik, B. Geyer, F. M. Dittes and J. Horejsi, Fortsch. Phys. **42**, 101 (1994).

[296] X. D. Ji, Phys. Rev. Lett. **78**, 610 (1997).

[297] E704 Collaboration, A. Bravar et al., Phys. Rev. Lett. **77**, 2626 (1996).

[298] K. Heller, in Proceedings of Spin 96, C. W. de Jager, T. J. Ketel and P. Mulders, Eds., World Scientific (1997).

[299] R. J. Glauber, Phys. Rev. **100**, 242 (1955).

[300] V. N. Gribov, Sov. Phys. JETP **30**, 709 (1970) [Zh. Eksp. Teor. Fiz. **57**, 1306 (1969)].

[301] L. Stodolsky, Phys. Rev. Lett. **18**, 135 (1967).

[302] S. J. Brodsky and J. Pumplin, Phys. Rev. **182** (1969) 1794.

[303] B. L. Ioffe, Phys. Lett. B **30**, 123 (1969).

[304] L. L. Frankfurt and M. I. Strikman, Nucl. Phys. B **316**, 340 (1989).

[305] B. Z. Kopeliovich, J. Raufeisen and A. V. Tarasov, Phys. Lett. B **440**, 151 (1998) [arXiv: hep-ph/9807211].

[306] D. E. Kharzeev and J. Raufeisen, nucl-th/0206073, and references therein.

[307] A. H. Mueller and A. I. Shoshi, Nucl. Phys. B **692**, 175 (2004) [arXiv:hep-ph/0402193].

[308] J. w. Qiu and I. Vitev, arXiv:hep-ph/0405068.

[309] A. D. Martin, M. G. Ryskin and G. Watt, arXiv:hep-ph/0406224.

[310] C. Adloff *et al.* [H1 Collaboration], Z. Phys. C **76**, 613 (1997) [arXiv:hep-ex/9708016].

[311] M. Ruspa, Acta Phys. Polon. B **35**, 473 (2004).

[312] J. Kuti and V. F. Weisskopf, Phys. Rev. D **4**, 3418 (1971).

[313]

[313] M. Arneodo, Phys. Rept. **240**, 301 (1994).

[314] S. J. Brodsky, I. Schmidt and J. J. Yang, arXiv:hep-ph/0409279.

[315] K. S. McFarland *et al.*, Int. J. Mod. Phys. A **18**, 3841 (2003).

[316] R. Petti, (NOMAD collaboration) presented at ICHEP(2004).

[317] Steve Geer, hep-ph/0210113, Talk given at 4th NuFact '02 Workshop (Neutrino Factories based on Muon Storage Rings), London, England, 1-6 Jul 2002.

[318] E. L. Berger, ANL-HEP-CP-86-78 *Invited paper given at Int. Symp. on Weak and Electromagnetic Interactions in Nuclei, Heidelberg, West Germany, Jul 1-5, 1986*

[319] A. Accardi *et al.*, arXiv:hep-ph/0308248.